

THE PHYSIOLOGICAL FUNCTION AND REGULATORY MECHANISMS
OF THE UNFOLDED PROTEIN RESPONSE AND ENDOPLASMIC
RETICULUM ASSOCIATED DEGRADATION

A Dissertation

Presented to the Faculty of the Graduate School
of Cornell University

In Partial Fulfillment of the Requirements for the Degree of
Doctor of Philosophy

by

Zhen Xue

January 2014

© 2014 ZHEN XUE

ALL RIGHTS RESERVED

THE PHYSIOLOGICAL FUNCTION AND REGULATORY MECHANISMS
OF THE UNFOLDED PROTEIN RESPONSE AND ENDOPLASMIC
RETICULUM ASSOCIATED DEGRADATION

Zhen Xue, Ph.D.

Cornell University 2014

ER protein homeostasis plays an important role in normal organism physiological and pathological conditions. ER stress induces activation of the unfolded protein response, which reacts to reset ER homeostasis by enhancing protein folding capacity, reducing protein translation load and up-regulating ER associated degradation. It is important to understand the physiological role of each main UPR or ERAD component as well as their molecular regulatory mechanisms.

IRE1 α , the most conserved UPR sensor protein, is a bifunctional enzyme containing both a kinase and RNase domain that are important for trans-autophosphorylation and *Xbp1* mRNA splicing, respectively. However, the amino acid residues important for structural integrity remain largely unknown. This research has identified a highly conserved proline residue at position 830 (P830) that is critical for IRE1 α structural integrity, hence the activation of both kinase and RNase domains. Further structural analysis reveals that P830 could form a highly conserved structural linker with adjacent tryptophan and tyrosine residues at positions 833 and 945 (W833 and Y945) thereby bridging the kinase and RNase domains. This finding may facilitate the identification of small molecules which specifically compromise IRE1 α function.

Previously, ER stress has been shown to activate inflammatory responses. Yet, whether this is true with ERAD in vivo remains to be demonstrated. Using macrophage-specific Sel1L (a key protein component of the Sel1L-Hrd1 ERAD complex) knock-out mice, our data challenges the causal link between ER stress and inflammation in a physiological setting. This research shows that Sel1L is dispensable for normal macrophage innate immunity functions. Although these macrophages exhibited elevated protein levels of a subset of ER chaperones and dilated ER cisternae at the basal conditions, surprisingly these changes are uncoupled from macrophage antigen presenting function, cytokine secretion function, and inflammatory responses against bacterial pathogens as well as in obese adipose tissues. Thus, we conclude that physiological mild ER stress may not play a causal role in inflammation in macrophages.

BIOGRAPHICAL SKETCH

Zhen Xue was born in Shanghai, China 1983 when China just started to open up to the world. By the time she could go to school, her parents provided all they could to support her study. Her grandmother was a nurse and it was her father's dream to become a medical doctor. Zhen showed great interest in biology since childhood and participated in national biology competitions in high school. She later went to Fudan University Shanghai Medical College in 2002 and graduated from the 7-year clinical medicine program, which included a one-year internship and two years of resident training. Following her love of science and her curiosity to know more about the molecular mechanisms of human diseases, she joined Prof. Ling Qi's lab at Cornell University Department of Nutritional Sciences in August 2009. Her research focuses on the physiological functions and molecular mechanisms of the unfolded protein response and ER associated degradation.

To My Father Bing-Shi Xue and Mother Wei-Ming Zhang.

ACKNOWLEDGMENTS

I would like to thank my PhD advisor Dr. Ling Qi for taking me into his lab. I am especially grateful to have visualized the development of a new lab over the years through collaborative hard work and the spirit of “keep trying”. I thank Dr. Qi for his guidance and support during my study. I will always appreciate the good role model he set for me and the good scientific habits he instilled in me to produce high quality work. I would like to thank my committee members Dr. Martha Stipanuk, Dr. Qiaoming Long and Dr. Sylvia Lee for their support, encouragement and advice on my projects as well on this thesis. Thank you also to Dr. Qiaoming Long, Dr. Helene Marquis, Dr. Zhenglong Gu, Dr. Yuxin Mao, Dr. Zhanguo Gao and Dr. Yihong Ye for their collaborations. I would also like to give special thanks to my lab members who provided tremendous help during my PhD study: Dr. Yin He, Dr. Liu Yang, Dr. Hui Chen, Dr. Yewei Ji, Dr. Haibo Sha, Dr. Guojun Shi, and the soon-to-be doctors: Shengyi Sun, Hana Kim and among many others, undergraduates Steven Ham, Robert Guber, Xin Shu. Finally, deepest thanks to all the supportive faculty members and classmates at Cornell, all my old friends in China and my new friends in the US, and my dear family for their infinite love and support.

TABLE OF CONTENTS

BIOGRAPHICAL SKETCH.....	iii
ACKNOWLEDGMENTS.....	v
TABLE OF CONTENTS	vi
LIST OF FIGURES	ix
LIST OF SUPPLEMENTARY FIGURES	x
LIST OF TABLES	xi
Chapter 1 INTRODUCTION AND LITERATURE REVIEW	1
1.1 THE ENDOPLASMIC RETICULUM.....	1
1.2 PROTEIN HOMEOSTASIS	3
1.2.1 Protein synthesis.....	3
1.2.2 Chaperone-assisted protein folding in the ER	4
1.2.3 Lectins and protein quality control in the ER.....	5
1.2.4 Disulfide bond formation.....	6
1.2.5 Substrate-specific chaperones.....	7
1.2.6 Protein sorting from the ER	7
1.2.7 ER STRESS.....	9
1.3 THE UNFOLDED PROTEIN RESPONSE (UPR)	11
1.3.1 IRE1 α PATHWAY	11
1.3.2 PERK PATHWAY	21
1.3.3 ATF6 PATHWAY.....	22
1.4 ER ASSOCIATED DEGRADATION (ERAD).....	24

1.4.1 MAJOR STEPS OF ERAD PROCESS	28
1.4.2 THE CONCEPT OF ERAD TUNING	34
1.5 ER STRESS AND DISEASES.....	35
1.5.1 ER STRESS AND METABOLIC DISEASES	36
1.5.2 ER STRESS AND IMMUNE DISEASES.....	44
1.6 RESEARCH AIM AND DISSERTATION ORGANIZATION	48
Chapter 2 A CONSERVED STRUCTURAL DETERMINANT LOCATED AT THE INTERDOMAIN REGION OF IRE1α	51
2.1 ABSTRACT.....	52
2.2 INTRODUCTION	52
2.3 EXPERIMENTAL PROCEDURES	55
2.4 RESULTS.....	58
SUPPLEMENTARY FIGURES	78
2.5 DISCUSSION	80
2.6 ACKNOWLEDGEMENTS	81
2.7 APPENDIX	82
2.7.1 The P830-containing structural linker of IRE1 α is important for cell growth.....	82
2.7.2 Analysis of IRE1 α phosphorylation sites on the activation loop	88
2.7.3 Summary of IRE1 α mutants and corresponding XBP1s levels	102
Chapter 3 The Sel1L-Hrd1 ERAD Complex in Macrophages Re-sets ER Homeostasis and is Dispensable for Innate Immunity.....	107
3.1 ABSTRACT.....	108

3.2 INTRODUCTION	109
3.3 EXPERIMENTAL PROCEDURES	113
3.4 RESULTS.....	119
SUPPLEMENTAL FIGURES.....	145
3.5 DISCUSSION	156
3.6 ACKNOWLEDGEMENTS	161
Chapter 4 SUMMARY AND FUTURE DIRECTIONS.....	162
REFERENCES	167

LIST OF FIGURES

Figure 1.1 Mechanisms which maintain ER protein homeostasis	10
Figure 1.2 Schematic figure of IRE1 α	12
Figure 1.3 Mammalian IRE1 α signaling pathways	13
Figure 1.4 Three major steps of mammalian ERAD process	27
Figure 2.1 The P830L mutation identified in human cancers abolished IRE1 α phosphorylation and activation.	61
Figure 2.2 The P830L mutation abolished IRE1 α phosphorylation and activation.....	64
Figure 2.3 P830 is located in the highly conserved hydrophobic patch connecting two domains of human IRE1 proteins.	67
Figure 2.4 The structural element consisting of P830-W833-Y945 is critical for IRE1 α function.....	71
Figure 2.5 The P830-containing structural linker of IRE1 α is important for its stability.....	74
Figure 2.6 The P830-containing structural linker of IRE1 α is critical for its oligomerization in response to ER stress.....	77
Figure 3.1 Characterization of MKO mice	122
Figure 3.2 ERAD deficiency and alterations in ER homeostasis in MKO macrophages.	126
Figure 3.3 Sel1L/HRD1 ERAD deficiency caused a mild UPR activation in MKO macrophages.	130
Figure 3.4 Increased sensitivity to ER stress in MKO macrophages.....	133
Figure 3.5 Normal innate function of MKO macrophages in vitro.	137
Figure 3.6 Sel1L is not required for inflammatory responses against pathogens in vivo.	141

Figure 3.7 Sel1L in macrophages is not required for chronic inflammatory responses in obesity.	144
---	-----

LIST OF SUPPLEMENTARY FIGURES

Figure S2.1 Xbp1 mRNA splicing.....	78
Figure S2.2 Confocal analysis of intracellular localization of IRE1 α WT and mutants.....	79
Figure. Appendix.1.1 P830-L941-Y945 linker mutation causes cell growth retardation.	85
Figure. Appendix.2.1 S724 and S726 are two phosphorylation residues of human IRE1 α	92
Figure. Appendix.2.2 S726D IRE1 α mutant shows full phosphorylation ability.....	95
Figure. Appendix.2.3 Alignment of yeast and human IRE1 α two monomers in an oligomerization model.	97
Figure. Appendix.2.4 Possible interaction between S726 and K574 in hIRE1 α	99
Figure S3.1 Distribution of Sel1L protein level in MKO mouse model.....	145
Figure S3.2 Normal spleen T cell and B cell population in naïve WT and MKO mice.....	147
Figure S3.3 Normal Mitochondria number and morphology in MKO peritoneal macrophages.	149
Figure S3.4 UPR genes in MKO peritoneal macrophages.	150
Figure S3.5 Accumulation of IRE1 α and PERK by blocking cytosolic proteasomes.....	151
Figure S3.6 The half-life of UPR and ERAD component proteins in MKO macrophages.	152
Figure S3.7 MKO peritoneal macrophage inflammatory response model in vitro.....	154
Figure S3.8 P2X7 levels in MKO peritoneal macrophages.....	155

LIST OF TABLES

Table 1 Summary of IRE1 α phosphorylation, XBP1 mRNA splicing and protein levels with mutation(s) identified in cancers in the ER stress condition.103

Table 2 Summary of IRE1 α phosphorylation, XBP1 mRNA splicing and protein levels with mutation(s) in the IRE1 α kinase domain in the ER stress condition.104

Table 3 Summary of IRE1 α phosphorylation, XBP1 mRNA splicing and protein levels with mutation(s) in the IRE1 α activation loop in the ER stress condition.105

Table 4 Summary of IRE1 α phosphorylation, XBP1 mRNA splicing and protein levels with mutation(s) in the IRE1 α RNase domain in the ER stress condition.106

Chapter 1 INTRODUCTION AND LITERATURE REVIEW

1.1 THE ENDOPLASMIC RETICULUM

All eukaryotic cells have an endoplasmic reticulum (ER). It is organized by interconnected flattened sacs and tubules and is continuous with the outer nuclear membrane. Thus, the ER membrane and the outer nuclear membrane form an enclosing internal space, called the ER lumen or the ER cisternal space, which often occupies more than 10% of the total cell volume.

The ER is structurally and functionally diverse among different cell types in order to meet diverse functional demands. Even within a cell, distinct regions of the ER may be highly specialized. In general, the ER is divided into rough ER and smooth ER. Mammalian cell proteins are translated in the cytosol. Secretory proteins or membrane proteins are then cotranslationally transported to the ER (1). Electron microscopy shows membrane-bound ribosomes coating the surface of the ER; therefore these regions are termed rough ER. Regions that lack membrane-bound ribosomes are termed smooth ER. Some smooth ER and transitional ER (the parts of ER between the rough and the smooth ER) form buds off vesicles carrying newly synthesized proteins or lipids for transportation to the Golgi apparatus where proteins are further modified.

The first and major function of the rough ER is protein sorting, where proteins become fully folded, matured, modified, and transported to their destined locations: plasma membrane, lysosomal vesicles or extra-cellular space. This process requires abundant protein chaperones that assist protein folding and quality control. The main function of smooth ER lies in lipid metabolism. The ER membrane synthesizes nearly all the major classes of lipids -- for example phospholipids and cholesterol. The second ER function is lipogenesis, because the enzymes that synthesize the lipid components of the lipoprotein particles are located in the membrane of the smooth ER. The third function of ER is calcium storage. A Ca^{2+} pump transports Ca^{2+} from the cytosol into the ER lumen where a high concentration of Ca^{2+} binding proteins facilitates calcium storage. Following many rapid responses to extracellular signals, a release of Ca^{2+} from the ER to the cytosol initiates important physiological reactions -- for example -- myofibril contraction in the muscle cells.

Approximately one-third of cell's proteins are secretory or membrane proteins that rely on ER for protein sortation (1). Previous studies have established the Signal Recognition Particle (SRP) pathway for ER resident or secretory proteins (2-5). Newly exported mRNAs yield the synthesis of an N-terminal signal sequence that is recognized by the SRP which suppresses protein synthesis. The ribosome-nascent polypeptide-SRP complex is recruited to the ER via binding interactions with the ER resident SRP receptor. Upon binding of the SRP receptor, SRP is released, translation resumes and the growing peptide is cotranslationally translocated into the ER.

ER plays a significant role in the expression of the mRNA transcriptome. Previous studies have demonstrated an enhanced half-life for ER-associated mRNA (6). Additionally, ER-associated mRNAs are excluded from the stress granule-directed trafficking pathways (7). Recently, studies on the mRNA translation and partitioning have further revealed the importance of ER in protein synthesis. Nicchitta's lab has reported two primary observations based on cell fractionation and ribosome profiling (8, 9): First, mRNAs encoding cytosolic proteins were broadly represented in the ER ribosome-associated mRNA pool and second, steady-state ribosome loading on ER-bound mRNAs was substantially higher than in the cytosol. These findings suggest that the ER might serve as a preferred locale for the synthesis of proteins. The existence of two compartments (ER and cytosol) in protein translation indicates that many RNA-binding proteins modulate a wide range of post-transcriptional processes (10) and confer compartment-specific translational efficiency (11); therefore, they are compartmentally segregated between cytosolic and ER-bound polysomes.

1.2 PROTEIN HOMEOSTASIS

1.2.1 Protein synthesis

Protein synthesis is operated by ribosomes. At the AUG start codon on the 5' end of mRNA, the large (60S) and the small (40S) ribosomal subunits form an initiation complex. Transfer tRNAs donate amino acids to elongate nascent

polypeptides at a rate of ~4-5 amino acids/second in mammalian cells (12). At the 3' end of mRNA, when a stop codon (UAG/UGA/UAA) is read, the large and small subunits of ribosomes disassemble and so translation stops. Translation has an error rate of about 1 amino acid in 10^3 - 10^4 (13-16). In addition to a high error rate in protein translation and transcription, proteins destined for the plasma membrane, lysosomal or extracellular space are folded in the ER at a 2.5-4 times faster rate than proteins synthesized in the cytosol (17). These ER dependent proteins also require more modifications to create structural complexity, thereby requiring the complicated regulation and quality control system discussed below.

1.2.2 Chaperone-assisted protein folding in the ER

The ER houses factors that assist protein folding and maturation in a challenging environment -- high concentrations of calcium ions and oxidizing conditions. Classical chaperones are grouped in several subfamilies: Hsp40, 60, 70, 90 and 100 kDa in size (18). Their synthesis is strongly enhanced under conditions of ER overload, glucose deprivation, and disruption of calcium or redox homeostasis (19, 20). BiP, for example, also known as GRP78 protects immature proteins from aggregation by binding to extended hydrophobic domains with relatively low affinity (1-100 mM) (18). BiP also plays an important role in the preparation of terminally misfolded ER proteins for dislocation into the cytosol for degradation (21-24); BiP also contributes to the unfolded protein response (25).

1.2.3 Lectins and protein quality control in the ER

Glycosylated proteins are decorated with a preassembled oligosaccharide core N-acetylglucosamine₂-mannose₉-glucose₃ (Glc₃Man₉GlcNac₂) at selective asparagine (N) residues (in Asn-X-Ser/Thr consensus site) by the oligosaccharyltransferase (OST) from a lipid pyrophosphate donor on the ER membrane, dolichol-PP (26, 27). After peptide translocation, the α -glucosidases I and II remove the two outermost glucose residues to produce a mono-glucosylated core glycan (28). Then two homologous ER lectins, calnexin (CNX) and calreticulin (CRT), in association with ERp57, an oxidoreductase that catalyzes disulfide bond formation, interact with the substrate to perform protein folding (29). Once folded, the innermost glucose residue is rapidly removed by glucosidase II while mis-folded or non-native deglycosylated glycoproteins are recognized by the ER folding sensor UDP-glucose:glycoprotein glucosyltransferase (UGT1) (30). UGT1 specifically re-glucosylates folding intermediates released from the CNX/CRT cycle so they will remain in the ER to enter more rounds of CNX/CRT-assisted folding. These additional rounds of CNX/CRT-assisted folding serve to delay aggregation and loss of folding competence (31, 32). This process is called the CNX/CRT cycle. The substrates that fail to acquire their native well-folded structure are eventually cleared by ER-associated degradation (ERAD) (33). In contrast, properly folded proteins released from CNX/CRT are transported to the Golgi compartment and assisted by mannose-binding lectins, such as ERGIC-53, VIPL, ERGL (34, 35).

Although in cultured cells, a single deletion of a single chaperone does not cause evident ER stress (36, 37), in vivo whole-body deletion of ER components such as ERP57 (38) or calreticulin (39, 40) results in embryonic lethality in mice. Calnexin-deficient mice displayed obvious motor disorders associated with a dramatic loss of large myelinated nerve fibers (41). The physiological functions of a specific type of chaperone or lectin are probably tissue-specific or specific during the development period (41, 42). MHC class I molecules expressed in a calreticulin-deficient cell line exhibited defective peptide loading and impaired T cell recognition (38, 43). These results all indicate the importance of lectins in maintaining normal ER homeostasis in cellular physiology.

1.2.4 Disulfide bond formation

The formation of disulfide bonds also serves to stabilize ER proteins. The incorrect pairing of cysteine residues usually prevents the folding of a protein into its native conformation (44). Prokaryotic and eukaryotic cells share similar pathways of disulfide-bond formation. In eukaryotic cells, protein disulfide - bonds are predominantly formed in the lumen of the ER. In vivo, the most common mechanism for the formation of protein disulfide bonds is a thiol-disulfide exchange reaction (44). Protein disulfide isomerase (PDI) was one of the first-identified thiol- disulfide oxidoreductases (45, 46) (47). Individual PDI homologues facilitate the maturation of discrete sets of proteins and they might also differ in their redox activity within the cell. Additionally, ERP57, a PDI

family member, acts in a unique pathway together with calnexin and calreticulin to assist in the maturation of a class of glycoproteins (48, 49).

1.2.5 Substrate-specific chaperones

While most proteins can be well folded by the traditional chaperone and lectins system, other proteins require a subgroup of specific chaperones for proper folding and maturation due to their unique expression levels or protein structure. For example, an LDL receptor needs the assistance of Receptor-Associated Protein (RAP) to prevent aggregation and premature ligand binding when being escorted to the Golgi (50, 51). Collagen also requires Hsp47 for its proper maturation in the ER (52) because Hsp47 mice display collagen deficiency and premature death (53).

1.2.6 Protein sorting from the ER

The ER proteins that are destined for the Golgi apparatus or beyond are transported in the form of COP-II coated vesicles. Proteins must be properly folded in order to exit from the ER. Despite the unclear mechanism of ER luminal protein transportation to the Golgi apparatus, it is known that many membrane proteins are actively concentrated in the specialized ER regions called ER exit sites. As vesicles bud from the ER, they start to merge with other vesicles that have matching SNARES. The clusters are moved quickly along microtubules to the Golgi apparatus while selective proteins with ER retrieval signals (KKXX

sequence at the C-terminal end for membrane proteins or KDEL sequence at the C-terminal end for soluble ER proteins) are returned to the ER through vesicles coated with COPI.

The Golgi apparatus is a polarized organelle consisting of cis, medial and trans cisternae. Proteins and lipids move from the cis to the trans cisternae by vesicular transport, by progressive maturation of the cis cisternae migrating continuously or, most likely, by a combination of the two mechanisms. The Golgi apparatus contains many sugar nucleotides and glycosyl transferase enzymes. Proteins undergo further glycosylation reactions and modifications, e.g. the O-linked (Pyrolysine-linked) glycosylation occurs within the Golgi. N-linked (Asparagine-linked) oligosaccharides glycosylation initially occurs in the ER and the oligosaccharides are usually removed in the Golgi. The finished protein in the trans- Golgi will be packed into vesicles and further transported into destined locations: lysosome, plasma membrane or extracellular space.

Terminally misfolded proteins in the ER are removed to the cytosol where they are degraded by the ubiquitin-proteasome system. This process is called ER-associated degradation (ERAD) (54). It is used for physiological protein turnover and is also utilized by viruses for structural protein breakdown. ERAD is an important aspect of the protein quality control system. The details will be discussed in 1.4.

1.2.7 ER STRESS

The ER protein homeostasis is maintained at a dynamic state of balance in which the input of newly synthesized proteins and the export of mature proteins, or degradation of misfolded proteins, remain equal. Accumulation of misfolded proteins in the ER causes ER stress. Two main mechanisms are adopted by the cells to maintain ER protein homeostasis: the unfolded protein response (UPR) and the ER associated degradation (ERAD) (**Figure 1.1**). The unfolded protein response (UPR) is activated to enhance protein folding machineries for the purpose of increasing protein output from the ER. UPR is also activated to attenuate protein translation in order to reduce the accumulation of misfolded proteins. The details of unfolded protein response (UPR) will be discussed in 1.3. The ERAD components can also be enhanced by UPR signaling pathways. Activation of ERAD will lead to ER protein translocation into the cytosol where these proteins are degraded by the cytosolic proteasome system. The details of ERAD will be discussed in 1.4.

ER stress can be caused by multiple physiological or pathological conditions: nutrient deprivation (55), virus infection (56) or calcium depletion (57). Most of the time, ER stress is caused by mutations of ER proteins such as anti-trypsin (58) or Parkin (59). The most common ER stress inducing drugs include thapsigargin (Tg), which inhibits ER calcium transport ATPase (60), tunicamycin (Tm), which blocks protein glycosylation (61) and dithiothreitol (DTT) which disrupts disulfide bond formation.

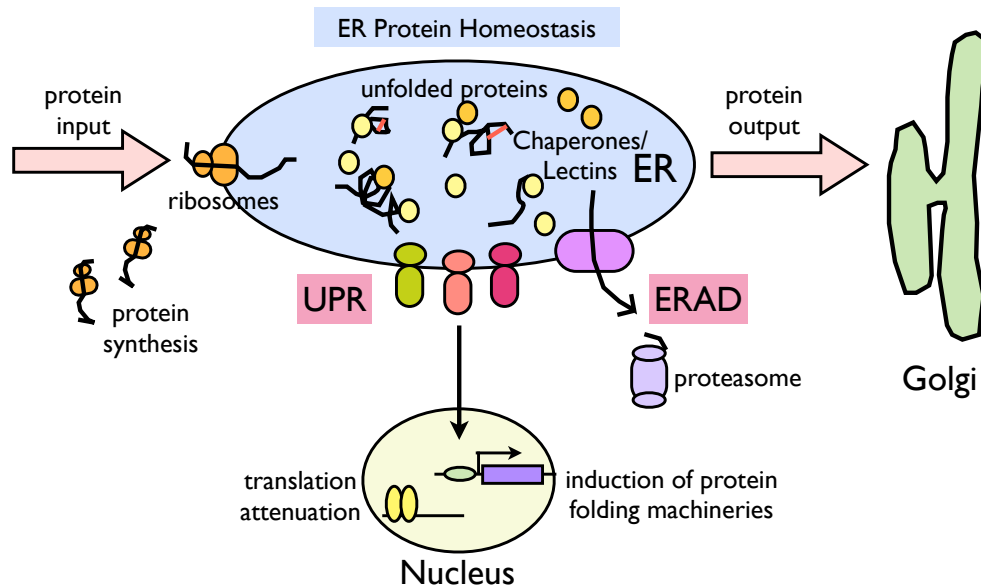


Figure 1.1 Mechanisms which maintain ER protein homeostasis.

The ER protein homeostasis is maintained by a balance between the protein input into the ER and the protein output for transportation or degradation. An accumulation of misfolded proteins in the ER leads to ER stress accompanied by increased levels of protein chaperones and lectins in the ER. The unfolded protein response (UPR) and the ER associated degradation (ERAD) are the two major mechanisms which reduce ER stress. Activation of UPR enhances ER protein folding machineries and attenuates protein translation. ERAD activation promotes protein translocation into the cytosol where the proteins are degraded by the proteasomes.

1.3 THE UNFOLDED PROTEIN RESPONSE (UPR)

In response to ER stress, organisms have developed an evolutionarily conserved ER-to-nucleus signaling pathway. The pathway is called the unfolded protein response (UPR) and copes with the stress for survival (62). The activation of UPR promotes protein export and reduces input by up-regulating ER protein folding capacity, enhancing ER-associated degradation, attenuating global translation, or inducing apoptosis when the stress is irreversible (63). IRE1 α -XBP1, PERK, and ATF6 pathways are known to mediate unfolded protein response in mammalian cells.

1.3.1 IRE1 α PATHWAY

Inositol requiring kinase 1 α (IRE1 α) is the most conserved UPR pathway as it is the only identified UPR initiation protein in yeast (64, 65). IRE1 α is a type I transmembrane protein that consists of four major domains: an N-terminal luminal sensor domain, a single transmembrane domain, a C-terminal cytosolic kinase domain and an endoribonuclease (RNase) domain. The schematic figure of IRE1 α protein is shown below (**Figure 1.2**). IRE1 α knock-out mice exhibited embryonic lethality after 12.5 days of gestation (66). IRE1 α has a homolog which is IRE1 β . IRE1 β is expressed selectively in the digestive tract and plays a distinctive role in mucin-secreting goblet cells. IRE1 β knock-out mice showed aberrant mucin 2 (MUC2) accumulating in the ER of goblet cells. The mice also showed ER distension and elevated ER stress which signaled increased XBP1

mRNA splicing (67). Most studies of the mammalian UPR signaling pathway are focused on IRE1 α . Activation of IRE1 α kinase and RNase domain cleaves XBP1 mRNA (X-box binding protein 1) (1.3.1.1), mediates mRNA decay (1.3.1.2), regulates inflammatory signaling pathways and determines cell fate (1.3.1.3) (Figure 1.3).

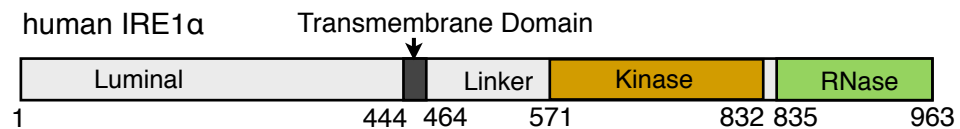


Figure 1.2 Schematic figure of IRE1 α

IRE1 α is composed of an N-terminal luminal sensor domain, a single transmembrane domain and C-terminal cytosolic kinase domain and an endoribonuclease (RNase) domain. The numbers of the amino acids indicate the position of each domain.

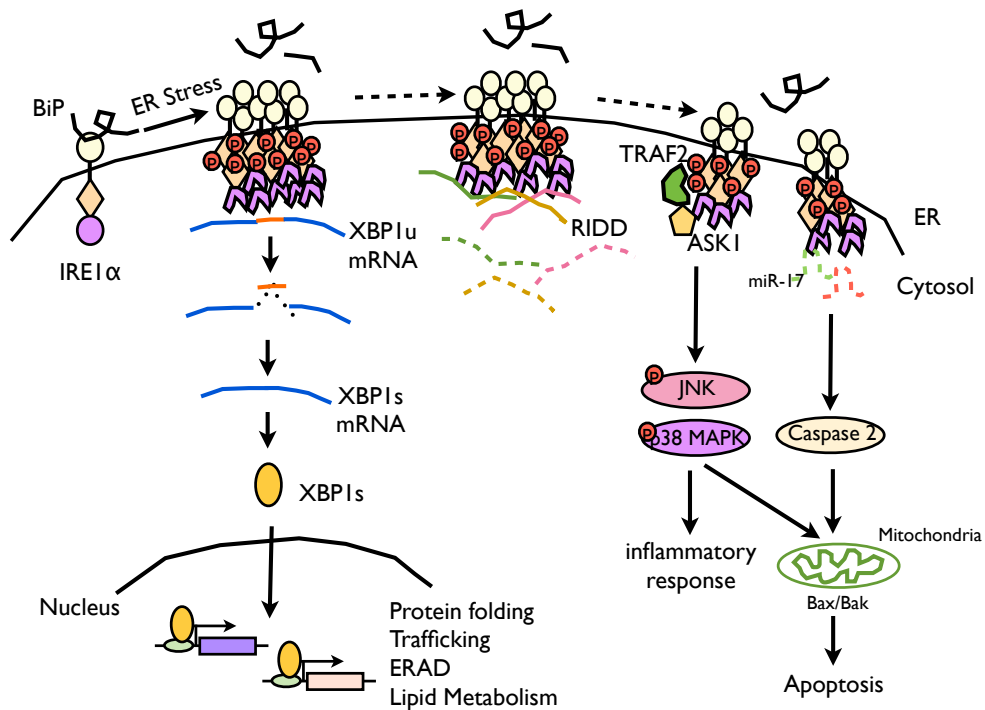


Figure 1.3 Mammalian IRE1 α signaling pathways

Under ER stress conditions, BiP dissociates from the IRE1 α luminal domain and then monomers of IRE1 α undergo oligomerization, phosphorylation and conformational changes that expose the active nuclease sites. Activated IRE1 α RNase domain cleaves XBP1 mRNA. The spliced form -- XBP1s -- is translated into a transcriptional factor that enhances protein folding machineries and ERAD. Regulated IRE1 α -dependent mRNA decay (RIDD) reduces protein load in the ER under ER stress. Activated IRE1 α can also form a complex with TRAF2 and ASK1 to induce JNK and MAPK pathways that regulate inflammatory responses and determine cell fate. IRE1 α also induces apoptosis through the caspase signaling by degrading miR-17/-34a/-96/-125b.

1.3.1.1 The physiological role of IRE1 α -XBP1s signaling pathway

Upon activation, IRE1 α can function as an endoribonuclease that cleaves a unique mRNA called XBP1 (X-box binding protein 1) in metazoans. After the cleavage at two specific positions flanking an intron, the exons are then ligated to form XBP1s mRNA which is translated into XBP1s protein. Splicing of XBP1 mRNA cuts out 26 nt and results in a frame shift at 165 aa. Hereafter, unspliced XBP1u and spliced XBP1s encode proteins of 261 and 376aa respectively (68). XBP1s binds to CRE-like sequences. The function of XBP1u is not fully understood yet. XBP1u contains a C-terminal degradation domain and a nuclear exclusion signal. It is known that XBP1u forms a complex with XBP1s. The complex can be transported to cytosol and rapidly degraded by the proteasome because of the degradation motif of XBP1u. Therefore, XBP1u may serve as a negative regulator of XBP1s (69).

XBP1s is a transcription factor that contributes to lipid biosynthesis, ER expansion, chaperones that enhance protein folding, ERAD and secretory pathways. Studies with XBP1 knock-out mice show that it is required for cardiac myogenesis, hepatogenesis, plasma cell differentiation and for the development of secretory tissues (70-73). XBP1 targets a diverse range of genes. These genes include (74): 1) In UPR pathways, ER chaperones and ERAD components such as ER degradation enhanced mannosidase alpha-like 1 (EDE1), DnaJ/Hsp40 homolog subfamily B member 9 (ERDJ4/DNAJB9) and DnaJ/Hsp40 homolog subfamily C member 3 (P58IPK/DNAJC3). 2) Tissue specific metabolic genes. For example, Mist 1 in skeletal muscles, C/EBP α in adipocytes and lipogenic

genes in hepatocytes are all XBP1s targets. 3) Disease-associated genes. For example several targets are linked to neurodegenerative diseases (e.g. Cdk5, Cdk5rap3, and Sil1) and myodegenerative diseases (e.g. Als2, Lmna, and Mbnl2). Specifically, γ -secretase complex components Ncstn, Psen1 and Psenen are involved in processing the amyloid precursor protein (APP) to generate amyloid beta peptide (A β). 4) Metabolic genes including those that regulate glycosylation, carbohydrate metabolism, glycolysis, gluconeogenesis, lipid and fatty acid metabolism, and apoptosis/cell survival. 5) Regulators of gene expression and chromosomal architecture, cell growth and differentiation, RNA processing and export, signal transduction, ubiquitin-associated processes, ion channels, transporters and proton pumps as well as DNA replication and repair, redox homeostasis and oxidative stress response. These functional targets suggest that XBP1 plays dual roles in both adjusting to the increased demand from the biosynthesis in the ER and neutralizing the byproducts produced in the process.

1.3.1.2 Regulated IRE1 α -dependent mRNA decay (RIDD)

IRE1 α independently mediates the rapid degradation of a specific subset of mRNAs (75). This function is processed by direct IRE1 α endonucleolytic cleavage, since IRE1 α showed a reduced specificity similar to its closest homolog, ribonuclease (RNase) L (76). Alternatively, IRE1 may rapidly recruit or activate a second ribonuclease. IRE1 α may also promote translational stalling and cleavage by no-go decay (75, 77). The substrates of RIDD are divergent in eukaryotes. RIDD operates only in fission yeast, but not in budding yeast, and it is

the only identified mechanism of UPR in fission yeast (78). Detailed mechanisms of RIDD are still unknown and require further investigation.

Recently it has been discovered that sustained IRE1 α RNase activity causes rapid decay of microRNAs (miR-17, -34a, -96 and -125b) that normally repress caspase-2 mRNA (79), therefore inducing apoptosis. The molecular mechanisms and implications of microRNAs and ER stress response await further investigation.

1.3.1.3 IRE1 α is a cell fate determinant

IRE1 α was not only identified as a positive regulator of cell survival but was also identified as a regulator of stress-induced apoptosis through cross talk between the ER and mitochondria. First, Bax-inhibitor 1 (BI-1/Tmbim6) is a highly conserved multi-transmembrane protein that resides predominantly in the ER. It serves to suppress IRE1 α kinase and endoribonuclease activity. This suppression has implications for controlling cell death and autophagy (80). Second, when attempts to restore ER protein homeostasis fail, IRE1 α can repress adaptive responses (81-83) and activate apoptosis through IRE1 α dependent degradation of miR-17/-34a/-96/-125b, thereby up-regulating Caspase 2 (84). Third, IRE1 α stimulates activation of the Apoptotic-Signaling Kinase-1 (ASK1) through formation of an IRE1-TRAF2-ASK1 complex (85). ASK1 activates the c-Jun N-terminal kinase (JNK) and the p38 MAPK kinase which, in turn, signal cascades that promote ROS-induced apoptosis in a mitochondria-

dependent pathway (86). ASK1 also plays a role in cell adaptation by opposing various stresses (86). Moreover, ER stress induces activation of mTORC1, which reduces AKT phosphorylation and induces activation of IRE1-JNK pathway and apoptosis (87).

Among the apoptosis-inducing substrates of JNK are two members of the BH3-only subgroup of Bcl2-related proteins, Bim and Bmf, which are normally sequestered by binding to dynein and myosin V motor complexes. Once phosphorylated by JNK, Bim and Bmf are released from the motor complex and induce Bax/Bak-dependent mitochondrial apoptosis (88). Bax and Bak also function in the ER membrane and bind to the cytosolic domain of IRE1 α for activation (89). In addition, the transcription factor CHOP is downstream of IRE1 α and regulates apoptosis. This regulation functions in part by enhancing DR5 (90) and Bim (91) while directly inhibiting Bcl-2 transcription (92, 93). Therefore, IRE1 α closely interact with BCL-2 family proteins in regulating stress-induced apoptosis through a cross talk between the ER and mitochondria.

1.3.1.4 IRE1 α activation mechanism

IRE1 α is activated upon sensing the accumulation of unfolded proteins in the ER. The activation process of IRE1 α can be divided into several steps: the luminal domain sensing the ER stress; auto-phosphorylation; oligomerization and conformational change. For the ER stress sensing mechanism, the N-terminal luminal region of yeast IRE1 α is composed of five sub-regions, termed I-V,

extending from the N-terminus to the transmembrane region (94). When the core luminal domain (cLD) binds to unfolded proteins or to peptides that are primarily composed of basic and hydrophobic residues (95), dimerization and oligomerization of IRE1 α occur, mediated by subregions II-IV interacting as homodimers (96). The homodimer formation can be impaired by an internal deletion on subregion IV S103P mutation (96). S103P mutation on the luminal domain of yeast IRE1 α led neither to BiP dissociation nor to a change in self-association. However, S103P mutant IRE1 α remained constitutively activated upon ER stress, indicating that self-association and BiP dissociation are not required for activation of yeast IRE1 α (97). Analysis of the yeast IRE1 α crystal structure revealed that the core luminal domain dimerizes to form a shared central groove, and its architecture is similar to the peptide binding domains of major histocompatibility complex (MHC). Therefore, it is proposed that the cLD directly binds unfolded proteins, which changes the conformational structure of IRE1 α monomers and in turn positions the cytosolic kinase domains prone to autophosphorylation (98). On the contrary, the mammalian IRE1 α binds to BiP at basal conditions, and the activation of IRE1 α is strongly dependent on the disassociation of BiP (99). Recently, it has been proved that BiP provides a buffer system against mild stress because BiP binding accelerates IRE1 α deactivation and deoligomerization. Therefore BiP modulates the sensitivity and kinetics of IRE1 α (94, 100). Unlike mammalian IRE1 α , the luminal domain of its homolog IRE1 β does not interact with BiP, but it interacts with unfolded proteins instead (101).

Once sensing the ER stress signal, either by direct binding to unfolded proteins or by disassociation of BiP, interactions between cLD initiate dimer formation which is required to configure higher-order oligomers necessary for UPR activation (98). It was also reported that the dimer contained an intermolecular disulfide bond formation (102). The dephosphorylated cytosolic portion of the crystal structure of human IRE1 α , when bound with ADP, showed a face-to-face dimer complex which was distinct from the back-to-back yeast IRE1 α dimer conformation (103). Transient dimer, or oligomerization, positions the kinase domain for trans-autophosphorylation among the adjacent IRE1 α activation loops. It also orders the RNase domain to form an interaction surface which is required for the Xbp1 specific ribonuclease activity (103, 104). In mammalian cells, higher orders of IRE1 α oligomers were found to comprise four or eight IRE1 α molecules (105). Yet it is still believed that dimer rather than oligomer is the basic functional unit of IRE1 α activation, because loss of foci formation only delays downstream signaling (106).

IRE1 α foci formation upon ER stress can be visualized by attaching a GFP tag to a IRE1 α expressing plasmid. With TM treatment, 293T cell IRE1 α starts foci formation after two hours and reaches a peak after four hours with fewer and larger foci. After six hours, IRE1 α foci start to dissociate and vanish completely at eight hours. Interestingly, IRE1 α phosphorylation, XBP1 mRNA splicing and the kinetics of BiP induction all synchronize well with IRE1 α foci formation. The IRE1 α signal attenuates after prolonged ER stress. Attenuation includes cluster dissolution, dephosphorylation and a decline in endoribonuclease activity.

However, reactivation of IRE1 α can still occur after the reset of ER homeostasis under additional stimuli (105).

Lipid composition in mammalian membrane phospholipid also serves as an important activator of UPR. It has been reported that stearoylCoA desaturase 1 (SCD1) knockdown causes an increase in the amount of saturated fatty acids and a decrease in the amount of monounsaturated fatty acids in phospholipids. This process does not affect the amount or the composition of the free fatty acid pool. SCD1 knockdown also induces expressions of CHOP and GRP78, and the IRE1 α mediated splicing of XBP1 mRNA (107). Lipid induced UPR activation can be alleviated by treating molecular chaperones (108). This indicates that lipid-induced ER stress is associated with increased misfolded proteins (109). Similarly, cholesterol loading was found to deplete endoplasmic reticulum calcium stores, induce UPR, and eventually activate caspase-3 mediated apoptosis -- an event likely to promote the progression of atherosclerosis (110). Despite an association with increased misfolded protein, the mechanism of IRE1 α activation (as well as PERK) also lies in an ER-spanning transmembrane domain that may directly sense lipid composition of the ER membrane. This is because deletion of the IRE1 α luminal sensing domain does not repress the responsiveness to ER stress induced by increased lipid saturation (111).

1.3.2 PERK PATHWAY

PERK is also a type I transmembrane protein composed of an ER luminal stress sensor and a cytosolic kinase domain. The activation mechanism of mammalian PERK is similar to that of IRE1 α . BiP dissociation from the N-terminus of PERK initiates homo-dimerization/oligomerization and autophosphorylation of the kinase domain (112). Unlike IRE1 α , PERK phosphorylates the α -subunit of eukaryotic translation initiation factor-2 (eIF2 α) at Serine 51. This phosphorylation blocks the guanine nucleotide exchange factor so eIF2 α cannot bind to GTP to form its active state. Instead, it remains bound to eIF2B and therefore inhibits translation initiation (113).

Once eIF2 α is phosphorylated, a global effect of translation attenuation occurs, thus reducing the burden of peptides entering the ER. Furthermore, PERK also enhances ERAD and expressions of prosurvival genes such as cIAP (cellular inhibitor of apoptosis) (114). However, not all protein translation is attenuated. EIF2 α phosphorylation promotes translation and expression of ATF4, CHOP and BiP. The transcription factor ATF4 drives pro-survival functions and is responsible for amino acid import, glutathione biosynthesis and oxidative stress resistance (115). Interestingly, ATF4 also induces a transcription factor C/EBP-homologous protein (CHOP/GADD153). CHOP actively promotes apoptosis primarily by repressing Bcl2 and other bZIP transcription factors expression (92). CHOP also induces Bcl-2 family protein Bax translocation from cytosol to mitochondria (116).

PERK is inhibited by P58IPK which binds to the cytosolic kinase domain of PERK (117, 118). Alternatively, PERK induces a negative feedback through CHOP. CHOP induces GADD34 expression and GADD34 dephosphorylates eIF2 α by forming a phosphatase with protein phosphatase 1 (PP1) (119). In addition, CReP (a constitutive repressor of eIF2 α phosphorylation) encodes the substrate targeting subunits of two phosphatase complexes that independently dephosphorylate eIF2 α constitutively (120). With these mechanisms, PERK pathway can be rapidly reversed within minutes when ER homeostasis is reset, and activated PERK is dephosphorylated (121).

1.3.3 ATF6 PATHWAY

ATF6 is also a transmembrane UPR initiator with a large luminal domain, a transmembrane domain and a cytosolic domain. Upon ER stress, it is transported from the ER to the Golgi apparatus where it is sequentially cleaved by S1P (site 1 protease) and S2P (site 2 protease) to remove the luminal domain and transmembrane anchor, respectively (122, 123). For this process, ATF6 shares the same protease with sterol response element binding protein (SREBP). After cleavage, the remaining cytosolic N-terminal domain of ATF6 is then translocated to the nucleus to serve as a transcription factor that up-regulates UPR target genes such as chaperones (BiP and Grp94) and protein disulfide isomerase (63). Similar to IRE1 α and PERK, ATF6 also binds to BiP, and BiP is released under ER stress to initiate the ATF6 Golgi localization process (124). In addition,

underglycosylated ATF6, in association with Calreticulin, has a higher rate of Golgi transportation and activation. This also serves as a mechanism to sense ER stress (125). Under basal conditions, ATF6 remains as a monomer, dimer or oligomer due to the intermolecular and intramolecular disulfide bonds between two conserved cysteine residues in the luminal domain. Upon ER stress, the extent of disulfide bond reduction correlates with activation, and only reduced ATF6 monomer reaches the Golgi apparatus (126). Details of the ATF6 activation mechanism under ER stress remain to be further investigated (63).

Cleaved ATF6, referred to as P50ATF6, (uncleaved ATF6 is of 90KD in size) regulates gene transcription in association with other bZIP transcription factors and co-regulators. In mammalian systems, the UPR is mediated by the cis-acting ER stress response element (ERSE). For example, ERSE mediates the transcription factors XBP1 and CHOP induction. The ERSE consensus sequence is CCAAT-N9-CCACG (127). Activated ATF6 binds to CCACG when CCAAT is bound by the general transcription factor NF-Y/CBF (128). Direct interaction of ATF6 and ERSE is critical for transcriptional induction of ER chaperones and UPR transcription factors. Recently ERSE-II has been revealed as the second ER stress response element; it is composed of ATTGG-N-CCACG. The activation of ERSE-II is similarly dependent on ATF6 (128).

Overall, ATF6 induces a cytoprotective gene expression program. ATF6 upregulates BiP, protein disulfide isomerase (PDI), ER degradation-enhancing alpha-mannosidase-like protein 1 (EDEM1), XBP1 (68) and CHOP, etc (121).

ATF6 also induces the Regulator of Calcineurin 1 (RCAN1) expression which leads to anti-apoptotic activity through Bcl2 and the Bcl2-antagonist of cell death (BAD) pathway (129) (130). In addition, there are many ATF6 homologs that are processed like ATF6; however, their functions are not yet fully understood. These include OASIS, CREBH, LUMAN/CREB3, CREB4, and BBF2H7 (131). In addition to protein homeostasis, ATF6(N) also binds to SREBP2(N) and inhibits SREBP2 targeted genes in liver cell lipogenesis (132).

Within the inactivation mechanism of ATF6, it is known that XBP1u regulates ATF6 degradation. XBP1u has a cytoplasm relocation signal NES and a proteasome-mediated degradation signal DEG; both are in the C-terminus of XBP1u. XBP1u directly interacts with ATF6 for translocation into the cytosol where they are both degraded by the proteasome system (133).

1.4 ER ASSOCIATED DEGRADATION (ERAD)

Many misfolded proteins are removed from the ER to be degraded by the cytosolic proteasome system. This process is called ER-associated degradation (ERAD). The major steps of ERAD include: 1) substrate recognition, 2) substrate relocation and 3) proteasome degradation (134). A transmembrane complex composed mainly of an E3 ligase, together with multiple cofactors, is called an ERAD component. Understanding both yeast and mammalian ERAD pathways is not enough. The total number of ERAD components remains unclear. Equally unclear are the relationships among different ERAD components and the identity

of the endogenous substrates for each E3 ubiquitin ligase. This lack of clarity is the result of previous research focusing on the model exogenous substrates to study their specificity to each ERAD component.

E3 ubiquitin ligases are at the center of ERAD transmembrane complexes. The ERAD complexes are responsible for substrate recognition, translocation and ubiquitination. The E3s usually have several transmembrane domains with a cytosolic RING finger domain (135). They are also associated with cytoplasmic AAA-ATPase Cdc48p/p97 that is thought to provide energy for substrate release from the ER. In yeast, one conserved E3 ligase complex is composed of E3 ligase Hrd1p and ER membrane proteins Der1p. Hrd3p is a substrate recruitment factor and is associated with Cdc48p (136). Two additional cofactors, Kar2p and Yos9p, are chaperones that can bind to substrates in association with Hrd1p. Another yeast E3 ligase is Doa10. Doa10 requires the Ub-conjugating enzymes Ubc6 and Ubc7 as well as the Ubc7 cofactor Cue1 and Cdc48 ATPase complex (the AAA-ATPase Cdc48p, and its cofactors Ufd1 and Npl4) (137, 138). The Cdc48 ATPase is only required for degradation of membrane-embedded Doa10 substrates, but not for any soluble substrates (137).

In mammalian systems, the ERAD complex is more complicated and diverse than that in yeast systems. For E3 ligases, gr78/RNF45/AMFR complex, HRD1/Sel1L complex, TCR8 and TEB4 are the known mammalian ERAD components, and more are being investigated (139). E2 ligases are also more diverse in mammalian systems. Yeast E2 ligase Ubc6 and Ubc7, for example,

have two mammalian homologs: Ube2j1, Ube2j2 (140-142) and Ube2g1, Ube2g2 (59, 143, 144), respectively (139). Similar to the yeast ERAD system, three major steps apply to the mammalian ERAD process (**Figure 1.4**). The details are discussed below.

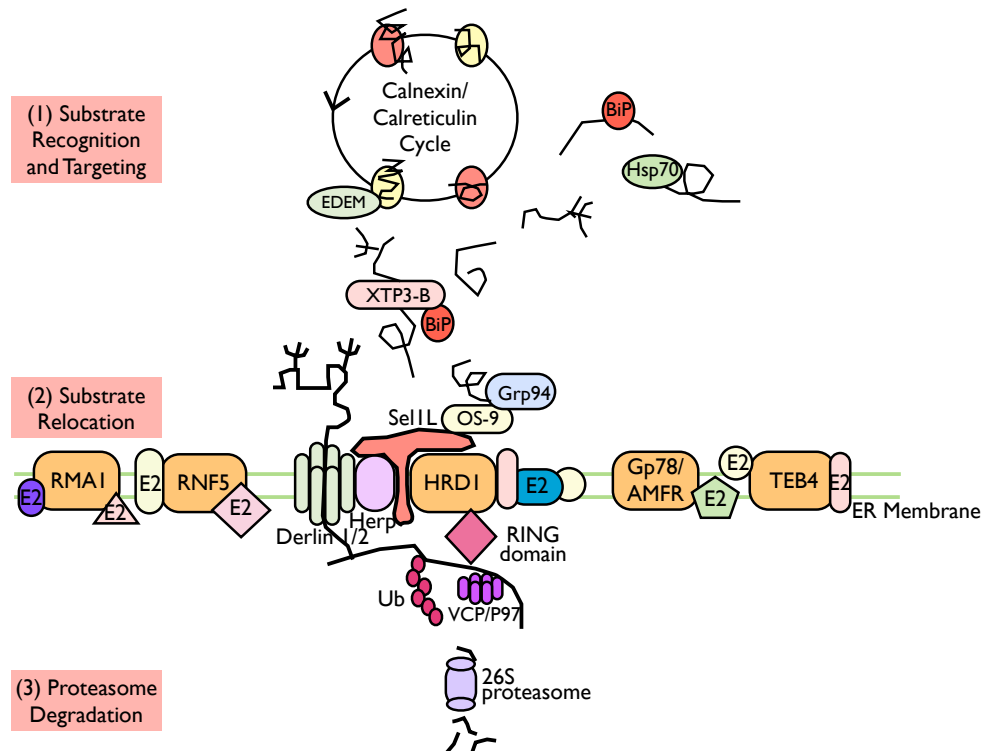


Figure 1.4 Three major steps of mammalian ERAD process

(1) Substrates are folded in the calnexin/calreticulum cycles. If they fail to achieve native states or contain lesions, they are recognized by lectins and chaperones for ERAD. N-linked glycosylation serves as a marker in this step. A variety of known transmembrane E3 ligases are shown in orange in the figure. Diversified E2s are indicated in different colors and shapes. HRD1, one of the most well known E3 ligases, needs a cofactor, Sel1L, for its own stability and for recognizing specific substrates. Lectins and chaperones recognize protein substrates and transport them to different E3 ligase complexes. Lectins XTP3-B and OS-9 are specifically recognized by HRD1/Sel1L ERAD components. (2)

After substrate recognition and targeting, the proteins are translocated through a channel composed of Derlin1/2. Herp connects Derlin1/2 translocon to HRD1/Sel1L complex. The Ring domain on HRD1 or other E3 ligases add ubiquitin to the translocated substrates with the help of ATPase P97. (3) After translocation, the protein substrates are finally degraded by 26S proteasomes.

1.4.1 MAJOR STEPS OF ERAD PROCESS

1.4.1.1 Substrate Recognition

Substrates of ERAD include soluble and integral membrane proteins, polypeptides that have failed to be post-translationally modified or are otherwise damaged or misfolded, and unassembled members of multiprotein complex, as well as regular physiological proteins. For example, the cystic fibrosis transmembrane conductance regulator (CFTR) relies on the ERAD for regular protein turnover and for prevention of toxic protein aggregation (145).

Chaperones, such as the heat-shock protein (Hsp70) family, bind to short polypeptide motifs with hydrophobic properties to prevent protein aggregation and maintain soluble status. Although molecular chaperones facilitate recognition of some ERAD substrates (146, 147), it is still not clear whether the chaperones are required for recognition of every ERAD substrate. It is clear though that BiP mutant knock-in mice showed defects that were consistent with compromised ER quality control and displayed profound brain development defects (148).

N-linked oligosaccharide (GlcNAc2-Man9-Glc3) also plays a role in ERAD substrate recognition. After the calnexin-calreticulin folding cycle, the glycoprotein contains a GlcNAc2-Man9 residue which is a signal for exit from ER or transit to its final destinations. On the contrary, if the glycoprotein contains hydrophobic patches or is in a molten globule-like state, a glucose molecule will be added to the glycoprotein by UDP-glucose:glycoprotein glucosyltransferase (UGGT) so it will re-enter the calnexin-calreticulin cycle (149) (150, 151). To prevent glycoproteins from becoming permanently trapped in a re-glucosylation and folding cycle, mannosidases act as timers. In later ERAD steps, mannosidases are required for delivery of certain glycoproteins from EDEM1 to lectins (152, 153).

Mammalian PDI and its homologs also participate in ERAD substrate translocations. PDI enables the retrotranslocation of the cholera toxin and the simian virus-40 (SV40) polyoma virus (45, 154). The PDI homologue, ERDJ5 accelerates formation of the monomer form of null Hong Kong (NHK) from disulfide-linked dimers for degradation (155).

1.4.1.2 Substrate Targeting

The ERAD system must be able to differentiate among actively folding, fully folded or misfolded proteins. It is still not clear how different types of substrates are recognized by a subgroup of chaperones followed by different E3 ligase complexes. One method is to divide substrates on the site of the misfolded lesion.

In yeast, it is hypothesized that there is a sequential check point mechanism to determine the destiny of ERAD substrates: if the lesion is in the cytosol (ERAD-C), then the misfolded protein is targeted for ERAD; if the lesion is in the luminal domain (ERAD-L), then the misfolded protein is targeted for the ER-to-Golgi transport system (156). Another theory postulates ERAD-L and substrates with transmembrane domain lesions (ERAD-M) use Hrd1p/Hrd3p ligase complex. The substrate forms a complex together with Der1p via the linker protein Usa1p and is recognized by Yos9p (157). ERAD-M differs from ERAD-L in that it is independent of Usa1p and Der1p. ERAD-C substrates are directly targeted by Doa10p complex for degradation. All three pathways share the Cdc48p ATPase complex (158).

Several ER-resident targeting lectins were recently discovered to deliver ERAD substrates to the retrotranslocation channel. EDEM (including EDEM1, EDEM2 and EDEM3) interacts with calnexin and possibly receives substrates from the calnexin cycle (159-164). Yos9 was shown to bind to misfolded proteins and form a complex with BiP. Yos9 possibly regulates the selectivity of Hrd1 for substrate targeting (157, 158, 165). Yos9p and Hrd3p, having similar mechanisms, both serve as “gatekeepers” in recognizing substrates (138). In the absence of Hrd3p and Yos9p, overexpression of Hrd1p can still degrade substrates. They can bind to substrates for ERAD independent of their carbohydrate groups, but still require the site-specific group processed by α -mannosidase I. Yos9 mammalian homologues, OS9 and XTP3-B were found to have similar functions. OS9, interacting with GRP94, recruits NHK for HRD1

complex (166). XTP3-B forms a complex with BiP and interacts with HRD1/Sel1L (167).

ERAD substrates must be ubiquitylated before degradation by the proteasome in the cytosol. The ubiquitylation process involves an E1 ubiquitin-activating enzyme, E2 ubiquitin-conjugating enzymes, E3 ubiquitin ligases and, in some cases, E4 ubiquitin-chain-extension enzymes (168-170). In yeast, Doa10-dependent ubiquitylation prefers Ubc6 and Ubc7 (137, 171) whereas Hrd1 uses Ubc7.

Mammalian orthologues of E2 ligases are more diverse and the specificity of E2 to different substrates and E3 ligases needs further investigation. The complexity of E3 is also less studied, and the research is based only on limited substrate examples. For instance, F-box only protein (SCF) E3 complex binds to glycosylated substrates and affects the stability of the α -subunit of TCR α (172). GP78, in cooperation with RMA1, promotes the ubiquitylation of the mutant CFTR as an E4-like activity for ERAD (173). Parkin, another E3 ligase, works with UBC6 and UBC7 homologues and ubiquitylates a putative G protein-coupled transmembrane polypeptide named Pael receptor. The Pael receptor interacts with Parkin and is responsible for autosomal recessive juvenile Parkinsonism (ARJP) (59).

Apart from lectins and E2 as important cofactors for substrate targeting, there are other important cofactors controlling E3-substrate interactions. Hrd3p in yeast

and its metazoan counterpart SEL1L are the most thoroughly characterized adaptors and will be discussed more in depth in 1.4.4. Housekeeping chaperones Hsp70 and Ssa1p facilitate substrate interaction with Doa10p (174). Hsp70s and Kar2p interact with Yos9p-Hrd3p (157). In mammals, BiP interacts with OS-9/XTP3-B/Sel1L complex (167).

Interestingly, E3s are autoubiquitylated and trigger their own degradation. Yeast Hrd3p inhibits Hrd1p degradation and ensures Hrd1p is active only in the presence of controlled substrate delivery (175). In mammals, transient expressed SEL1L is rapidly degraded but is stabilized when HRD1 is coexpressed (175). In yeast, Hrd1 oligomerization is also essential for its activity and is regulated by Usa1p (176).

1.4.1.3 The retrotranslocon

Previously, Sec61 α was thought to compose the retrotranslocon channel. However, using real-time fluorescence to detect the ERAD substrates, it was discovered that retrotranslocation was blocked by antibodies against Derlin-1 but not against Sec61 α (177). More studies now show that the Derlin family functions as the retrotranslocation channel. In yeast, Der1 interacts with a Ubl-domain-containing protein, the U1 SNP-associating protein-1 (Usa1), which is a Herp homologue and forms a complex together with Hrd1 (158). In mammalian systems, Derlin-1 associates with different substrates and the inactivation of Derlin-1 results in ER stress. Derlin-1 interacts with US11, which is encoded by a

virus and specifically targets MHC class I heavy chains for export from the ER. Moreover, Derlin-1 interacts with VIMP which recruits the p97 ATPase and its cofactor (178). Derlin-1 also interacts with US11, which recruits MHC products to Derlin-1 (179). Derlin-1 has a rhomboid pseudoprotease domain, and mutation of this domain stabilizes NHK at the cytosolic face of the ER without disrupting the p97/VCP interaction. Therefore it is proposed that the rhomboid domain is responsible for substrate interaction whereas the C terminus of Derlin-1 is independently responsible for p97/VCP recruitment (180).

1.4.1.4 Cytoplasmic extraction and proteasome degradation

Ubiquitylated substrates can follow multiple dynamically controlled pathways to be degraded in the cytosol. The AAA adenosine triphosphatases (ATPase) Cdc48p (or p97 in metazoans), or at times the proteasome lid, play an important role in the extraction of substrates from the ER membrane (181). Once in the cytosol, peptide N-glycanase (PNGase), recruited by p97, removes the N-linked glycans from the substrates before entering into the proteasome (182, 183)(184). Deubiquitination is also required in the process of dislocation and is processed by YOD1 (185). During the entire process, ERAD is tightly coupled to substrate dislocation in a complex manner (134).

1.4.2 THE CONCEPT OF ERAD TUNING

It is proposed that a complex comprised of SEL1L and LC3-I acts as an ERAD tuning receptor and regulates the COPII-independent vesicle-mediated removal of the luminal ERAD regulators EDEM1 and OS-9 from the ER. This model suggests that during basal condition, SEL1L disengages and the absence of ERAD substrates possibly causes E3 ligase-induced ubiquitylation and degradation of the retro-translocon. EDEM1 and OS-9 are segregated in ER-derived ERAD tuning vesicles with the intervention of SEL1L and LC3-I. However during ER stress with accumulated proteins in the ER, elevation of the intraluminal levels of ERAD substrates competitively bind Sel1L, thus reducing the interaction of SEL1L with EDEM1, OS-9 and LC3-I. The dislocation machineries are stabilized, so the intraluminal concentration of ERAD factors and ERAD activity are enhanced (186). In short, the ERAD tuning pathways offer rapid and readily reversible adaptation response to deal with transient problems which may arise in the folding compartment. Activation of UPR, on the other hand, requires more time for transcription and translation regulations (186).

The concept of ERAD tuning is based on three pieces of evidence (187): 1) Several ERAD factors including ERManI (188, 189), EDEM1 (190-193), OS-9 (186), XTP3-B (167), HERP (194, 195), SEL1L (196, 197), the E3 ligases SMURF1 (198, 199) and gp78 (200, 201), JAMP (202) and ataxin-3 (203, 204) are subjected to faster turnover than conventional ER-resident chaperones and enzymes. This indicates that they may be involved in the ubiquitin proteasome

system, autophagy or autophagy-like pathways. 2) Some ERAD factors are constitutively segregated from the ER (186, 205). 3) Luminal expression of misfolded polypeptides may delay the turnover of ERAD factors, may retain them in the ER by interfering with their vesicle-mediated segregation from the compartment, or may directly affect the composition of ERAD complexes and their activity (186, 206, 207).

The ERAD tuning theory is also proved in the coronaviruses (including SARS and mouse hepatitis virus, MHV) during their infection cycle. The viruses hijack components of the ERAD tuning machinery and presumably co-opt EDEM1/OS-9/LC3-I-containing vesicles for replication (186, 192).

1.5 ER STRESS AND DISEASES

Increasing numbers of diseases are discovered to be associated with misfolded protein accumulation. In many cases, the unfolded protein response is specifically activated to reverse the ER stress by enhancing protein folding, ERAD or global translation attenuation. The type of diseases that result from mutations that interfere with proper protein folding or trafficking are called “conformational diseases” (208, 209). These misfolded proteins can lead to the accumulation of aggregated forms of the protein which become toxic for the cell (210). Typical examples include prion encephalopathies, neurodegenerative diseases (Alzheimer’s, Parkinson’s, Huntington’s), type 2 diabetes, amyloidosis, etc. On the other hand, when the aberrant conformer of a protein undergoes abnormal

degradation by the ubiquitin-proteasome system, it can lead to a loss-of-function effect (211). One example of loss-of-function disease is cystic fibrosis which is characterized by a loss of the functional Cystic Fibrosis Transmembrane Conductance Regulator (CFTR) (201, 212, 213).

Chemical chaperones are low molecular weight compounds that stabilize proteins in their native conformation. Chemical chaperones are effective in rescuing processing defects in the mutant protein. They can inhibit protein aggregation and enable the mutant proteins to escape the quality control systems (214). Compounds such as receptor ligands or enzyme inhibitors that selectively recognize the mutant proteins were found to rescue conformational mutants and were termed pharmacological chaperones (215-217). Increasing evidence has suggested that chemical and pharmacological chaperones could be effective in treating conformational diseases (218). In this introduction, I will focus on metabolic and immune conformational diseases.

1.5.1 ER STRESS AND METABOLIC DISEASES

1.5.1.1 ER stress and obesity and diabetes

UPR has been proposed as the intermediate link between obesity and diabetes. ER stress has been shown to exist in metabolic tissues, mostly liver, pancreas and adipose tissues. Activation of the IRE1 α -JNK pathway in liver and fat leads to suppression of the insulin receptor signal by suppressing serine phosphorylation of the insulin receptor substrate-1 (IRS-1) (219). XBP-1 deficient mice develop

insulin resistance (219). In the hypothalamus of obese mice, increased endoplasmic reticulum stress and activation of the unfolded protein response inhibits leptin receptor signaling (220). Moreover, chemical chaperones, 4-phenyl butyric acid (PBA) and tauroursodeoxycholic acid (TUDCA) improve leptin-sensitivity (220).

XBP1 β -cell specific knock-out mice display modest hyperglycemia and glucose intolerance resulting from decreased insulin secretion from β cells. This is due to a decreased number of insulin granules, impaired proinsulin processing, blunted glucose-stimulated insulin secretion and inhibited cell proliferation (221). A negative feedback activation of IRE1 α also contributes to β -cell dysfunction in XBP1 mutant mice (221). Meanwhile, XBP1 deficiency in the liver results in hypocholesterolemia and hypotriglyceridemia, indicating that hepatic XBP1 is responsible for lipogenesis (222). On the contrary, liver IRE1 α deletion displays modest hepatosteatosis, and was found to be necessary for efficient secretion of apolipoproteins upon disruption of ER homeostasis. Furthermore, IRE1 α represses expression of key metabolic transcriptional regulators including CCAAT/enhancer-binding protein (C/EBP) β , C/EBP δ , peroxisome proliferator activated receptor γ (PPAR γ) and enzymes involved in triglyceride biosynthesis (223).

PERK-eIF2 α pathway plays an important role in pancreas development. Ser51Ala eIF2 α mutant mice die after birth with pancreatic β cell deficiency (224). PERK is highly expressed in a mouse pancreas, although the exocrine and

endocrine pancreas develop normally in PERK $-/-$ mice. Postnatally, IRE1 α activation and increased cell death lead to progressive diabetes mellitus with exocrine pancreatic insufficiency, progressive degeneration of the islets of Langerhans and loss of insulin-secreting β cells followed by loss of glucagon-secreting α cells (225, 226). PERK deficiency causes suppression of insulin mRNA and does not lead to uncontrolled protein synthesis (227). Instead it leads to impaired ER-to-Golgi anterograde trafficking, retrotranslocation from the ER to the cytoplasm, proteasomal degradation, enlarged ER and retention of proinsulin (228). Liver specific suppression of eIF2 α phosphorylation results in lower liver glycogen levels and susceptibility to fasting hypoglycemia in lean mice and glucose tolerance and diminished hepatosteatosis (229). Attenuation of eIF2 α phosphorylation also correlates with the lower lipogenesis transcription factor, PPAR γ , and its upstream regulators C/EBP α and C/EBP β (229). Therefore, PERK-eIF2 α mediates the translation of key hepatic transcriptional regulators of glucose and lipid metabolism and thereby contributes to obesity and diabetes.

It is also believed that CHOP is a fundamental factor linking protein misfolding in the ER to oxidative stress and apoptosis in β cells under conditions of increased insulin demand. CHOP deletion in multiple type 2 diabetes mouse models result in improved glycemic control and expanded β cell mass, improved β cell ultrastructure and prolonged cell survival (230). In addition, islets from CHOP deletion mice show increased expression of UPR and oxidative stress response genes and reduced levels of oxidative damage (230).

1.5.1.2 ER stress and cardiovascular diseases

UPR activation is associated with the pathophysiology of heart failure in humans. The hearts showed a marked increase of GRP78 expression and morphological change of ER (231, 232). In the mouse model, after transverse aortic constriction (TAC), activation of the UPR was found in both hypertrophic (1 week after TAC) and failing hearts (4 weeks after TAC). While CHOP was activated, JNK or caspase-12 was not, indicating that CHOP may be involved in the transition from cardiac hypertrophy to heart failure. ASK1, as previously discussed is a kinase to phosphorylate JNK. The ASK1 knock-out mouse model also showed fewer cardiac dysfunctions and cardiac apoptosis cells after TAC (233). The expression of sarco/endoplasmic reticulum calcium ATPase isoform 3f (SERCA3f) was found to be up-regulated in failing human hearts (234).

Moreover, atherosclerosis plaques were found to have ER stress and UPR activation in endothelial cells, macrophages and smooth muscle cells (235). In normal conditions, macrophages ingest ApoB containing lipoproteins cholesterol and the ER esterifies the cholesterol to form cholesterol ester. Excessive amounts of free cholesterol, as well as oxysterols induce ER stress and ER stress induced apoptosis (110, 236-238). The apoptosis pathway is dependent on CHOP and involves the release of ER calcium, the mitochondrial release of apoptogens and activation of the death receptor Fas (239-241). For macrophages particularly, the ER stress-induced apoptosis usually requires a “second hit” either by pattern recognition receptors or by toll-like receptors (242, 243). Oxidized phospholipids activate a CD36-TLR2 pathway that initiates an oxidative burst. This oxidative

burst further amplifies the CHOP pathway mediated primarily by NADPH oxidase (244). Activation of the IRE1 α pathway and CHOP was also found in smooth muscle cells in the culture treated by 7-ketocholesterol (245), unesterified cholesterol (246), homocysteine (247) or glucosamine (248). The mechanism of ER stress-induced apoptosis is still not fully understood in smooth muscle cells. Apoptotic endothelial cells are procoagulant, and increase the adhesiveness of platelets, at least partially, by the mechanism that disturbs blood flow and is associated with IRE1-XBP1 branch activation (249, 250). Homocysteine (251, 252) and modified forms of LDL (253, 254) are associated with both IRE1 and CHOP activation. Activation of IRE1 α partially phosphorylates JNK or, by a direct interaction with BAX or BAK on the ER membrane, regulates the mitochondria dependent apoptosis. On the other hand, PERK or ATF6 activation can, in turn, activate Fas signaling pathway to initiate mitochondria independent apoptosis, which is mediated by CHOP. Details were discussed previously in 1.3.

Increased expression of UPR-related genes has been reported in cardiomyocytes close to the site of myocardial infarction in mice and humans (255, 256). Cardiomyocytes infected with a recombinant adovirus encoding dominant-negative XBP1 showed an increased hypoxia/reoxygenation-induced apoptosis, suggesting that the XBP1 arm of the UPR may have a cardioprotective role against hypoxic insults (255). ATF6 transgenic mice showed increased expression of ER resident chaperones GRP78 and GRP94 and better functional recovery after ex vivo ischemic/reperfusion (I/R). They also showed significantly less necrosis and apoptosis (257). Adenoviral-mediated transfer of the PDI gene

also showed significantly reduced cardiomyocyte apoptosis and a smaller left ventricular end-diastolic (256). These findings all suggest that activation of the UPR plays a protective role against I/R injury. However, with prolonged stimuli, ER stress induces the expression of PUMA. PUMA is a pro-apoptotic member of the Bcl-2 family. The suppression of PUMA expression leads to inhibition of cardiomyocyte apoptosis induced by a pharmacological ER stressor (258). This means ER stress can induce both protective UPR and apoptotic signaling in ischemic heart diseases, depending on the severity and length of stimuli induced by I/R.

1.5.1.3 ER stress and cancer

Following initiation of malignancy, rapid tumor growth results in microenvironmental stress and a change of ER protein homeostasis. Hypoxia, glucose deprivation, lactic acidosis, oxidative stress and decreased amino acid supplies as well as intrinsic stressors -- such as errors in glycoproteins and lipid biosynthesis that result from an increased mutation rate -- all contribute to UPR induction (259). Activation of UPR both protects neoplastic cells from apoptosis and permits recurrence of tumor growth once favorable growth conditions have been restored (260, 261). However, if the stress persists, UPR will promote tumor cell apoptosis.

Indeed, ATF6 nuclear translocation has been observed to increase in various types of cancers, for example human hepatocellular carcinoma (HCC) (262) and

Hodgkin's lymphoma (263). ATF6 primarily induces cytoprotective responses including ER biogenesis, chaperone up-regulation and protein degradation (264, 265). ATF6 also induces transcription of XBP1 that can adjust the ER capacity to match demand. Therefore ATF6 has been hypothesized as a survival factor for quiescent carcinoma cells. ATF6 is also responsible for the adaptation of tumor cells to chemotherapy which is regulated by the Ras homolog enriched in brain (RHEB) and by the mammalian target of rapamycin (mTOR) (266). The ATF6-RHEB-mTOR pathway could be the possible target for the reduction of the metastatic cancer relapse rate (259).

IRE1 α has been shown to promote cell proliferation through XBP1, because XBP1 splicing itself could lead directly to tumorigenesis. Elevated XBP1s levels in B and plasma cells drive multiple myeloma pathogenesis and promote hallmark myeloma characteristics (267-269). Moreover, IRE1 is required for tumor angiogenesis and also contributes to VEGF expression (270, 271). VEGF can also induce internalization of VEGF receptors, and subsequently induce IRE1 α activation and XBP1 splicing (272). XBP1s also increases BCL-2 levels after antiestrogen stimulation in breast cancer cells, and it suppresses apoptosis (273). On the other hand, IRE1 α prolonged RIDD activation has also been reported to induce apoptosis by interacting with TRAF2, which further triggers JNK and caspase-12 activation (274, 275). Thus, IRE1 α plays a dual role in tumor cell survival.

Similar to IRE1 α , PERK has been implicated in tumor progression and angiogenesis. PERK mutation or dominant negative PERK leads to smaller tumors and impaired angiogenic abilities (276, 277). PERK knock-down in human esophageal and breast carcinomas also results in ROS accumulation, oxidative DNA damage and subsequently, cell-cycle arrest at the G2/M phase through the PERK downstream transcription factor NRF2 (278, 279). On the contrary, pharmacologically activated PERK can also induce growth arrest and suppress tumor growth because eIF2 α phosphorylation-induced translational arrest down-regulates cell-cycle regulators and arrests the cells in the G1 phase (280). After acute ER stress, eIF2 α phosphorylation stalls protein synthesis to reduce the stress. However, if the stress persists, severe ER stress eventually leads to ROS and ultimately apoptosis.

ER stress activates UPR in an overlapping mechanism. CHOP is a downstream target of all PERK, IRE1 α and, to a milder degree, ATF6, although PERK-CHOP branch shows stronger activity during prolonged ER stress (281). Most targets can be regulated separately by each pathway, while each pathway activates its own specific down stream transcriptional activities. Some targets require the concomitant activation of two initiators, e.g. P58IPK depends on both ATF6 and IRE1 α activation (264). Finally, some downstream effectors exhibit multiple mechanisms in reducing ER stress. The three UPR pathways can also shift balance between cytoprotection and apoptosis based on the timing of ER stress. For example IRE1 α and PERK initially attenuate ER stress. However, sustained PERK activation upregulates CHOP levels, and accumulation of CHOP

until it reaches a sufficient level will stimulate the pro-apoptotic BCL-2 family proteins. Currently, the way tumor cells adapt to long-term ER stress is unclear, and tissue-specific UPR activation also complicates the research. Due to the incomplete understanding of UPR pathway redundancy, the timing effect, and the interplay between all the UPR pathways, understanding the mechanisms of UPR in cancers remains a challenge (259).

1.5.2 ER STRESS AND IMMUNE DISEASES

The UPR can initiate inflammation in variable cells and tissues. The fundamental link between UPR and inflammation is now thought to be an important aspect of the pathogenesis of inflammatory diseases. The interconnection mechanisms include the production of reactive oxygen species (ROS), the release of calcium from the ER, the activation of the transcription factor nuclear factor- κ B (NF- κ B), JNK, and the induction of the acute-phase response (282).

The process of disulfide-bond formation requires a robust driving force based on molecular oxygen because the terminal electron recipient leads to the production of ROS (283). Furthermore, additional oxidative stress can result from the depletion of reduced glutathione, which is consumed to reduce unstable and improperly formed disulfide bonds (284). PERK activates its downstream ATF4 and phosphorylates nuclear factor-erythroid-derived 2-related factor 2 (NRF2). Following phosphorylation, NRF2 translocates to the nucleus, and activates a set

of antioxidant plus oxidant-detoxifying enzymes in order to maintain the cellular level of glutathione as a redox buffer in the cell.

As discussed in 1.3.1, IRE1 α activation induces a conformational change so that its cytosolic domain binds to the adaptor protein tumor-necrosis factor α receptor-associated factor (TRAF2) (285). IRE1 α -TRAF2 complex recruits I κ B kinase (IKK), and IKK phosphorylates I κ B, which exposes a nuclear-localization signal in NF- κ B (286). NF- κ B is a transcriptional factor that is responsible for numerous inflammatory genes. Similarly, IRE1 α -TRAF2 complex recruits the protein kinase JNK, which activates JNK. JNK induces inflammatory genes by phosphorylating the transcription factor activator protein 1 (AP1) (287). PERK-eIF2 α also contributes to the activation of NF κ B, because global translation attenuation causes a faster degradation of I κ B to NF κ B due to a shorter half-life (288).

UPR participates in the development of autoimmunity. Inadequate UPR and aberrant protein folding contribute to autoimmunity through the following four mechanisms (289): 1) misfolded proteins overwhelm the UPR and act as autoantigens that promote autoimmunity; 2) UPR-related genes themselves act as autoantigens, and it has been suggested that patients with rheumatoid arthritis present BIP specific autoantibodies; 3) Defective UPR pathways in non-immune cells may still allow autoimmunity by overwhelming normal mechanisms of immune tolerance; 4) upregulating ERAD confers resistance to UPR-mediated apoptosis or a survival advantage to autoreactive cells.

UPR plays an important role in B-cell development and lymphopoiesis, since XBP1 is responsible for terminally differentiated immunoglobulin secretions during the development of plasma cells (72, 290). Rag (recombination activating gene-2 RAG2 blastocyst complementation system) was used to study the role of XBP1 in B cells. XBP1-deficient B cells expressed normal cellular markers of B220, IgM and IgD. However, *Xbp1^{-/-} Rag^{-/-}* chimeric mice had decreased basal levels of all immunoglobulin isotypes, and failed to produce antibodies in response to antigens or viral infection. They also did not express CD138 marker for plasma cells, and showed a lack of plasma cell development (72). It is believed that the phenotype of *Xbp1^{-/-} Rag^{-/-}* mice was due to a lack of UPR in these B cells (290, 291). The upstream transcription factor B-lymphocyte-induced maturation protein 1 (BLIMP1) is also upregulated in XBP1 deficient B cells as a lack of negative feedback (291). Interestingly, *IRE1 α ^{-/-}* B cells showed similar phenotype as *Xbp1^{-/-} Rag^{-/-}* mice, because the B cells have defects in antibody production (292). ATF6 cleavage is also found in stimulated B cells, indicating its function in terminal B cell differentiation (293). Yet, *PERK^{-/-}* B cells develop normally into plasma cells (292, 294). The malignant transformation of plasma cells form myeloma. Early experiments also showed that Xbp1 was highly expressed in myeloma cells (295), and patients with myeloma have high Xbp1s levels in the bone marrow (269). Bortezomib, a therapeutic agent for the treatment of myeloma, has a potent and selective inhibiting effect on 26S proteasome. Therefore the mechanism of selectivity for myeloma cells can be explained by an increased susceptibility of myeloma cells to endoplasmic reticulum induced

apoptosis; for example, activation of PERK, CHOP and ATF6, as well as JNK (296, 297).

In macrophages, TLR2/4 specifically activates the IRE1 α -XBP1 pathway and activates transcription profiles similar to those under ER stress induction, and TLR2/4 is required for optimal expression of cytokines including IL-6, IL-1 β , TNF and IFN- β (298-300). XBP1 is also essential for dendritic cell (DCs) development and survival. Lymphoid chimeras lacking XBP-1 possessed decreased numbers of DCs, whereas overexpression of XBP1 rescues and enhances DC development (301). On the other hand, prior engagement of TLR3/4 suppresses CHOP and ATF4 expression in splenic macrophages, renal tubule cells, and hepatocytes. Suppression of CHOP and ATF4 prevent renal dysfunction and hepatosteatosis, the effect of which is dependent on TRIF. These mechanisms might be beneficial for TLR-expressing cells to survive when experiencing prolonged levels of ER stress in the process of inflammatory reactions (302).

It has now been reported that ER stress plays a role in inflammatory bowel diseases (IBD). XBP1 specific knock-out in intestinal epithelial cells showed susceptibility to colitis induced by dextran sodium sulfate and resulted in apoptosis of Paneth cells (303). Furthermore, XBP1 deletion in gut epithelia also results in the reduction in size and number of goblet cells. In addition, autophagosome formation is activated in hypomorphic Paneth cells via PERK, eIF2 α and ATF4 (304). Commensal microbiota and increased intestinal epithelial cell death induce ileitis, and activate the IRE1-NF κ B pathway when autophagy is

deficient. ATG16L1 is shown to ameliorate ER stress induced intestinal inflammation and eases the NF- κ B pathway (304). Similarly, dextran sodium sulfate (DSS) induced colitis was found in gastrointestinal IRE1 β knock-out mice. Therefore, a tight regulation of UPR and inflammatory pathways regulate the development of inflammatory diseases including inflammatory bowel diseases.

1.6 RESEARCH AIM AND DISSERTATION ORGANIZATION

Since the identification of UPR sensors in the early 1990s, it has been concluded that UPR plays an essential role in maintaining ER protein homeostasis. Activation of UPR is known to be required in important physiological and pathological regulations. IRE1 α -XBP1 is the most famous pathway required for plasma cell development and production of immunoglobulins and cytokines. Altering the IRE1 α signaling pathway is also known to affect the severity of diseases including obesity and diabetes, cancer, inflammatory diseases and neurodegenerative diseases. In this thesis, chapter 1 reviewed facts about UPR and ERAD and their relationship to metabolic and inflammatory diseases.

Pursuant to this research, the IRE1 α -XBP1 pathway is the most revolutionarily conserved and well-studied UPR pathway. A comprehensive understanding of the regulatory mechanisms underlying mammalian IRE1 α activation is critical to understanding the UPR and future interventions. Kinase activity and trans-autophosphorylation of IRE1 α protein are important for the

activation of the RNase domain. Moreover, the two cytosolic domains of IRE1 α protein are functionally linked via autophosphorylation. One outstanding question remains: How is the activation of IRE1 α RNase and kinase domain coherently regulated? And, is phosphorylation of IRE1 α dispensable in the activation of its RNase domain? Chapter 2 discusses the molecular mechanism of human IRE1 α activation, and in particular, reveals that the internal link between the kinase and RNase domain is required for the coordinated activation of IRE1 α and foci formation. In appendix A, the importance and mechanism of IRE1 α phosphorylation based on more mutant variables will be discussed.

Growing evidence has further suggested a close interaction between UPR and inflammatory responses. In response to ER stress, IRE1 α -TRAF2-JNK pathway is activated, as well as NF- κ B and CREBH transcription factors that promote pro-inflammatory responses and acute-phase responses. On the other hand, ER stress can also be triggered by inflammation. TNF α causes the activation of all three UPR mammalian pathways in fibrosarcoma cells (305). TNF α , IL-1 β and IL-6 also induce UPR activation in hepatocytes (306). ER stress can also be triggered by excess metabolic factors such as lipids, glucose, cytokines, and neurotransmitters. These stimuli activate UPR, and UPR further causes more inflammatory responses and disruption of metabolic functions. Such a cycle exacerbates inflammatory signaling and stress signaling and deteriorates metabolic phenotypes.

Equally important as UPR, ERAD degrades unfolded and misfolded proteins from the ER lumen in the cytosolic proteasome and acts upon UPR. Defects in ERAD are known to cause accumulation of misfolded proteins or early degradation of physiologically required proteins. However, the molecular mechanisms of variable mammalian ERAD components remain largely unexplored. More research is needed to understand the diversity of E3 ligases, their physiological functions in each tissue type and their relevant temporal expressing manners. An intriguing question is whether ERAD contributes to inflammatory responses. In chapter 3, a macrophage specific Sel1L deletion model is used to study the interconnection between ERAD and inflammatory responses. Surprisingly, the study shows that Sel1L is dispensable in macrophage innate immunity functions. With a lack of Sel1L, macrophages remain intact in the functions of cytokine secretion, antigen presenting, pathogen defense and inflammatory responses in type 2 diabetes. This research challenges the notion of a dependence of UPR in inflammatory responses in highly secretory cell types. It also suggests a tightly regulated mammalian ERAD compensatory mechanism.

Finally, chapter 4 summarizes the research findings and discusses the direction of future research.

**Chapter 2 A CONSERVED STRUCTURAL
DETERMINANT LOCATED AT THE INTERDOMAIN
REGION OF IRE1 α**

Zhen Xue^{1,3}, Yin He², Kaixiong Ye^{1,3}, Zhenglong Gu^{1,2,3}, Yuxin Mao⁴, and
Ling Qi^{1,2,3}

¹ Graduate Program in Nutrition; ² Graduate Program in Genetics and
Development; ³ Division of Nutritional Sciences, Cornell University, Ithaca, NY
14853, USA

⁴ Weill Institute of Molecular and Cell Biology, Department of Molecular
Biology and Genetics, Cornell University, Ithaca, NY 14853, USA

Published: Journal of Biological Chemistry 286 (35), 30859-30866

Running title: Regulation of IRE1 α activation by a structural linker

Keywords: XBP1s, splicing, phosphorylation, Phos-tag, foci

2.1 ABSTRACT

The UPR sensor inositol-requiring enzyme 1 α (IRE1 α) is a bifunctional enzyme containing both kinase and RNase domains that are important for trans-autophosphorylation and *Xbp1* mRNA splicing, respectively, in response to ER stress. However, the amino acid residues important for structural integrity remain largely unknown. Here, through analysis of IRE1 α mutants associated with human somatic cancers, we have identified a highly conserved proline residue at position 830 (P830) that is critical for its structural integrity, hence the activation of both kinase and RNase domains. Structural analysis revealed that P830 may form a highly conserved structural linker with adjacent tryptophan and tyrosine residues at positions 833 and 945 (W833 and Y945), thereby bridging the kinase and RNase domains. Indeed, mutation of P830 to leucine (P830L) completely abolished the kinase and RNase activities, significantly decreased protein stability and prevented oligomerization of IRE1 α upon ER stress; similar observations were made for mutations of W833 to alanine (W833A) and to a lesser extent for Y945A. Our finding may facilitate the identification of small molecules to specifically compromise IRE1 α function.

2.2 INTRODUCTION

The unfolded protein response (UPR), a highly evolutionarily conserved endoplasmic reticulum (ER)-to-nucleus signaling pathway, is critical for maintaining ER homeostasis and has been implicated in the pathogenesis and

development of many human diseases including diabetes, cancer, and lung and heart diseases. UPR, the quality-control system designed to re-establish ER homeostasis, is initiated by the activation of three major sensors at the ER membrane: inositol-requiring enzyme 1 (IRE1), PKR-like-ER kinase (PERK), and activating transcription factor 6 (ATF6). Activation of UPR leads to the induction of chaperones and ERAD (ER-associated degradation) components, global translational attenuation, and is required for the maintenance of ER function, clearance of misfolded protein in the ER, and, if stress persists, induction of apoptosis (131). Among the three branches, the IRE1 α -initiated pathway is the most evolutionarily conserved and represents the only UPR branch in yeast (307, 308). Recent studies have shown that the IRE1 branch plays important roles in a wide range of physiological and disease conditions including B cell and adipocyte differentiation, secretory function for pancreas and salivary glands, neurodegeneration, and obesity and insulin resistance (131, 309). Hence, a comprehensive understanding of the regulatory mechanisms underlying mammalian IRE1 α activation is critical to the development of new therapeutic approaches.

In addition to a kinase domain, the cytoplasmic tail of the IRE1 protein also possessed endoribonuclease (RNase) activity, which cleaves *Hac1/Xbp1* mRNA (310, 311). The *Hac1/Xbp1* mRNA encodes for a potent transcription factor responsible for the upregulation of many genes involved in protein folding, degradation and trafficking (68, 312-314). The ER luminal domain of IRE1 α protein is critical for sensing ER stress and subsequent IRE1 α activation. While

earlier studies of human IRE1 α have suggested that IRE1 α dimers are sufficient for its activity (102, 315-317), recent studies showed that the formation of stress-induced IRE1 α foci is conserved between yeast and mammals (104, 105). The formation of IRE1 α foci in response to ER stress is believed to juxtapose the IRE1 α kinase and RNase domains, allowing for a more efficient way to relay signals emanating from the ER lumen.

One outstanding question remains as how important is the molecular mechanism underlying the activation of IRE1 α RNase and kinase domains. Some recent studies have shed light on this question. First, kinase-defective K599A mutant abolishes the RNase activity of IRE1 α , suggesting that kinase activity and trans-autophosphorylation of IRE1 α protein is important for the activation of its RNase domain (104). This is likely achieved by phosphorylation-induced conformational changes. Moreover, a previous study reported the failure to express stable forms of individual kinase and RNase domains (318). Together, these studies imply that the two cytosolic domains of IRE1 α protein are functionally linked via autophosphorylation. However, two recent studies suggested a dispensable role of phosphorylation of IRE1 α in activation of its RNase domain (319, 320). Thus, further studies are required to elucidate the relationship between the two domains.

Through analysis of IRE1 α mutants associated with human somatic cancers (321), our study identifies the interdomain linker region of the cytosolic domain of IRE1 α as an important structural determinant for its function. Thus, this region

may be used as a potential drug target for small molecules to regulate IRE1 α /UPR signaling.

2.3 EXPERIMENTAL PROCEDURES

Cell lines and reagents. IRE1 α ^{-/-} MEFs were generous gifts from Dr. David Ron (New York University School of Medicine). T-REx293 cell line and T-Rex293 stably expressing IRE1 α -3F6HGFP were recently described (105, 322) and provided Dr. P. Walter and Han Li (University of California, San Francisco). HEK293T, T-REx293 and Phoenix cells as described (322) were maintained in DMEM supplemented with 10% FBS (Hyclone) and 1% penicillin/streptomycin. Thapsigargin (Tg) (EMD Calbiochem) and stock cycloheximide (Sigma) were dissolved in DMSO and ethanol, respectively. Cells were treated with Tg at indicated concentrations for the indicated times and immediately snap-frozen in liquid nitrogen. Phos-tag was purchased from the NARD Institute (Japan).

Plasmids and mutagenesis. The pDsRed2-ER (Clontech) plasmid was provided by Dr. Fenghua Hu (Cornell University). pMSCV-IRE1 α -HA encoding wildtype human IRE1 α (89) was a gift from Dr. C. Hetz (University of Chile). IRE1 α -3F6HGFP plasmid (105) was provided by Dr. P. Walter and Han Li (University of California, San Francisco). Mutagenesis was performed and sequenced as described (323).

Transfection, retroviral transduction and stable cell lines. HEK293T were transfected with plasmids using polyethylenimine (PEI, Sigma) as we recently described (323). Cells were snap-frozen in liquid nitrogen 24 h post-transfection followed by Western blot. To avoid experimental variations due to transfection efficiency, stable IRE1 α ^{-/-} MEF lines expressing various IRE1 α constructs were generated using retroviral transduction as described (322). Stable cell lines were selected in hygromycin (VWR) at 125 μ g/ml. Stable cell lines were made and tested independently at least twice.

Analysis of IRE1 α foci formation. It was performed essentially as described (105) with the following modifications. T-REx293 cells were transfected with 0.2-0.5 μ g IRE1 α -3F6HGFP plasmid and 1 μ g OG44 (Invitrogen) for 24 hours followed by 62.5 μ g/ml hygromycin (VWR) selection for 2-3 weeks. Cells were treated with doxycycline (VWR) at 10nM for 24 h to induce the expression of IRE1-3F6HGFP followed by Western blot. Cells were treated with thapsigargin (Tg) at 300 nM for 4 hours to induce ER stress. Fluorescent microscopic picture of the T-REx293 were taken with the Zeiss 710 confocal microscope.

Intracellular localization of WT and mutant IRE1 α with ER marker. T-REx293 cells stably expressing WT or mutant IRE1 α -3F6HGFP were placed on the cover slip and grow until 50% confluent. pDsRed2-ER was transfected 1.5 μ g per well for 6-well for 12 hours followed by 10 nM Dox treatment for 24 hr. Fixed by 4% paraformaldehyde for 20 min, washed by PBS twice and d-water once, cover slip was then put onto glass slide and stained by prolong Gold

antifade reagent with DAPI (Invitrogen) and later concealed for observation under confocal microscope.

Western blot, phosphatase treatment and image quantification.

Preparation of cell lysates, nuclear extract, and Western blot were performed as we previously described (322, 323). Antibodies used in this study included XBP1 and HSP90 (Santa Cruz), IRE1 α (Cell Signaling) and PARP (a gift from Lee Kraus, UT Southwestern Medical Center). Phos-tag gel and phosphatase treatment were performed as described (322, 324, 325). Membranes were routinely strip-reprobed for HSP90 as a position control. Band density was quantitated using the Image Lab software on the ChemiDOC XRS+ system (Bio-Rad) and presented as mean \pm SEM from several independent experiments or as representative data from at least two independent experiments.

RNA extraction and XBP1 splicing assay. RNA extraction was described in the previous paper (322). XBP1 splicing assay was performed following David Ron's protocol at <http://saturn.med.nyu.edu/research/mp/ronlab/protocols.html>.

Structure of yeast and human IRE1 α . The crystal structure of the cytosolic domain of yeast IRE1 α (PDB accession number 3FBV) (104) and human IRE1 α (PDB accession number 3P23) (103) were used for structural analysis of IRE1 α mutants.

Cycloheximide treatment. Stable MEF cell lines with various IRE1 α constructs were treated with 100 μ g/ml cycloheximide (Calbiochem) for 0, 6, 9, 12, 16 and 24 hours. Cells were then snap-frozen in liquid nitrogen and analyzed by Western blot and image quantification.

Statistical analysis. Results are expressed as mean \pm SEM. Comparisons between groups were made by unpaired two-tailed Student *t*-test. $P < 0.05$ was considered as statistically significant. All experiments were repeated independently at least twice.

2.4 RESULTS

The S769F and P830L mutations abolish IRE1 α phosphorylation and activation. In a recent proteomic screening study, seven mutations (N244S, L474R, R635W, S769F, Q780-stop and P830L) were identified to be associated with various cancers (321) (Figure 2.1A). As they present in tumor cells in one copy (321), their significance in cancer is unclear. Nonetheless, the identification of these mutants allowed us to address how the cancer-associated mutation may affect IRE1 α structure and function. The relative positions of these mutations in the kinase domain of the active form of yeast IRE1 α protein (104), based on homology, are shown in Figure 2.1B.

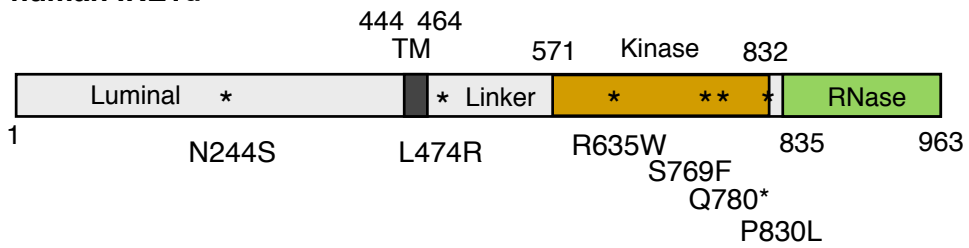
To determine the impact of these mutants on IRE1 α activity, we generated IRE1 α ^{-/-} MEF cells stably expressing the mutant proteins and assessed IRE1 α

phosphorylation in response to ER stress using Phos-tag gels as we recently described (322, 324, 325). Our previous studies have shown that the slower-migrating band on the Phos-tag gel represents the phosphorylated form of IRE1 α and the ratio of phosphorylated- to total- IRE1 α correlates with the amount of ER stress (324, 325). Strikingly, mutation of IRE1 α at either S769F or P830L, but not R635W nor L474R, completely abolished IRE1 α mobility shift upon thapsigargin (Tg) treatment, indicating defective IRE1 α kinase activity (lanes 7-14 of Figure 2.2A and lanes 1-8 of Figure 2.2B). Of note, we were not able to detect N244S and Q780stop mutant proteins due to technical reasons.

A

Tissue	Histology/type	cDNA annotation	AA annotation	Location
Renal	Clear cell carcinoma	A731G	N244S	ER lumen
Lung	Adenocarcinoma	T1421G	L474R	Cytosol (linker)
Stomach	Adenocarcinoma	C1903T	R635W	Cytosol (Kinase)
Brain	Glioblastoma	C2306T	S769F	Cytosol (Kinase)
Brain	Glioblastoma	C2338T	Q780* (STOP)	Cytosol (Kinase)
Ovary	Serous carcinoma	C2489T	P830L	Cytosol (Kinase)

human IRE1 α



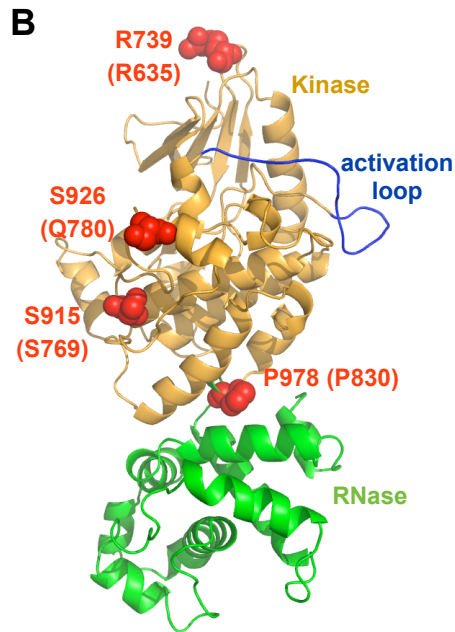


Figure 2.1 The P830L mutation identified in human cancers abolished IRE1 α phosphorylation and activation.

The list of mutations identified in human cancers (upper) and their distribution in human IRE1 α (lower). Mutations that abolish IRE1 α activity are highlighted in red. Luminal, luminal domain; TM, transmembrane; Kinase, kinase domain and RNase, RNase domain of human IRE1 α . (B) Location of four mutations in the kinase domain of yeast IRE1 α protein. Kinase domain in orange, RNase domain in green and activation loop in blue shown. The amino acid position in yeast, based on homology, indicated. Position in human IRE1 α protein indicated in parenthesis.

It is worth pointing out that it is necessary to use phos-tag gels to analyze phosphorylation of IRE1 α mutants, as p-IRE1 α did not separate well in regular gels under the same running conditions (Figure 2.2B-C). The kinase-dead K599A mutant (326) exhibited no IRE1 α phosphorylation while dimerization-defective D123P mutant (317) showed a 70% reduction (lanes 7-8 and 10-11, Figure 2.2C). As additional controls, mutations at S548D and T973D had no effect on IRE1 α phosphorylation upon ER stress (lanes 1-6, Figure 2.2A). Supporting the notion that the slower migrating band is due to phosphorylation, phosphatase treatment abolished the band shift in WT IRE1 α (lane 3, Figure 2.2C); by contrast, there was no change in the electrophoretic mobility of P830L IRE1 α following phosphatase treatment (lanes 4-6, Figure 2.2C). Quantifications of the percent of p-IRE1 α in total IRE1 α from at least two independent experiments are shown in Figure 2.2D and E.

To further examine the effect on RNase activity, we assessed the production of XBP1s protein by Western blot. K599A completely and D123P partially abolished XBP1s production (lanes 5-8, Figure 2.2F lower) while other mutations such as K748A and T973D (lanes 9-12, Figure 2.2F lower) had no effect. XBP1s protein was barely detectable in IRE1 α ^{-/-} MEFs expressing P830L or S769F (lanes 9-12, Figure 2.2F upper), but was less affected in cells expressing L474R or R635W (lanes 5-8, Figure 2.2F upper). This was also confirmed by RT-PCR analysis of *Xbp1* mRNA splicing (lanes 5-6, Figure S2.1). Taken together, among the 4 cancer-associated mutants, our data showed that P830L and S769F

mutations had detrimental effect on IRE1 α kinase and RNase functions whereas L474R and R635W had no major impact.

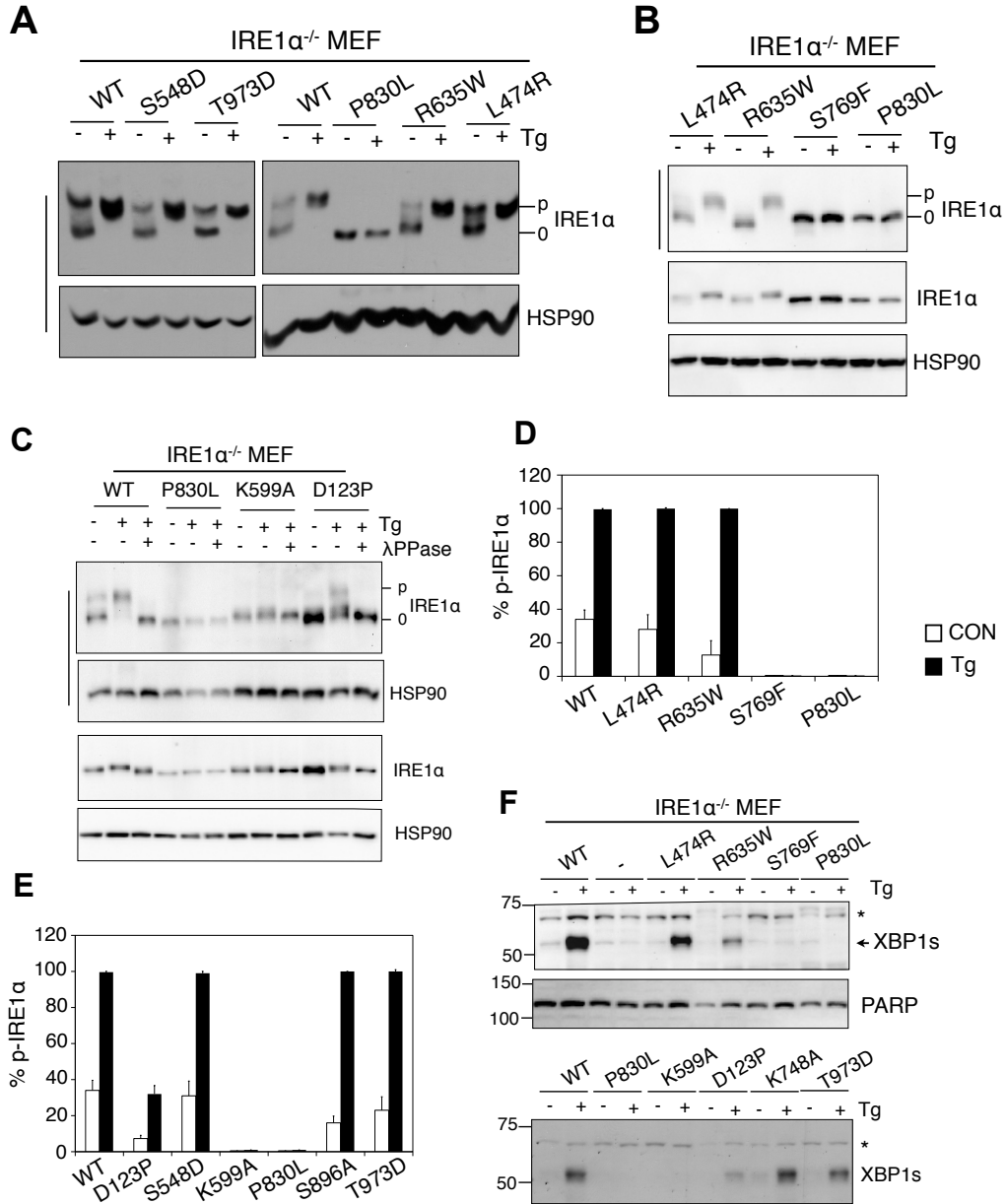


Figure 2.2 The P830L mutation abolished IRE1 α phosphorylation and activation.

(A-C) Western blot analysis of IRE1 α in cell lysates of IRE1 α ^{-/-} MEFs stably expressing wildtype or mutant IRE1 α . Cells were treated with 60nM Tg for 3 hr. In C, lysates were treated with λ PPase. Phos-tag gels indicated with a straight line on the left-hand side. HSP90, a loading control. Note the difference of IRE1 α pattern in Phos-tag gels vs. regular SDS-PAGE gels. (D-E) Quantitation of p-IRE1 α in Phos-tag gels shown in panels A-C. Results expressed as mean \pm SEM. All the *P* values <0.05 using unpaired Student's *t*-test comparing the P830L to other mutants or wildtype (except S769F and K599A). For simplicity, the *P* values are not indicated in the figures. (F) Western blot analysis of XBP1s protein in IRE1 α ^{-/-} MEFs stably expressing wildtype or mutant IRE1 α . Cells were treated with 60 nM Tg for 3 hr. *, a non-specific band. Data is representative of at least two repeats with two independent stable cell lines for each mutant.

P830 is located in a linker region bridging two domains of IRE1 protein.

We then analyzed potential effect of the two loss-of-function mutants on IRE1 α structure (Figure 2.3A). Based on the structure of human IRE1 α (103), S769 is located in the kinase domain (Figure 2.3A). Replacement of the serine with a bulky phenylalanine residue causes sterical collisions with at least two neighboring residues Y765 and C794 (Figure 2.3B), which may affect the stability and activation of the kinase domain. While C794 is not conserved, both S769 and Y765 are highly evolutionally conserved (Figure 2.3D).

Interestingly, P830 is located at the junction between the kinase and RNase domains (Figure 2.3A). Further analysis revealed that P830 may form a highly hydrophobic patch with W833 and Y945 or with L941 on the other side (Figure 2.3C). Based on this, mutation of P830 to L was not favored as the side chain of leucine (L) would contact the W833 and Y945 residues (Figure 2.3C), or L941 in the other direction (not shown), and hence, disrupt this structural element. All four residues involved in this structural motif (P830, W833, L941 and Y945) were highly conserved in both IRE1 α and IRE1 β proteins through evolution from yeast to humans (Figure 2.3E), suggesting that the P830-containing structural linker bridging the two domains of IRE1 may be critical for IRE1 activation in a highly conserved manner. We speculated that understanding the effect of P830L may provide some insight into the importance of the region linking the kinase and RNase domains of IRE1 α , hereafter termed the “linker”. Therefore, in the remainder of this study, we focused on the P830 residue.

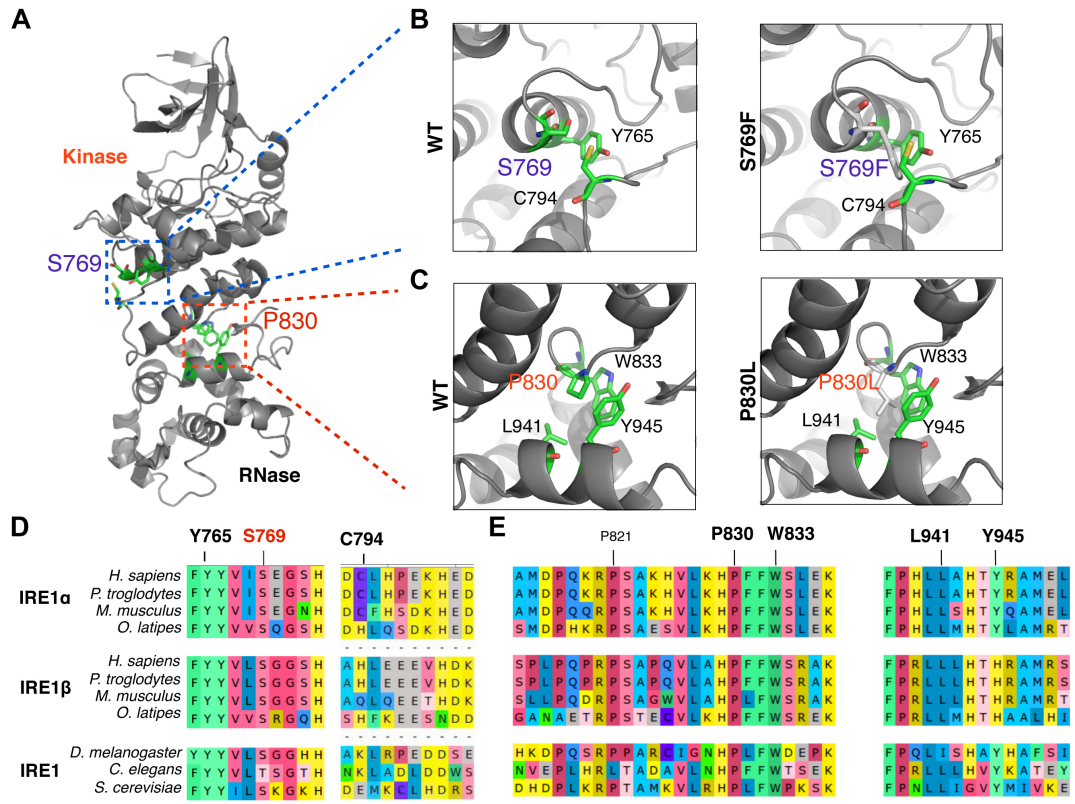


Figure 2.3 P830 is located in the highly conserved hydrophobic patch connecting two domains of human IRE1 proteins.

(A) Ribbon diagram of the cytosolic domain of human IRE1 α protein (PDB accession number 3P23) highlighting two cancer-relevant mutations, the S769F (in purple box) and P830L site (in red box). (B) A close view of the S769 site in wildtype (left) and the structural modeling of the S769F mutant (right). Residues (Y765 and C794) that in close contact with the modeled phenylalanine (F) are shown in sticks. (C) A close view of the P830 site in wildtype (left) and the structural modeling of the P830L mutant (right). Residues (W833, Y945, and L941) that may be in collision with the mutant leucine (L) are shown in sticks. P, proline; W, tryptophan; Y, tyrosine; L, leucine; S, serine and C, cysteine. (D-E) Amino acid sequence alignment showing the conservation of (B) S769, Y765 and C794 residues and (E) P830, W833 and Y945 and L941 residues in IRE1 proteins. Number refers to residue positions in human IRE1 α protein. *H. Sapiens*, human; *P. troglodytes*, chimpanzee; *M. mulatta*, macaque; *E. caballus*, horse; *M. musculus*, mouse; *G. gallus*, chick; *O. latipes*, fish; *D. melanogaster*, fly; *C. elegans*, worm; *S. cerevisiae*, yeast.

The structural element consisting of P830-W833-Y945 is critical for IRE1 α function. We next attempted to delineate the effect of this hydrophobic patch consisting of P830, W833 and Y945 or L941 on IRE1 α activation by mutagenesis. Interestingly, W833A caused a similar dramatic defect on IRE1 α phosphorylation as P830L in response to ER stress (lanes 7-8 Figure 2.4A), and to a lesser extent for Y945A (lanes 11-12 Figure 2.4A), but not L941A (lanes 9-10, Figure 2.4A). To exclude the possibility that the P830L effect was caused by random mutations generated at other sites during mutagenesis, we mutated P830L back to P (P830L \rightarrow P). Indeed, the P830L \rightarrow P mutation fully restored the WT phenotype (lanes 13-14, Figure 2.4B). Pointing to the importance of the P830 position, mutation at the nearby P821L, also a highly conserved residue (Figure 2.3E), had only a minor effect (~20%) on IRE1 α phosphorylation (lanes 5-6, Figure 2.4B). Moreover, mutation of P830 to alanine (P830A) caused a much milder defect in IRE1 α phosphorylation relative to the P830L mutant, with ~70% of IRE1 α being phosphorylated under ER stress (lanes 1-2, Figure 2.4B-C).

Next, we asked whether mutating Y945 or W833 to a smaller residue alanine could reverse the detrimental effect of P830L by accommodating P830L. However, the double mutants of P830L/Y945A or P830L/W833A exhibited the same phenotype as P830L with no IRE1 α phosphorylation in response to ER stress (lanes 7-8 and 11-12, Figure 2.4B). Quantification of IRE1 α activation in all mutants was shown in Figure 2.4C. Thus, these data suggest that the P830-W833-Y945 residues, not P830-L941, form a structural linker bridging the two cytosolic effector domains of IRE1 α .

Next we checked the RNase activity of these mutants by assessing the protein levels of XBP1s using Western blot. Indeed, XBP1s protein levels seemed to correlate with the extent of IRE1 α phosphorylation: The P830L, W833A or Y945A mutations led to no XBP1s production in response to ER stress, and to a much lesser extent for L941A and P830A (Figure 2.4D). As a positive control, RNase-dead K907A mutant (327) with normal IRE1 α phosphorylation (lanes 5-6, Figure 2.4A) was defective in XBP1s production in response to ER stress (Figure 2.4D). Taken together, our data showed that three residues P830, W833 and Y945 likely form a structural linker that is critical for IRE1 α function.

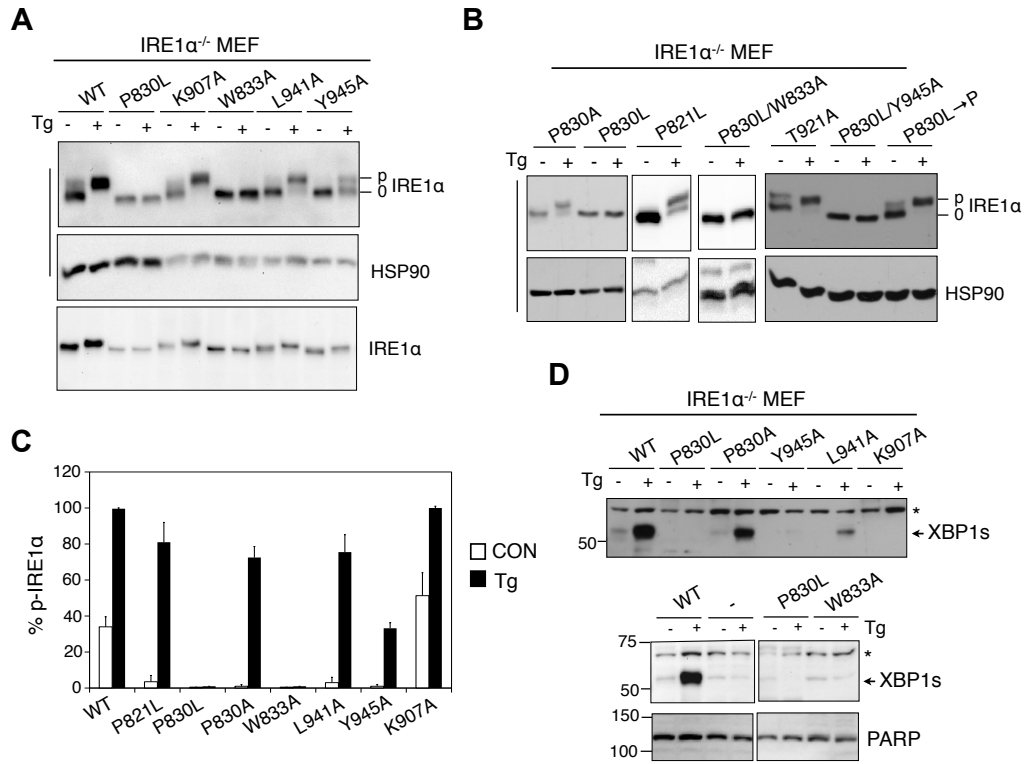


Figure 2.4 The structural element consisting of P830-W833-Y945 is critical for IRE1 α function.

(A-B) Western blot analysis of IRE1 α in cell lysates of IRE1 α ^{-/-} MEFs stably expressing wildtype or mutant IRE1 α . Cells were treated with 60nM Tg for 3 hr. (C) Quantitation of p-IRE1 α in Phos-tag gels shown in panels A-B. Results expressed as mean \pm SEM, an average of at least two independent experiments. All the *P* values <0.05 using unpaired Student's *t*-test comparing the P830L to other mutants or wildtype (except W833A). For simplicity, the *P* values are not indicated in the figures. (D) Western blot of XBP1s protein in IRE1 α ^{-/-} MEFs stably expressing wildtype or mutant IRE1 α . Cells were treated with 60nM Tg for 3 hr. Phos-tag gels indicated with a straight line on the left-hand side of the gel. *, a non-specific band. HSP90, a loading control. Data is representative of at least two repeats for each mutant.

The P830-containing structural linker of IRE1 α is important for its stability. To further shed light on the defects caused by P830L, we examined the stability of IRE1 α mutants under basal conditions. IRE1 α -/- MEFs stably expressing various mutant proteins were treated with cycloheximide, an inhibitor of protein synthesis, for the indicated time periods followed by Western blot analysis of IRE1 α protein levels. While K599A had a similar half-life as wild type protein ($t_{1/2}$ = 12 h, Figure 2.5A-B), the P830L, W833A and Y945A mutations dramatically reduced the half-life of IRE1 α to 6 hours or less (Figure 2.5D-F), pointing to the specificity of these three residues, but not L941A on IRE1 α stability (Figure 2.5C). Taken together, these results suggested that P830L, W833A and Y945A mutations at the linker region had a significant impact on IRE1 α protein stability, an effect distinct from the kinase-dead K599A mutation.

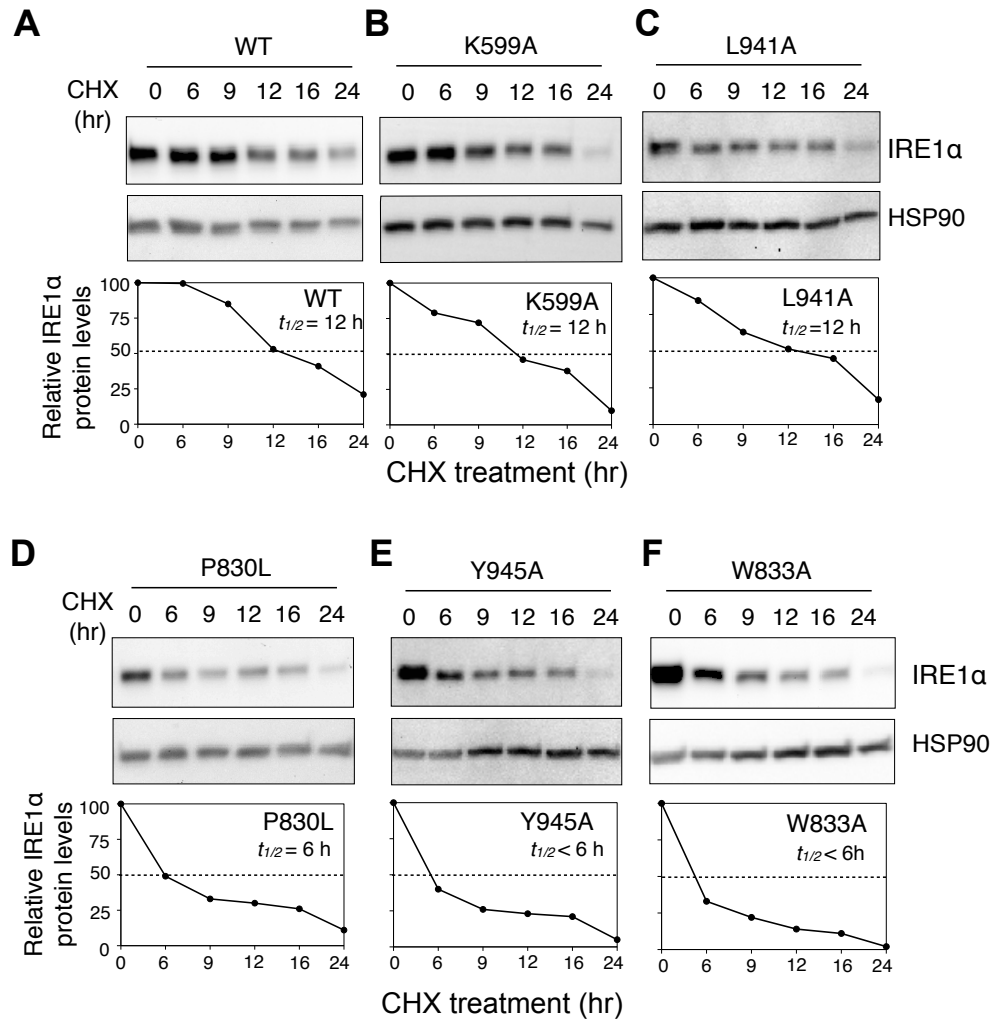


Figure 2.5 The P830-containing structural linker of IRE1 α is important for its stability.

Western blot analysis of IRE1 α (upper) and quantitation of IRE1 α half-life (lower) for IRE1 α ^{-/-} MEFs stably expressing wildtype or mutant IRE1 α . Cells were treated with cycloheximide (CHX) for the indicated time. IRE1 α protein levels at various time points were normalized to the 0 time point of its own protein. Protein half-life refers to the time at which protein levels reach to 50% of that at 0 time point. Data is representative of at least two repeats for each mutant. HSP90, loading control.

The P830-containing structural linker of IRE1 α is important for its oligomerization. As mammalian IRE1 α oligomerizes upon ER stress (105), we next tested the effect of P830L on its foci formation. To this end, we used an inducible system to detect IRE1 α foci formation in T-REx293 cells (105) (Figure 2.6A). Using co-expression of ER-localized dsRed encoded in the pDsRed2-ER plasmid, we first confirmed that exogenous wild type and mutant IRE1 α proteins were predominantly localized to the ER (Figure S2.2). In line with a previous study (105), foci formation peaked in cells expressing WT-IRE1 α protein upon 4 h treatment of 300 nM TG (Figure 2.6B and not shown). Interestingly, unlike wildtype IRE1 α protein, P830L IRE1 α protein failed to form foci upon ER stress (Figure 2.6C), so did the dimerization-defective D123P IRE1 α (Figure 2.6D). Thus, these results suggested that the P830-containing structural linker of IRE1 α affects its oligomerization in response to ER stress.

To test whether mutant IRE1 protein would have a dominant negative effect on endogenous IRE1 α protein, we transfected mutant proteins into HEK293T cells and tested for ER stress response. Despite being 10-fold more than endogenous protein, exogenous mutant proteins failed to significantly reduce IRE1 α activity as assessed by XBP1s protein levels (Figure 2.6E). This result suggested that the P830L mutant does not act as dominant negative mutation, rather might just act a loss-of-function mutation.

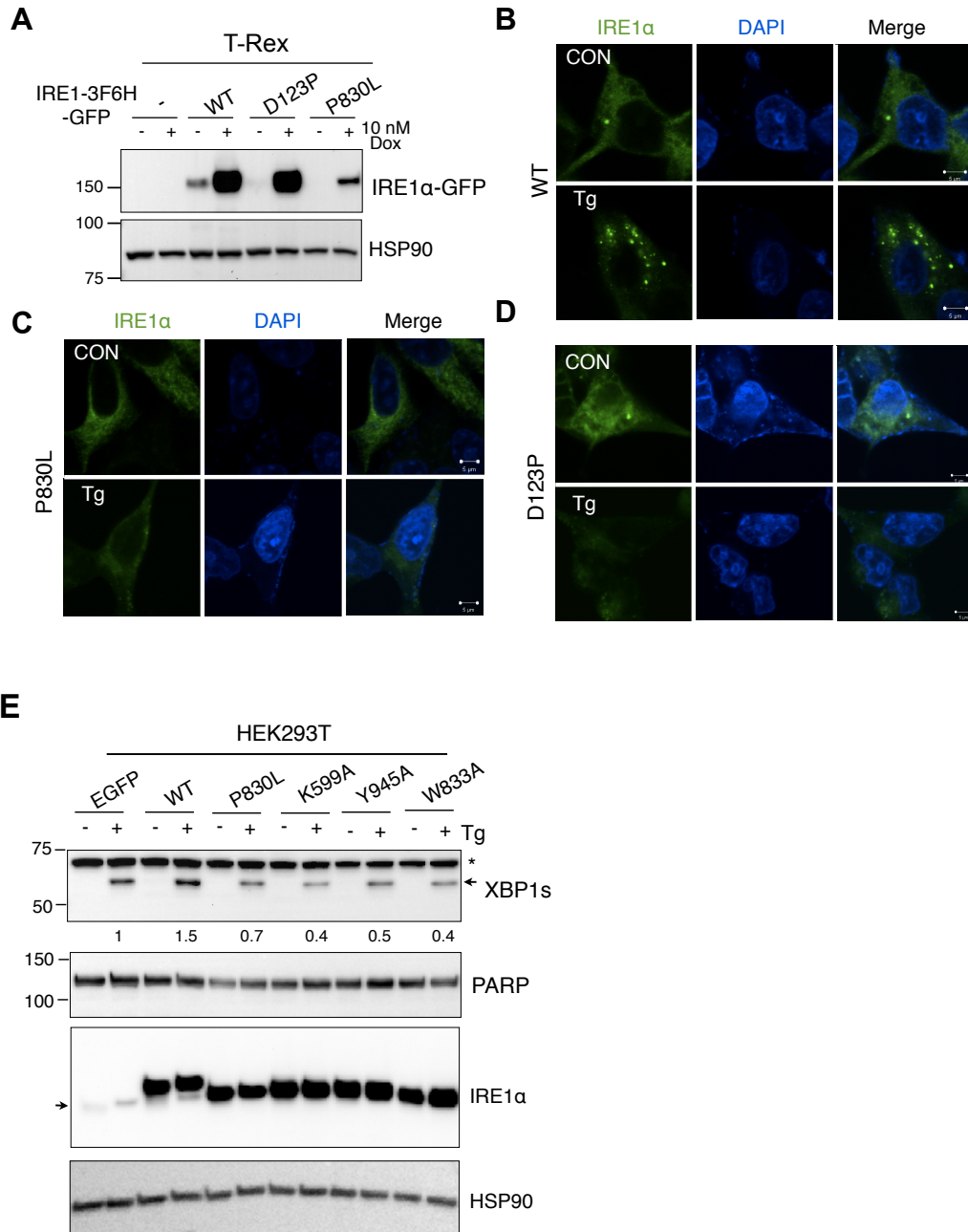


Figure 2.6 The P830-containing structural linker of IRE1 α is critical for its oligomerization in response to ER stress.

(A) Western blot of IRE1 α -GFP proteins in the T-REx293 system. Parental T-REx293 cells (-) or T-REx293 cells stably expressing different IRE1 α proteins, either WT or D123P or P830L, were treated with 10 nM Dox for 24 hr followed by Western blot. (B-D) Confocal microscopic images of IRE1 α foci in wildtype (B), P830L (C) and D123P (D)-expressing cells treated as in A with or without 300 nM Tg for 4 hr. Images are representatives of over 100 cells from 3 independent experiments. Scale bar, 5 μ m. (E) Dominant negative effect of P830L. Western blot analysis of XBP1s and IRE1 α following overnight transfection of HEK293T cells with near 100% transfection efficiency. Cells were treated with 300 nM Tg for 4 hr prior to harvest. PARP and HSP90, loading controls for XBP1s and IRE1 α , respectively. Representative of two independent experiments. Numbers shown below the XBP1s blot refer the relative abundance of XBP1s protein (after normalized with PARP). Arrow next to the IRE1 α blot indicates the endogenous IRE1 α band. The ratio of endogenous to exogenous IRE1 α protein levels is 1:10.

SUPPLEMENTARY FIGURES

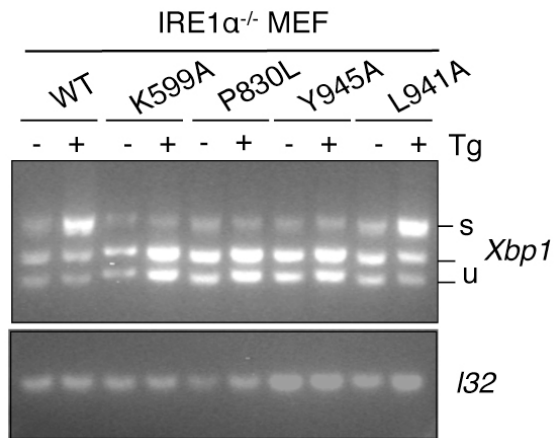


Figure S2.1 Xbp1 mRNA splicing.

RT-PCR analysis of Xbp1 mRNA splicing in IRE1 $\alpha^{-/-}$ MEF stably expressing various IRE1 α mutants. Cells were treated with 60 nM Tg for 3 hr. L32, a loading control. Xbp1u and s are shown. Representative of two experiments.

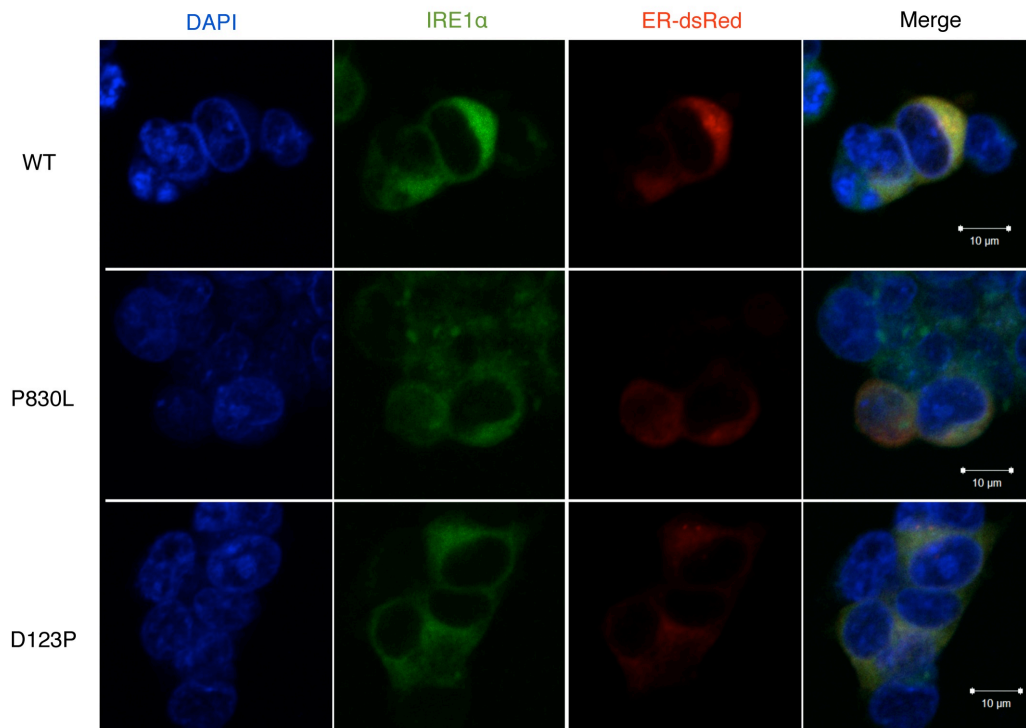


Figure S2.2 Confocal analysis of intracellular localization of IRE1 α WT and mutants.

Cells expressing wildtype (top), P830L (middle) and D123P (bottom) IRE1 α -3F6HGFP were co-transfected with ER-dsRed plasmid to mark the ER. No observable difference was found for WT or mutant IRE1 α location in the ER. Images are representatives of over 100 cells from 2 independent experiments. Scale bar, 10 μ m.

2.5 DISCUSSION

This is the first study addressing how cancer-associated IRE1 α mutations affect its structure and function. Here we have identified an important structural element that is critical for the function of IRE1 α . This structural linker consisted of P830, W833 and Y945 bridges the kinase and RNase domains of IRE1 α protein. Disturbance of this linker structure abolishes the activities of both the kinase and RNase domains of IRE1 α and prevents foci formation in response to ER stress. This mechanism is likely to be evolutionarily conserved as these three residues are highly conserved from yeast to humans. Although it remains unclear how P830L affect tumor development *in vivo* (This mutation is probably not tumorigenesis because it led to a defect in XBP1s pro-survival signaling. However, it is not the focus of this study), this study demonstrates that the P830L mutation is deleterious for IRE1 α stability and function.

How the folding and activation of two cytosolic domains of IRE1 α are coupled *in vivo* remains unclear. Currently, one prevailing model is that the activation of the RNase domain of IRE1 α depends on the trans-autophosphorylation of its adjacent kinase domain following dimerization or oligomerization (131, 318). Efforts to further understand this phosphorylation-mediated regulatory event is hampered by the fact that specific phosphorylated residues on mammalian IRE1 α protein remain unknown. In yeast, an estimated 17 Ser/Thr residues located at both the activation loop and the adjacent α EF- α F loop are believed to be phosphorylated under ER stress (104). While we predict that

trans-autophosphorylation of mammalian IRE1 α protein is not likely to be as extensive as in yeast, as indicated in the Phos-tag-based Western blots (322, 324, 325), the identities and the importance of these possible phosphorylation sites on the activation of mammalian IRE1 α protein remains an interesting question.

Our data suggest that the “P830-W833-Y945” residues in the IRE1 α hydrophobic core are important for its folding and activation. This linker region affects not only the activities of the kinase and RNase domains, but also its half-life and the ER-stress-induced oligomerization. The effect of P830-related mutations on IRE1 α function is indeed more severe than the kinase-dead K599A and dimerization-defective D123P mutants, suggesting that P830-related mutations may interfere with the folding process of IRE1 α protein. How we can translate this finding to therapeutic purposes require further studies.

2.6 ACKNOWLEDGEMENTS

We thank the Qi laboratory for helpful discussions; Carol J Bayles (Cornell University) for the help with confocal microscopy. Drs. D. Ron, P. Walter, C. Hetz, F. Hu and H. Li for reagents. This study is supported by the Cornell startup packages (to L. Q., Z. G. and Y. M.), American Diabetes Association (ADA) and NIH NIDDK RO1DK082582 (to L. Q.).

2.7 APPENDIX

2.7.1 The P830-containing structural linker of IRE1 α is important for cell growth.

Introduction

IRE1 α and its down stream XBP1s were previously reported to govern cell fate in a cell type specific and condition specific way (74). It was demonstrated that XBP1 expression was induced in cancers including multiple myeloma, acute myeloid leukemia, and breast cancer (273, 328-332). The role of XBP1 as a survival factor in cancer cell types makes it a potential drug target. The initial identification of P830L in ovary serous carcinoma (321) raised the crucial scientific question: What is the biological consequence of this mutation in cancer formation? Soft Agar Assay for colony formation is an anchorage independent growth assay, normally considered as the most stringent assay for detecting malignancy. Therefore, WT and P830L IRE1 α mutant, as well as P830A, K599A, L941A and L945A IRE1 α mutant MEFs were used to perform soft agar assay.

Experimental Procedures

Soft Agar Assay

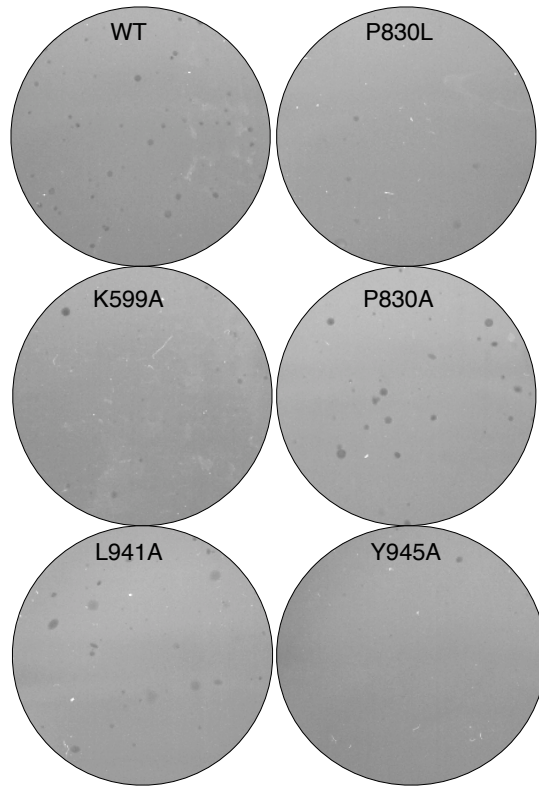
0.5% base agar (Sigma Agarose, Type VII (A4018-5G)) with 1X Dulbecco's Modified Eagle Medium (DMEM) and 10% fetal bovine serum (FBS) were prepared and 1ml was used in a well of a 6-well plate. The plates were stored at room temperature for more than 30 minutes to solidify. Top agar 0.3% with 1X

DMEM and 10% FBS were then prepared and preheated to 37 °C and mixed with 5000 cells to cover the top of the base agar. The cells were incubated under normal conditions and 1.5ml of regular media were added at the top biweekly. The cells were incubated to grow for 3 weeks. Then the number and size of the colonies were observed by light microscope (ZEISS SN 3832000516). Whole plate pictures were scanned by a printer.

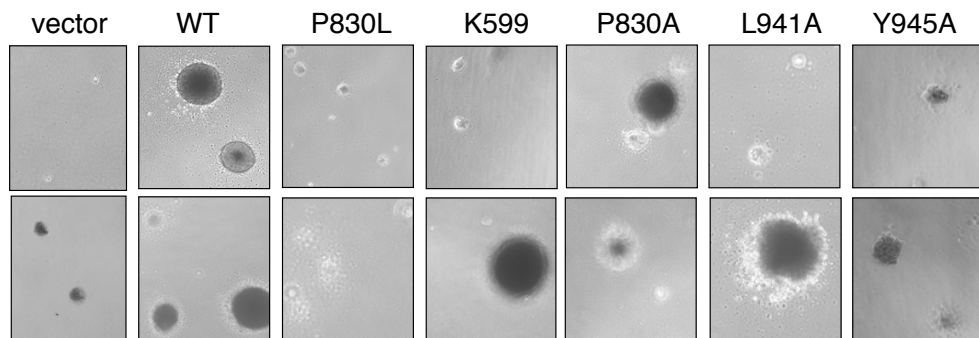
Results

Compared with IRE1 α $-/-$ MEFs transfected with wild type IRE1 α , P830L IRE1 α mutant MEF cells showed a much slower rate of growth. The P830 mutant group showed much fewer and smaller colonies; whereas a less severe growth retardation was observed in K599A, P830A, L931A and Y945A IRE1 α mutant MEFs (Figure. Appendix 1.1). This result was consistent with the XBP1s mRNA splicing and protein level and indicated that XBP1 plays a pro-survival role in MEFs and that the P830 containing linker region is critical for the effective cleavage event of XBP1.

A



B



c

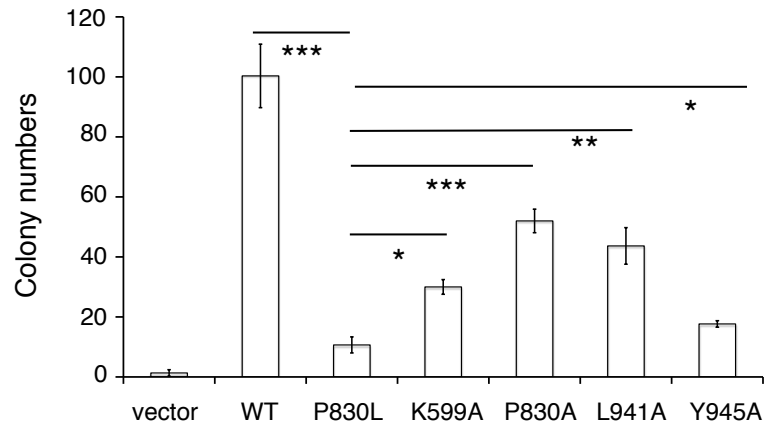


Figure. Appendix.1.1 P830-L941-Y945 linker mutation causes cell growth retardation.

IRE1 α $-/-$ MEFs expressing empty vector, WT, P830L, P830A, K599A, L941A, and L945A mutant IRE1 α were cultured to perform soft agar assay. (A) Pictures showed the formation of colonies in the wells of 6-well plates after three weeks. (B) Pictures showed the representative morphology and relative size of colonies under 10X5 ZEISS microscopy magnification. (C) The chart showed the quantification of average colony numbers in each well (n=3).

Discussions

It remains puzzling why IRE1 α mutants in cancer were proved to be anti-malignancy. One possible explanation is that these mutations were not a cause of malignant transformation. Instead, the lack of a DNA error correction system (e.g. P53) led to a random mutation which coincidentally depleted the IRE1 α normal function. Another potential explanation was the presence of a negative feedback due to increased pro-survival signaling in the cancer cells. However, the transcriptional regulation of IRE1 α appeared stable; therefore, this possibility was less likely. Nevertheless, the biological effect of P830L IRE1 α mutant in MEFs colony formation assay further proved the role of P830-containing linker in activating IRE1 α -XBP1 signaling. Currently the idea of developing a drug based on this residue seems promising.

In the past, IRE1 α has been shown to be a cell fate determinant. The downstream of IRE1 α , XBP1s, could therefore directly lead to tumorigenesis. Relevant evidence indicates that increased XBP1s levels in B cells could drive multiple myeloma pathogenesis (269). Evidence also indicates that XBP1s could promote cell proliferation by regulating cyclin A1 expression in prostate cancer cell lines (267). However, IRE1 α can also promote apoptosis by mediating JNK pathway (274) or by mediating prolonged RIDD (333). Activation of JNK can induce caspase-12 signaling pathway and apoptosis (274). Although the mechanisms remain unclear, prolonged RIDD activation also increases apoptosis (319). Therefore, it is important for us to understand that the biological effect of IRE1 α P830L mutant is depleted cell growth signaling. This further proves that

the linker region containing P830 can serve as a drug target to suppress cell growth in cancers.

Acknowledgement

We thank Dr. Nasun Hah from Dr. Lee Kraus's lab for assistance in the soft agar assay experiment.

2.7.2 Analysis of IRE1 α phosphorylation sites on the activation loop

Introduction

Controversy still surrounds the question: Is autophosphorylation of IRE1 α required for its activation? On one side, abundant evidence shows that in yeast the activation of the RNase domain of IRE1 α depends on the trans-autophosphorylation of its adjacent kinase domain. Following a signal, trans-autophosphorylation of the kinase domain makes the unfettered binding of nucleotide possible, which in turn, promotes dimerization or oligomerization to compose the ribonuclease activity (131, 318). On the other side, two papers suggest a dispensable role of phosphorylation of IRE1 α in activation of its RNase domain (319, 320). They show that a L745G mutant IRE1 α , which has a defect in kinase activity and phosphorylation, can constitutively activate all downstream functions in the presence of an ATP-competitive inhibitor 1NM-PP1 through conformational change in the kinase domain (319, 320).

The effort to further understand this phosphorylation-mediated regulatory event on mammalian IRE1 α protein is hampered by the fact that specific phosphorylated residues remain unknown. In yeast, an estimated 17 Ser/Thr residues located at both the activation loop and at the adjacent α EF- α F loop are believed to be phosphorylated under ER stress (104). While we predict that trans-autophosphorylation of mammalian IRE1 α protein is not likely to be as extensive as in yeast, as indicated in the Phos-tag-based Western blots (322, 324, 325), the

identities and the importance of these possible phosphorylation sites on the activation of mammalian IRE1 α protein still pose interesting questions.

From all the phosphorylation sites in yeast, we selected evolutionarily more conserved Serine (S) sites on the human IRE1 α activation loop as candidates, S724, S726 and S729. We mutated them either into smaller nonpolar amino acid Alanine (A) as a loss of phosphorylation mutation, or mutated them to the acidic polar residues Aspartic acid (D) or Glutamic acid (E) to determine if the mutations would enhance phosphorylation. The phosphorylation of IRE1 α was then evaluated in both the basal and ER stress conditions by phos-tag gels. Downstream effectors XBP1 splicing and XBP1s protein levels were evaluated to understand their relevant RNase activity.

Experimental Procedures

As described in chapter 2.3, alignment structure pictures were produced by PyMOL.

Results

S724 and S726 are two phosphorylation residues of human IRE1 α .

Stable cell lines were produced by using IRE1 α -/- MEFs cells expressing mutant human IRE1 α plasmids following mutagenesis. By aligning seven species' IRE1 α activation loops, two Serine (S) residues were found to be the most conserved -- S724 and S726 (Figure. Appendix 2.1 A upper). Structural pictures also showed that human IRE1 α S724 matched S841 in yeast, while S726 has a

different spacial position than S726 in yeast (Figure. Appendix 2.1 A lower). This indicates the phosphorylation status of mammalian IRE1 α might be differently regulated than that in yeast. Very interestingly, we found that S724A and S726A mutant cell lines both showed an almost complete abolishment of IRE1 α phosphorylation (Figure. Appendix 2.1 B) in the ER stress condition. The downstream effect of IRE1 α activation such as XBP1 splicing and chaperone induction (Figure. Appendix 2.1 C), as well as the XBP1s protein level (Figure. Appendix 2.1 B) were consistent with the phosphorylation level. Therefore, we concluded that for human IRE1 α , phosphorylation is important for its kinase and RNase domain activation. S724 and S726 are two phosphorylation sites of human hIRE1 α .

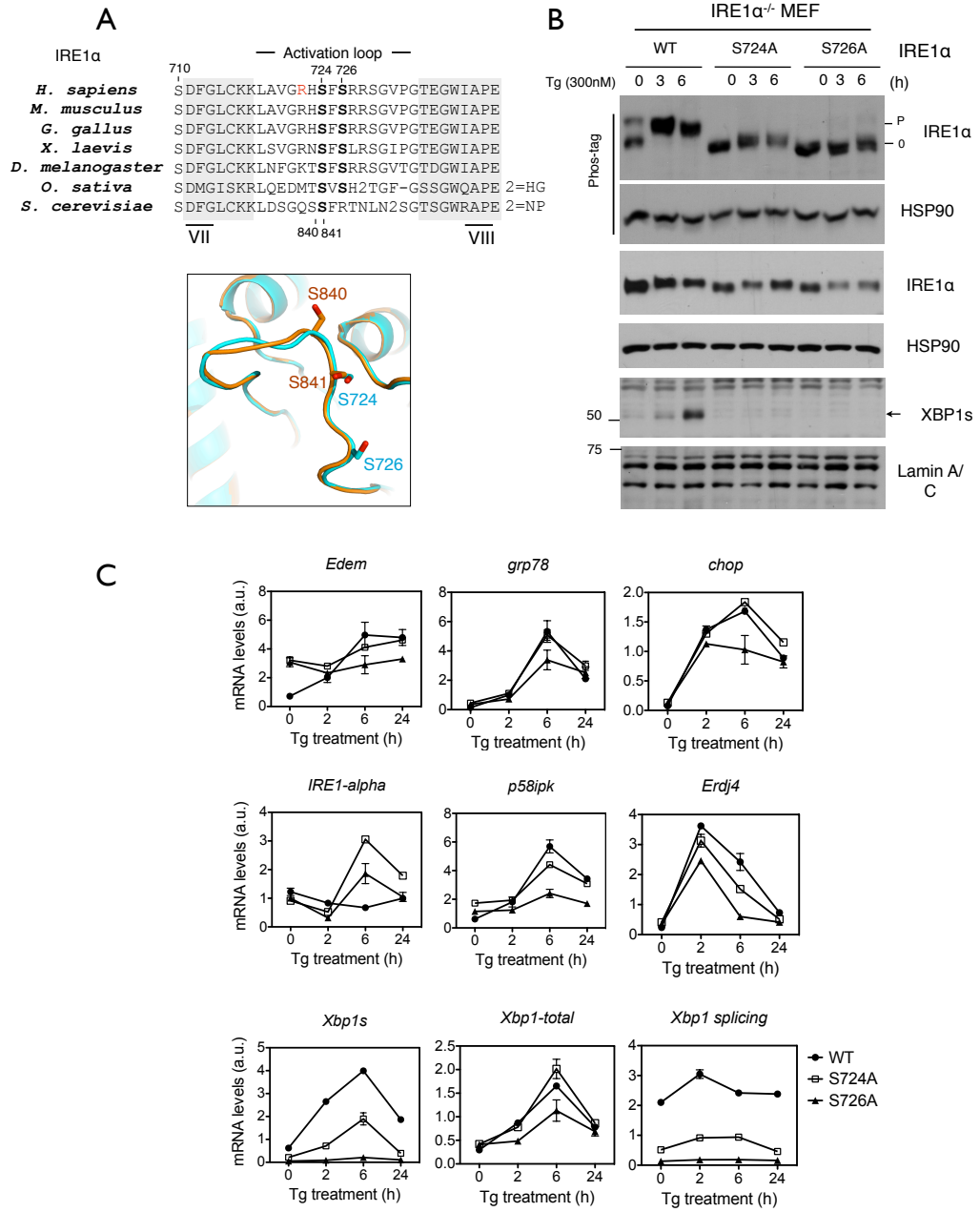


Figure. Appendix.2.1 S724 and S726 are two phosphorylation residues of human IRE1 α .

(A) Alignment of IRE1 α activation loop. The lower part shows the alignment of the activation loop between yeast (orange) and human (blue) IRE1 α in a 3D structure. (B) IRE1 α $-/-$ MEFs expressing WT, S724A and S726A IRE1 α plasmids treated with or without Tg in a time course. Hsp90 is the loading control for cytosolic fraction and Lamin A/C is the loading control for nuclear fraction XBP1s. Phostag gels show the phosphorylated and non-phosphorylated IRE1 α . (C) qPCR data showing the induction of UPR genes in three cell line groups in a Tg treatment time course.

When mutating the S724 and S726 to the acidic polar residues Aspartic acid (D) or Glutamic acid (E), S726D and S726E showed similar 100% phosphorylation under ER stress conditions, while at basal level, they do not exceed the phosphorylation level of WT (Figure. Appendix 2.2 B, data not shown). S726D IRE1 α also can induce full activation of XBP1s as WT (Figure. Appendix 2.2 A). S724D was found to be similar to S726D in its downstream effect shown as full XBP1s expression (Figure. Appendix 2.2 A). However, S724D appeared not to be fully phosphorylated upon ER stress. The phosphorylation condition of S724D was difficult to interpret because the phosphorylation band seemed to migrate more slowly than the non-phosphorylated band but faster than the fully phosphorylated bands of WT and S726D. It is not yet known whether there is a half-phosphorylated condition. (Figure. Appendix 2.2 B). This means that although S724 is a very important residue for IRE1 α phosphorylation and its RNase function, under certain conditions such as S724D mutation, phosphorylation can still be bypassed to permit XBP1s full expression. Non-conserved nearby residue S710 showed no defect in phosphorylation under ER stress. The less conserved residue S729 showed a half reduction in phosphorylation and XBP1s production compared to WT (Figure. Appendix 2.2 A,B). Kinase dead IRE1 α mutant K599A (326) and luminal domain mutant D123P (182) were used as controls (Figure. Appendix 2.2 C). PERK phosphorylation conditions were not affected by IRE1 α mutants (Figure. Appendix 2.2 B).

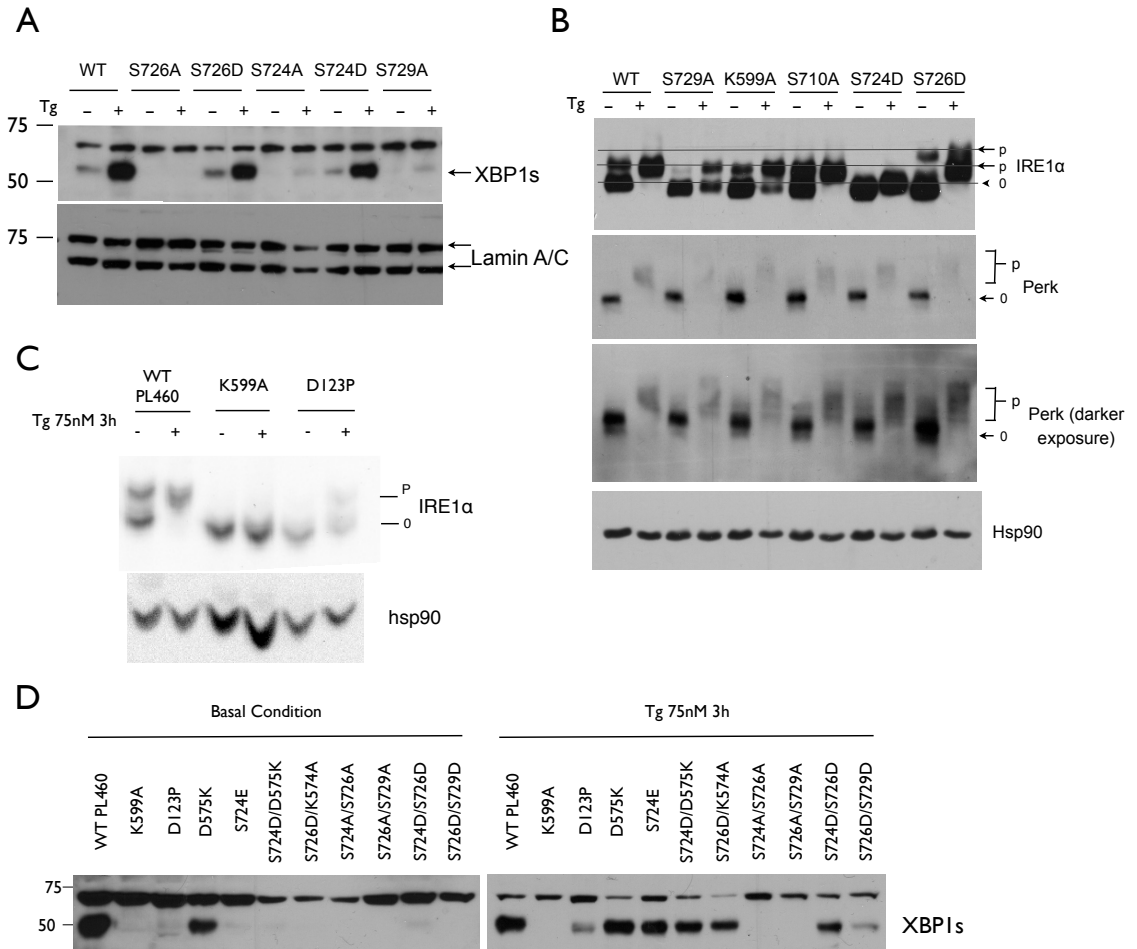


Figure. Appendix.2.2 S726D IRE1 α mutant shows full phosphorylation ability

IRE1 α $-/-$ MEFs expressing mutant IRE1 α plasmids, as indicated in the above figure, were treated with or without Tg. (A) (D) XBP1s protein level of IRE1 α mutants were shown in western blots. (B) (C) IRE1 α phosphorylation and PERK phosphorylation under the condition of various IRE1 α mutants were shown in western blots. Hsp90 is the loading control for cytosolic fraction (IRE1 α and PERK). Lamin A/C is the loading control for nuclear fraction.

Based on the previous discovery that S724, S726, and S729 to a lesser extent, are responsible for mammalian IRE1 α phosphorylation, we next wanted to know what are the possible residues interacting with these serine residues. Thus, we aligned human and yeast IRE1 α in a 3-D structure using the yeast oligomerization model (104). It was found that D575 in humans and K678 in yeast could be related to S724 and S841 in human and yeast IRE1 α , respectively (Figure. Appendix 2.3). K574 might be related to S726 (Figure. Appendix 2.3).

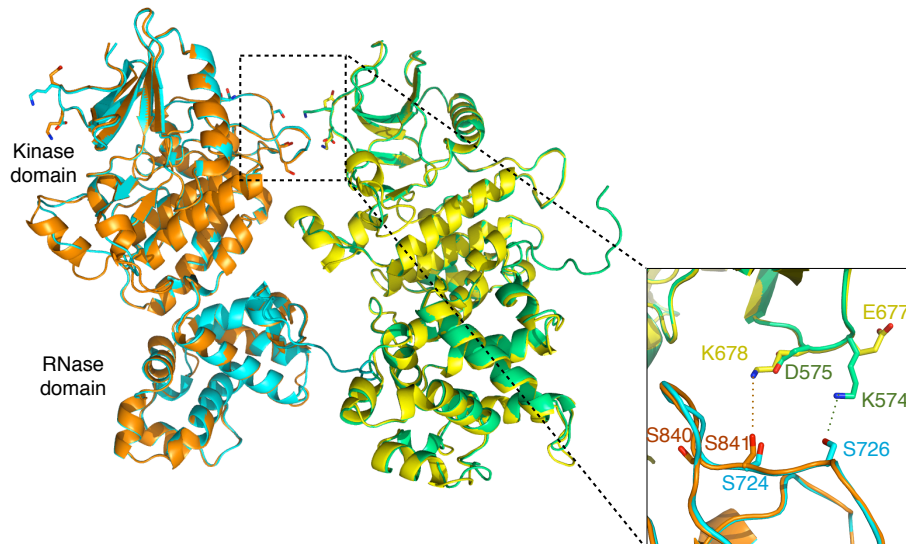


Figure. Appendix.2.3 Alignment of yeast and human IRE1 α two monomers in an oligomerization model.

Alignment of yeast (orange and yellow) and human (blue and green) IRE1 α in a 3D structure shows two monomers of IRE1 α in the oligomerization model. In the corner, magnified activation loops are shown and possible interaction between residues is indicated.

Based on the phenotype of a full phosphorylation ability of S726D, we made a double mutant S726D/K574A. Indeed, this double mutant showed abolition of phosphorylation under ER stress condition but K574 single mutant cells were not affected. This proved that K574 residue contributes to S726 phosphorylation; therefore possible residue interactions are likely to exist (Figure. Appendix 2.4 A, B). Similarly D575K mutant cell lines showed normal phosphorylation in ER stress. However, trying to rescue the phosphorylation defect in S724D mutant by changing the D575 to a positively charged residue lysine (K) failed to show any improvement (Figure. Appendix 2.4 C, D). Therefore, there is no conclusive association between D575 and S724. Further study is required to assess the exact conformational change based on S724D mutation. It is also puzzling that, even with a defect in IRE1 α phosphorylation, double mutant S726D/K574A and S724D/D575K both lead to only a slight reduction in XBP1s expression (Figure. Appendix 2.2 D). S724D/S726D and S726D/S729D have reduced XBP1s; S724A/S726A and S726A/S729A have no XBP1s expression (Figure. Appendix 2.2 D).

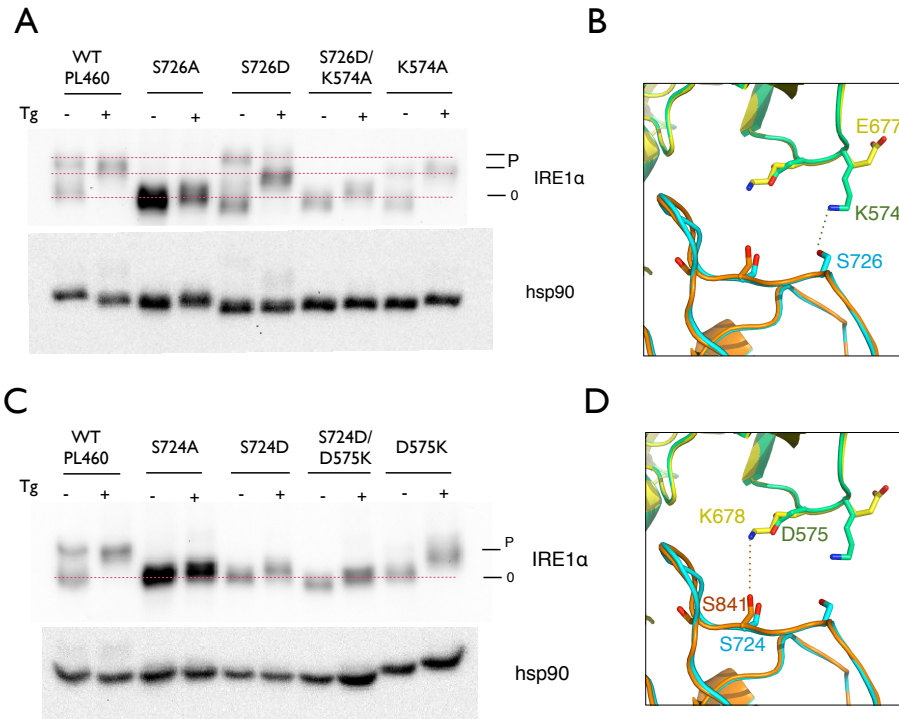


Figure. Appendix.2.4 Possible interaction between S726 and K574 in hIRE1 α

(A) (C) IRE1 α $-/-$ MEFs expressing mutant IRE1 α plasmids as indicated in the figure were treated with or without Tg. Hsp90 is the loading control for cytosolic fraction. Phos-tag gels show the phosphorylated and non-phosphorylated IRE1 α . (B) (D) 3D structural alignment shows a special relationship between the residues indicated.

Discussion

This appendix shows the importance of phosphorylation in human IRE1 α activation. It has been proved that by mutating S724 or S726 to alanine causes a defect in IRE1 α downstream functions including XBP1 splicing. However, it still cannot be concluded that phosphorylation of IRE1 α is absolutely required for its RNase function. Because situations were observed, such as S724D and S726D/K574A mutants, which does not present a full phosphorylation phenotype, still possessing almost normal XBP1s protein levels. Yet, in most situations, IRE1 α phosphorylation condition still correlates with the extent of XBP1 splicing. Therefore, the phos-tag gel measuring the percentage of IRE1 α is still a valuable tool to understand the activation status of human IRE1 α , especially under physiological conditions where the chances of having special kinds of genetic mutations and chemical compound activation are very rare.

Previously there were controversial opinions about whether IRE1 α activation is in the form of dimer or oligomers. One crystal structure of the kinase/RNase domain of Ire1 reveals a symmetric dimer with a back-to-back arrangement (318). This model does not support autophosphorylation on the activation loop, because it positions the phosphorylation sites more than 40Å away (104). This study, showing the importance of phosphorylation on the activation loop, supports the oligomerization model. It was proposed that a rod-shaped assembly, with no known precedence among kinases, and kinase assembly trans-autophosphorylates subsequently order the RNase domain to create an interaction surface for mRNA

binding (104). It is possible that human IRE1 α can be activated in the form of oligomers (334).

Acknowledgement

hIRE1 α structure pictures were provided by Dr. Yuxin Mao. Kaixiong Ye from Dr. Zhenglong Gu's lab helped with the alignment of different species of IRE1 α . My heartfelt appreciation goes to Dr. Haibo Sha and Dr. Yin He for their assistance in mutagenesis. And thank you Cindy Wang for the maxi-prep.

2.7.3 Summary of IRE1 α mutants and corresponding XBP1s levels

In order to identify the important residues responsible for IRE1 α autophosphorylation upon activation and to identify the importance of phosphorylation for the RNase domain function, all possible residues in the kinase domain, activation loop and RNase domain were mutated. The following tables summarize the results of multiple western blot repeats of variable IRE1 α mutant MEFs. P-IRE1 α % is measured on phos-tag gels in an ER stress condition (Tg 75nM for 3 hours). Raw data from each single repeat is shown in the table. XBP1 mRNA splicing levels and protein levels are repeated once to twice each. Detailed methods are described in chapter 2.3. Representative figures of p-IRE1 α , XBP1 mRNA levels and XBP1 protein levels are shown in Appendix 2.7.2.

Table 1 Summary of IRE1 α phosphorylation, XBP1 mRNA splicing and protein levels with mutation(s) identified in cancers in the ER stress condition.

Lab Number	Protein Annotation	p-IRE1 α %	p-IRE1 α %	p-IRE1 α %	Average p-IRE1 α %	Average p-IRE1 α Scale	XBP1 splicing	XBP1s protein
PL523	D123P	37	32	5	24.7	+	+	++
PL659	P830L	1.6	0.7	0	0.8	-	-	-
PL627	L474R	99.4	99.5		99.5	++++		
PL658	Q780Stop					no expression		
PL625	S769F					failed		
PL660	N244S					failed		

*WT “++++” is considered as 100%. Every other result is compared with WT. “-” means 0%; “+” means 1-25%; “++” means 25-50%; “+++” means 50-75%; “++++” means 75-100%. This applies to all the tables below.

Table 2 Summary of IRE1 α phosphorylation, XBP1 mRNA splicing and protein levels with mutation(s) in the IRE1 α kinase domain in the ER stress condition.

Lab Number	Protein Annotation	p-IRE1 α %	p-IRE1 α %	p-IRE1 α %	Average p-IRE1 α %	Average p-IRE1 α	XBP1 splicing	XBP1s protein
PL460	WT	96.4	95	96	95.8	++++	++++	++++
PL515	S710A	++++				++++		
PL524	K574A	97.5			97.5	++++		
PL525	K748A	100	98	89	95.7	++++	++++	
PL542	K599A	3.5	2	0	1.8	+	-	-
PL550	D575K	99.4	100	97.3	98.9	++++	+++	+++
PL607	K599A/D575K	2.1	2	2.3	2.1	+		
PL608	D123P/D575K	27.5	50		38.8	++		
PL609	K568A	98.2	99	99.5	98.9	++++		
PL611	V576A	92.9	95	98.8	95.6	++++		
PL616	D575A	96.9	95		96.0	++++		
PL624	R635W	99.8	100		99.9	++++		
PL652	S548A	100	100	100	100.0	++++		
PL653	S548D	97.1	97	99	97.7	++++	++++	
PL655	S551D	100			100.0	++++		
PL651	S533D	96			96.0	++++		

Table 3 Summary of IRE1 α phosphorylation, XBP1 mRNA splicing and protein levels with mutation(s) in the IRE1 α activation loop in the ER stress condition.

Lab Number	Protein Annotation	p-IRE1 α %	p-IRE1 α %	p-IRE1 α %	Average p-IRE1 α %	Average p-IRE1 α Scale	XBP1 splicing	XBP1s protein
PL500	S724A	1.5	0	0	0.5	+		+
PL501	S726A	40	0	1	13.7	+		-
PL512	S729A	++	++	++++		+++		+
PL516	S724D	++++		++++	68.0	++++		++++
PL517	S726D			97.7	97.7	++++		++++
PL527	S724/726A	++				++	-	-
PL529	S726/729A	++				++	-	-
PL530	S724/726D	+++				+++	+	++
PL532	S726/729D	++++				++++	+	+
PL539	S724E	97.6			97.6	++++	++	++++
PL540	S726E	++++				++++		
PL606	S724/726/729D	0.5			0.5	+		
PL549	S726D K574A	++++	66		66.0	+++	+++	+++
PL551	S724D D575K	+				+	+++	++++
PL617	R722D	47.9	44.5		46.2	++		
PL619	K716A	97.6	89	93.5	93.4	++++		
PL618	R722A	27	20		23.5	+		

Table 4 Summary of IRE1 α phosphorylation, XBP1 mRNA splicing and protein levels with mutation(s) in the IRE1 α RNase domain in the ER stress condition.

Lab Number	Protein Annotation	p-IRE1 α %	p-IRE1 α %	p-IRE1 α %	Average p-IRE1 α %	Average p-IRE1 α Scale	XBP1 splicing	XBP1s protein
PL513	K907A	100	85		92.5	++++		-
PL657	T973D	99.4	98	96	97.8	++++	++++	
PL659	P830L	1.6	0.7	0	0.8	-		
PL661	830LtoP	100			100.0	++++		
PL663	S896A	100			100.0	++++		
PL664	T921A	100			100.0	++++		
PL667	S952A	100	100		100.0	++++		
PL668	P830A	49	73	80	67.3	+++		++
PL669	Y945A	57	44	62	54.3	+++		-
PL670	L941A	46	68		57.0	+++		+
PL671	P830L/Y945A	0			0.0	-		
PL672	P830L/L941A	0	0		0.0	-		
PL687	W833A	91.8			91.8	++++		
PL689	P817L	0			0.0	-		

Chapter 3 The Sel1L-Hrd1 ERAD Complex in Macrophages Re-sets ER Homeostasis and is Dispensable for Innate Immunity

Zhen Xue¹, Yewei Ji^{2,8}, Shengyi Sun^{3,8}, Guojun Shi²; Hana Kim⁴, Zhanguo Gao⁷,
Helene Marquis^{4,5}, Qiaoming Long⁶, and Ling Qi^{1,2,3,4*}

¹Graduate Program in Nutrition, ²Division of Nutritional Sciences, ³Graduate Program in Biochemistry, Molecular and Cell Biology, ⁴Graduate program in Immunology and Infectious Diseases, ⁵Department of Immunology, ⁶Department of Animal Science, Cornell University, Ithaca, NY 14853; ⁷Antioxidant and Gene Regulation Lab,

Pennington Biomedical Research Center, Louisiana

⁸ These authors contribute equally223

Running title: The role of Sel1L in macrophages

*** Correspondence:**

Ling Qi, Ph.D., Email: lq35@cornell.edu; Phone: (607) 254-8857

Possible journals to submit:

Cell Metab/Dev Cell, JEM, PNAS, EMBO J,

3.1 ABSTRACT

Alterations in endoplasmic reticulum (ER) homeostasis or ER stress have been causally linked to inflammatory responses but the physiological evidence in vivo remains to be demonstrated. ER-associated degradation (ERAD) is responsible for the clearance of misfolded proteins in the ER, thus essential for the maintenance of ER homeostasis. Using macrophage-specific ERAD-deficient mice, our data challenges the causal link between ER stress and inflammation in a physiological setting. We show that Sel-1 homolog 1 (Sel1L), a key protein component of the Sel1L-Hrd1 ERAD complex, is required for the clearance of misfolded proteins and the maintenance of ER homeostasis in macrophages. Although Sel1L-deficient macrophages exhibit elevated protein levels of a subset of ER chaperones and dilated ER cisternae at the basal conditions with increased sensitivity to ER stress upon challenge, to our surprise, these changes are uncoupled from inflammatory responses against bacterial pathogens both in vitro and in vivo, as well as in obese adipose tissues, pointing to a dispensable role for ERAD in macrophage inflammation. Thus, we conclude that physiological mild ER stress may not play a causal role in inflammation in macrophages.

3.2 INTRODUCTION

Macrophages play a key role in inflammatory responses, such as autoimmunity, pathogen infection and obesity and type-2 diabetes. Indeed, it has been widely accepted now that macrophage activation dictates the quality, duration, magnitude and specificity of most, if not all, inflammatory responses. This is associated with two major functions of macrophages: First, macrophages phagocytose non-self antigens and act as professional antigen-presenting cells (APCs) via major histocompatibility complex (MHC)-peptide complexes to activate T lymphocytes of the adaptive immune system. Unpaired MHC class I molecule is a known misfolded protein that is normally cleared. Second, activated macrophages secrete a large amount of cytokines such as tumor necrosis factor α (TNF α), interferon γ (IFN γ), interleukin (IL) -6 and IL-1 β , all of which are key mediators of inflammatory responses (335). ER associated degradation (ERAD) recognizes ER misfolded or unfolded proteins in the ER and translocate proteins while ubiquitylating the substrates to be finally degraded in proteasome and ERAD is activated upon UPR (336). As the biosynthesis, folding and maturation of MHC protein and most cytokines occur in the endoplasmic reticulum (ER), we hypothesized that ERAD plays a critical role in macrophage innate immunity functions.

Indeed, ER stress response or unfolded protein response (UPR) has been implicated in macrophage function in inflammatory responses and metabolic diseases (235, 337). Upon lipopolysaccharide (LPS) stimulation, UPR may be

activated in Toll-like receptor (TLR)-dependent manner and the IRE1 α -XBP1 pathway of the UPR is required for the innate function (i.e. cytokine transcription/production) of macrophage (298). In X-box binding protein 1(*Xbp1*)-deficient macrophages, cytokine mRNA levels were impaired (298). Recently, UPR activation has been linked to inflammation, although the underlying mechanism is less well defined. ER stress activation may lead to the activation of JNK and NF- κ B (285, 288, 338), both of which are key mediators of inflammation. Moreover, ER stress or IRE1 α activation was recently directly linked to inflammasome activation in β cells and macrophages (339, 340), which may contribute to the cell death that occurs with prolonged treatment of pharmacological ER stress inducers (341, 342). However, as most studies used high nonphysiological concentrations of ER stress inducers such as thapsigargin, tunicamycin and DTT, whether ER stress plays a role in inflammation in vivo under various physiological settings remains to be demonstrated.

ER-associated degradation (ERAD) machinery recognizes, translocates and degrades misfolded proteins in the ER, acting as a component of the ER quality control system, and is critical for the maintenance of ER homeostasis (134). At least 10 different ubiquitin ligases have been implicated in ERAD in mammals (134, 343). Perturbations of ER homeostasis (caused by disturbance of ERAD, protein folding capacity, ER microenvironment etc) culminate in ER stress and activate the UPR (63, 344). Although the nature of substrate recognition and the physiological role of the complex in vivo largely remain unknown, recent studies using model antigens have shown that each ERAD system is responsible for a

subset of overlapping substrates. The physiological roles of ERAD in vivo and in macrophages have not been studied so far.

The most well-characterized ERAD machinery is composed of Hrd1 E3 ubiquitin ligase, and its complex with the Sel1L protein, an adaptor protein that regulates both stability and substrate specificity of Hrd1 (135, 345, 346). Sel1L and its function are highly conserved from yeast to humans (347). Mammalian Sel1L/yeast Hrd3 encodes an ER-resident single transmembrane protein with a large luminal domain and a short cytosolic tail (348, 349). Both mammalian Sel1L and yeast Hrd3 form a complex with E3 ubiquitin ligase Hrd1 and are responsible for the degradation of a subset of misfolded proteins in the ER (135, 166, 196, 350). While Hrd3-deficient yeast and Sel1-deficient worms are viable (135, 178, 346, 351), Sel1L-deficient mice are embryonic lethal (352). Variants in the Sel1L gene have been identified in Japanese patients with autoimmune thyroid diseases (353), and Sel1L has been identified as a candidate gene for canines and humans with progressive early-onset cerebellar ataxia (354) and Alzheimer's disease (355). Nonetheless, the physiological significance of the Sel1L-Hrd1 complex in vivo remains unknown.

One significant difference between ERAD-deficient animal models and UPR-deficient mice (such as IRE1 α -, PERK-, Xbp1-null and etc) is that ERAD-deficient cells are capable of mounting strong UPR in the face of accumulation of misfolded proteins in the ER, whereas UPR-deficient cells or mice are not. Upon accumulation of misfolded proteins (due to ERAD failure), the activation of UPR

branches may collectively alleviate misfolded protein load by elevation of ER chaperones (such as GRP78, calnexin and ERp57 and etc), expansion of ER membranes and attenuation of protein synthesis; if stress persists, cells may undergo apoptosis.

To study the role of Sel1L in ERAD and inflammation, we generated myeloid cell-specific Sel1L-deficient mice (MKO). We initially hypothesized that Sel1L deficiency in macrophages may lead to activation of the UPR, which may directly induce inflammatory responses. However, here we report a surprising finding that, although ERAD is essential for ER homeostasis, MKO macrophages have normal cytokine secretion, antigen presentation, pathogen defense, and other innate immunity functions both in vitro and in vivo. Thus, our findings suggest a dispensable role of HRD1/Sel1L ERAD complex in macrophages inflammatory responses.

3.3 EXPERIMENTAL PROCEDURES

Mice The *SellL*^{fllox/+} ES cells on the C57BL/6N background were purchased from the KOMP Repository Project (ID CSD44577, UC Davis, <http://www.knockoutmouse.org/martsearch/project/44577>). Exon 6 of *SellL* gene was flanked with two *loxP* sites (floxed). The lacZ-neo cassette was deleted by crossing the animals onto the β Actin-FLPe deleter mice (356). The *SellL*^{fllox/fllox} animals were then crossed with myeloid-specific Lyz2-Cre mice (B6.129P2-*Lyz2tm1(cre)Ifo/J*, JAX 004781), which have been backcrossed onto the C57BL/6J background for more than 5 generations prior to arrival at our facility. The last stage of cross generated *MKO* and the control cohort *SellL*^{fllox/fllox} littermates without Cre (termed “WT” hereafter) at 1:1 ratio. HFD contained 60% fat, 20% carbohydrate and 20% protein (Research Diet D12492) while ND consisted of 13% fat, 67% carbohydrate and 20% protein (Teklad 2914). All animal procedures have been approved by the Cornell IACUC (#2007-0051).

Preparation of Primary Macrophages Peritoneal macrophages were obtained 4 days after intraperitoneal injection of 2 ml aged 4% brewed thioglycollate broth (Inc and catalog #). Mice were euthanized by CO₂ and the abdomens were soaked with 70% alcohol. Retract the abdominal skin manually to expose the intact peritoneal wall, and use 6-ml syringe with room temperature PBS to inject along the left side of peritoneal wall, and fluids were aspirated and removed to regular polypropylene centrifuge tubes. Centrifuge the peritoneal exudate cells (PEC) at ~1,000 rpm for 10 min. 200 μ l lysis buffer for red blood cells was added to the cell suspension after centrifuge, and the reaction was stopped by the addition of 15 ml PBS. Peritoneal macrophages were counted using hemocytometer. 3×10^6 cells were plated in each well of a 6-well plate for

western blot or other biochemistry analysis. For bone marrow derived macrophages (BMDM), femur bones were collected and flushed with a 27 1/2-gauge needle. After centrifugation, cells were seeded onto 10-cm Petri dishes at approximately 1×10^7 cells/plate in DMEM (Sigma) containing 10% FBS and 20% L929 cell conditioned media as a source of macrophage colony-stimulating factor (M-CSF) for 5-8 days. Flow cytometric analysis shows that nearly 95% cells were BMDM.

Drug Treatment and Cell Culture Thapsigargin (Tg, EMD Calbiochem) was dissolved 0.6 mM in DMSO. Lipopolysaccharides (LPS, Sigma L4130) was dissolved in culture media at 1 μ g/ml. Aliquots were stored at -20°C . MG-132 (FISHER NC9937881) was dissolved in DMSO at 10mM and stored at -80°C . In most experiments, cells were treated with various drugs over a time course as indicated in the figures and figure legends.

Transmission Electron Microscopy (TEM) Peritoneal macrophages were seeded on 6 well plates as described above with 1.5×10^6 cells each well and fixed with 5% glutaraldehyde, 4% paraformaldehyde in 0.1M phosphate buffer for 2 h and post fix in 1% osmium tetroxide in 0.1 M phosphate buffer. The further processing and imaging acquisition were performed on a fee-for-service basis by the Electron Microscopy & Histology Core Facility at Weill Cornell Medical College.

Western Blot and Image Quantitation Preparation of cell lysates, PPase treatment and Phos-tag and regular Western blot were performed as previously described (322, 324). IRE1 α phosphorylation allows directly visualization of ER stress response and accurate assessment of stress in the ER (322, 324, 325). Antibodies used in this study: HSP90 (rabbit, 1:5,000), GRP78 (goat, 1:1000),

Caspase 3 (rabbit, 1:2,000) from Santa Cruz; IRE1 α (rabbit, 1:1,000), PERK (rabbit, 1:1,000), eIF2 α p-Ser51 (rabbit, 1:2000), eIF2 α (rabbit, 1:2000), LC3B (rabbit, 1:1000), I κ B α (rabbit, 1:2000), ACC (rabbit, 1:2000) from Cell Signaling; SellL (rabbit, 1:1,000) from Abcam; HRD1 (rabbit, 1:8000) from Novus Biologicals; PDI (rabbit, 1:10,000), ERp57 (rabbit, 1:2,000), Calnexin (rabbit, 1:10,000) from Assay Design; Hsp70 (mouse 1:1,000) from LifeSpan BioSciences; Derlin1 (rabbit, 1:5,000) and Derlin2 (rabbit, 1:5,000), gifts from H. Ploegh (MIT); iRhom2 (rabbit, 1:5,000), a gift from M. Freeman (Cambridge, UK). Of note, to ensure sufficient signal for cleaved caspase 3, the membrane for caspase 3 was cut around the 25 kDa line and then probed separately with caspase 3 antibody. Band density was quantitated using the Image Lab software on the ChemiDOC XRS⁺ system (Bio-Rad) and presented as mean \pm SEM from several independent experiments or as representative data from at least two independent experiments.

RNA Extraction and qPCR RNA from cells and tissues were extracted using Trizol and Qiagen RNA miniprep kit and performed as previously described (322). qPCR primer sequences have been previous reported (322, 324).

Cell Survival Assay 3×10^6 peritoneal macrophages in wells of 6 well plate were treated with Tg 300nM for 6.5 hour. Scrape the cells up, and count cell number to plate 1×10^6 in a 10cm dish and change fresh media every 3 days. 12 days later, the cells were briefly washed in PBS and fixed in freshly prepared 3.7% formaldehyde in PBS for 15 min followed by 30 min incubation in 0.05% crystal violet in distilled water (filtered before use) with gentle rocking at room temperature. Cells were washed 3 times for 5 min each with ddH₂O, permeabilized with methanol for 15 min and sampled aliquots were read at OD 540 nm with Bio-Tek Synergy 2 plate reader (Bio-Tek Inc.).

Brefeldin-A BODIPY, Cell Surface Marker Analysis and Flow Cytometry

Cells were incubated at 37°C for 30 - 45 min with 0.4 µg/ml Brefeldin A-BODIPY (Invitrogen) in culture media followed by flow cytometric analysis using a BD FACSCalibur flow cytometer. For surface marker analysis, fluorochrome- or biotin- conjugated antibodies against CD4 (GK1.5), CD8 (YTS169), F4/80 (BM8), CD11b (M1/70), Gr1 (RB6-8C5), B220 (RA3-6B2), CD45 (30-F11), CD69 (H1.2F3), and isotype control antibodies were purchased from BioLegend, UCSF Flow Core Facility or BD Biosciences. Following incubation with anti-CD16/CD32 antibody to block Fc receptors, 1×10^6 cells were incubated with 20 µl of antibodies diluted at optimal concentrations for 20 min at 4°C. Cells were washed three times with PBS and then resuspended in 200 µl PBS for analysis. Data was analyzed using the CellQuest and FlowJo software.

T cell and NKT Cell Activation Assay BMDM from both WT and MKO were cultured in 96 well (4×10^5 BMDM/well), as well as 4×10^5 CD8⁺ T cells, isolated from OT1 mouse splenocytes. To each well, 5µM OVA257-264 (SIINFEKL, Biomatik) or CON-DMEM (not shown) were added and incubated in 37°C incubator for 48 hours. The supernatant was collected at the end of incubation and analyzed for IL-2 analysis using ELISA. (C) NKT cells (1×10^4 /well) and 1×10^5 peritoneal macrophages were co-cultured in a 96 well for 12 hours and culture medium were then spin and collected for analyzing IL-2 by ELISA.

LPS Challenge 8-w-old female mice were injected i.p. with LPS at 40mg/kg body weight and observed for survival every 4 h. In some experiments, 200 µl serum was collected at 0, 3 and 6 h time points post injection for cytokine analysis.

***Listeria monocytogenes* Infection** Mice were anesthetized with isoflurane and infected with 10^4 *Listeria monocytogenes* strain 10403S by retro-orbital injection. Mice were sacrificed at 3 days post-infection and blood, liver and spleen were collected. Tissues were homogenized in 0.05% NP-40 solution and serial dilutions were plated on LB-agar to determine bacterial loads. Cytokines levels of TNF α and IFN γ in serum were quantified using eBioscience Ready-Set-Go ELISA kits.

Cytokine Analysis TNF- α , IL-6 and IL-1 β ELISA kits were purchased from eBioscience or Biolegends. All ELISAs were performed per supplier's protocols.

Inflammasome Activation Inflammasomes activation, in vivo and in vitro, was performed as previously described (357). Briefly, 8w-old mice were injected i.p. with LPS at 2 ng/g BW (Sigma L4130) 1.5 h prior to the ATP challenge i.p. (50mM ATP, adjusted to pH 7 with NaOH, Sigma) at 10 μ l per gram of body weight. 1 h later, mice were euthanized. Blood and peritoneal lavage fluid were collected to measure cytokines and Gr-1⁺ CD11b⁺ neutrophils. The IL-1 β level was measured by ELISA and the neutrophil levels were measured by the flow cytometer. In vitro, peritoneal macrophages were treated with 0.1 μ g/ml LPS (Sigma L4391) for 5 h followed by addition of 5 mM ATP (Sigma) for 30 min followed by protein extraction.

H&E Staining Tissues were collected at what condition and fixed in 10% formaldehyde and sent to Cornell Histology Core Facility for sectioning and HE staining on a fee-for-service basis. Pictures of HE staining sections were taken by a Leica microscope (Leica Microsystems, Buffalo Grove, IL).

Glucose/Insulin Tolerance Test (GTT/ITT) Male mice on HFD for 20 weeks (from the age of 8 weeks) were subjected to the glucose tolerance test (GTT). Mice were fasted for 18 hours before the test, and injected i.p. glucose (Sigma) 1 g/kg body weight. During ITT, mice were fasted... Blood glucose was monitored using One-Touch Ultra Glucometer at 0, 30, 60, 90 and 120min post-injection.

Statistical Analysis Results are expressed as mean \pm SEM unless indicated otherwise. Comparisons between groups were made by unpaired two-tailed Student's t-test, where $p < 0.05$ was considered as statistically significant. All experiments were repeated at least two to three times and representative data are shown.

3.4 RESULTS

Generation of myeloid-cell specific Sel1L-deficient (MKO) mice. In macrophages, Sel1L is a transmembrane glycoprotein residing in the endoplasmic reticulum (346, 352) as confirmed by its complete sensitivity to endoH (**Figure 3.1A**). It is expressed in embryonic and cancer cells (348, 358-360), as well as organs with a high protein secretion function (**Figure S3.1A**). During the process of cell differentiation, from bone marrow progenitor cells into mature macrophages with the stimulation of CSFs (colony-stimulating factor produced by L929 cell lines), Sel1L protein level increased (**Figure S3.1B**), indicating its important role in BMDM. ER stress, but not LPS, induced Sel1L mRNA levels by 50% (**Figure 3.1B**). To study the role of Sel1L/HRD1 ERAD complex in macrophages inflammatory responses, we generated myeloid-cell specific Sel1L KO mice, hereafter termed *MKO* mice. In the *Sel1L*^{fllox/+} ES cells, exon 6 of *Sel1L* gene was flanked with two *loxP* sites (*Sel1L*^{fllox/fllox}) (**Figure 3.1C**). The *Sel1L*^{fllox/fllox} animals were crossed with myeloid-specific *Lyz2-Cre* mice. The last stage of crosses generated *MKO* and the control cohort *Sel1L*^{fllox/fllox} littermates without Cre (termed WT hereafter) at 1:1 ratio as expected (**Figure 3.1F**). Western blot analysis revealed significant reduction of Sel1L protein in bone marrow-derived macrophages and thioglycollate-elicited peritoneal macrophages of *MKO* mice compared to WT mice, but not in other tissues (e.g. liver, spleen, and pancreas, **Figure 3.1D**). Of note, it is not clear what the bands underneath Sel1L bands are. They could be non-specific bands bound by Sel1L antibodies, or could be unknown alternatively spliced isoforms of Sel1L. However, the size of

these lower bands does not match any Sel1L isoforms that are currently known (348). *MKO* mice on low-fat diet (LFD) appeared normal and exhibited no body weight differences up to 16 weeks of age (**Figure 3.1E**). The amount of myeloid-derived macrophages and neutrophils in spleens of naïve or thioglycollate-challenged mice were comparable between *MKO* and WT mice (**Figure 3.1G, Figure S3.2**), suggesting that Sel1L deficiency does not affect myeloid cell differentiation and proliferation. Finally, total peritoneal macrophages cell numbers were the same between the two cohorts (**Figure 3.1H**). This indicates that Sel1L deficiency does not affect myeloid cell activation and infiltration.

Figure 3.1 Characterization of MKO mice.

(A) Sel1L protein is sensitive to endoH in peritoneal macrophages. (B) Sel1L mRNA level induced by Thapsigargin (Tg) and lipopolysaccharide (LPS) measured by qPCR. (C) Schematic gene structure of mouse Sel1L manipulated in transgenic mice. Exon 6 was flanked with two floxP sites. Exons are shown in purple and introns in black line. (D) Sel1L expression level in different tissues in WT and Sel1L KO mice. (E) Growth curve (body weight) of WT and MKO from week 3 to 9 after birth. (WT n=10, MKO n=6) (F) Observed ratio of birth between WT and MKO mice was consistent with expected ratio. (G) Naïve or Thioglycollate-injected mice spleen were dissected and performed FACS. CD11b, Gr1 and F4/80 antibodies were used to gate and quantify the percentage of macrophages. (H) Cell count of collected peritoneal macrophages from each WT (n=5) and MKO (n=5) mouse.

ERAD deficiency and alterations in ER homeostasis in Sel1L deficient macrophages. (Thereafter Sel1L deficient macrophages are referred to as MKO macrophages, and Sel1L myeloid-cell specific knock-out mice are referred to as MKO mice). In line with the observations in yeast (135) and in mammalian cell lines (345, 350), but in contrast to one mammalian cell study (361), loss of Sel1L significantly reduced the level of Hrd1 by 50-60% in macrophages (**Figure 3.2A-B**), highlighting the importance of Sel1L in Hrd1 stability and in the formation of the HRD1 ERAD complex. Sel1L deficiency had few effects on other ERAD components. Derlin 1 and 2 protein levels were only slightly affected (by 20-30%) in Sel1L-deficient macrophages (**Figure 3.2B**).

To directly visualize ER homeostasis, we next performed transmission electron microscopy (TEM) to visualize organelle morphology in cells. Dramatically, ER cisternae in the MKO cells were dilated (arrows in **Figure 3.2D**). The normal flat cisternae of ER are expanded into a ballooned structure in Sel1L KO peritoneal macrophages. In the ER of MKO macrophages, we also noticed significantly higher luminal density, possibly representing an accumulation of misfolded proteins (**Figure 3.2D**). There was no difference in cell size and intracellular granule particles between the two cell groups (**Figure 3.2D**). In addition, Sel1L KO macrophages showed normal numbers of mitochondria with no differences in average size and morphology (**Figure S3.3**), suggesting that mitochondrial reactive oxygen species (ROS) were unlikely to cause an increase of proinflammatory cytokine production (362, 363) in this case. We also measured ER expansion in MKO peritoneal macrophages by the flow

cytometer using ER/Gogi mass specific Brefeldin A-Bodipy staining (**Figure 3.2C**).

We then determined the consequence of Sel1L-Hrd1 ERAD deficiency on ER homeostasis. To this end, we either mock-treated or treated primary macrophages (bone marrow-derived (BMDM) and thioglycollate-elicited peritoneal macrophages) obtained from WT and MKO mice with thapsigargin (Tg) or lipopolysaccharides (LPS) to induce ER stress and inflammation, respectively. Interestingly, while PDI and calnexin protein levels were not affected (**Figure 3.2F**), a subset of ER chaperones including ERP57 and GRP78 were upregulated by 2-4 fold in MKO macrophages (**Figure 3.2E**), indicating a chaperone specific effect in resetting ER homeostasis. Similar results were confirmed by qPCR measuring GRP78, Grp58 and Calnexin mRNA levels (**Figure S3.4**). Under the condition treated, cytosolic chaperones such as HSP70 were not affected by Sel1L knock-out (**Figure 3.2F**), pointing to a specific effect of Sel1L on resetting ER homeostasis.

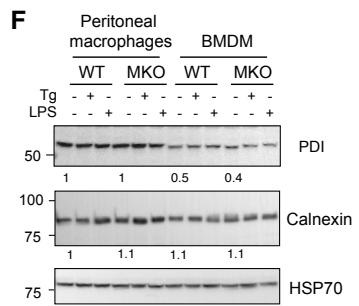
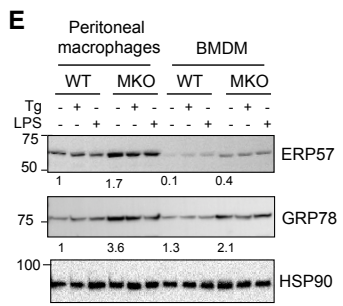
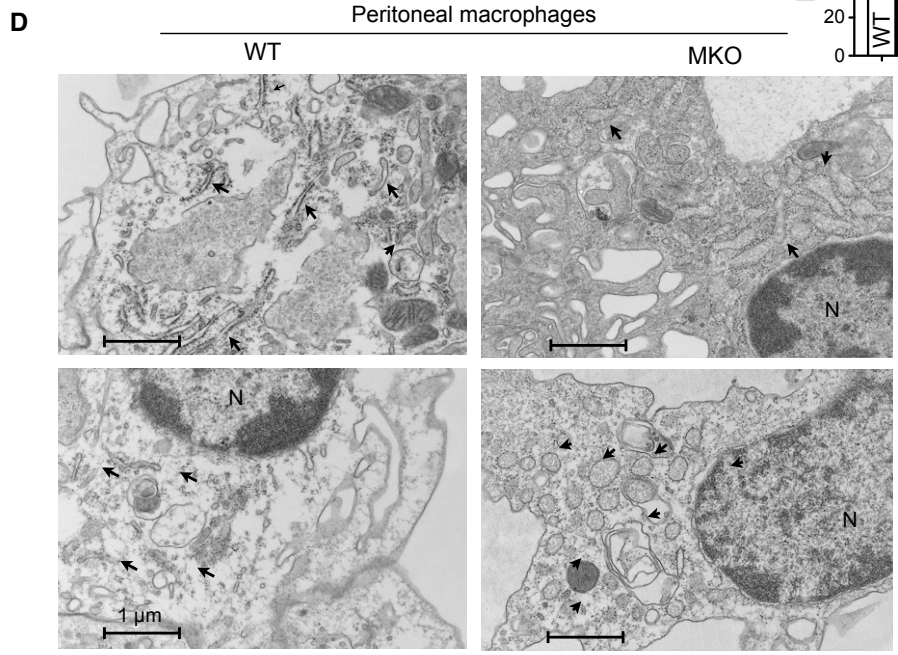
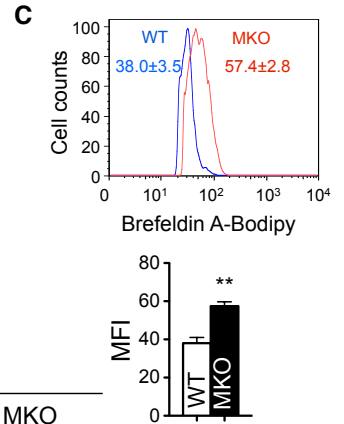
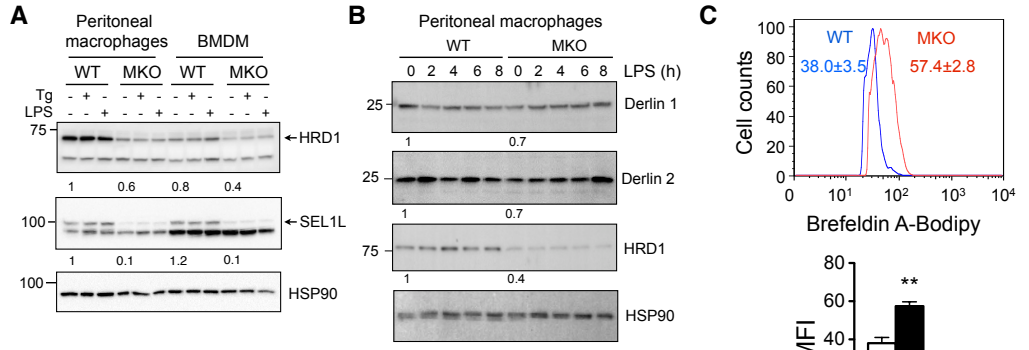


Figure 3.2 ERAD deficiency and alterations in ER homeostasis in MKO macrophages.

(A) Thioglycollate induced peritoneal macrophages and bone marrow derived macrophages (BMDM) were cultured and treated by Thapsigargin (Tg, 300nM) or lipopolysaccharides (LPS, 1000ng/ml) for 4 hours or as indicated time course. Whole cell lysates were extracted and performed SDS-page western blots. Data were representative of 2 independent experiments. Both peritoneal macrophages and BMDM showed decreased HRD1 protein levels in MKO. Quantification of untreated state was shown in numbers below. (B) WT and MKO peritoneal macrophages and BMDM were treated by LPS in 2, 4, 6, 8 hours and western blots showed MKO Derlin 1 and Derlin 2 level remained comparable to WT. (C) FACS data of WT and MKO peritoneal macrophages stained with Brefeldin A-Bodipy showed increased ER size in MKO (n=4). Quantification of mean fluorescence index (MFI) was listed below. (D) Representative TEM images of peritoneal macrophages. Scale bar was shown in the picture. Arrows indicated ER, N indicated nucleus. (E) (F) WT and MKO peritoneal macrophages and BMDM were treated in the same condition as (A). Western blots showed up-regulation of ER chaperones ERP57 and GRP78, but not PDI and Calnexin. Quantification of untreated state data shown in numbers below. HSP90, HSP70 were loading controls.

Increased sensitivity to ER stress induced cell death in MKO macrophages. We next directly assess the activation status of UPR pathways, mostly the IRE1 α and PERK pathways as we previously described (324). A dramatic increase of IRE1 α protein was observed in both MKO peritoneal macrophages and bone marrow derived macrophages (BMDM) by 10-30 fold (**Figure 3.3A-B**), similar to the *Xbp1*- or *Derlin 2*- deficient cells (79, 364). However, the absolute amount of phosphorylated IRE1 α in MKO macrophages under basal conditions was comparable to that in WT, but the amount of p-IRE1 α was highly increased in MKO cells compared to WT cells with Tg treatment (**Figure 3.3A-C**). However, the percent of total IRE1 α that was phosphorylated was reduced in MKO cells at both basal and Tg-treated conditions, reflecting up-regulation of IRE1 α in MKO cells (**Figure 3.3A-C**). *Xbp1* mRNA splicing was significantly elevated in *MKO* macrophages compared to WT macrophages under basal conditions (**Figure 3.3D**), while upon ER stress challenge, *Xbp1* mRNA splicing was comparable between the two cell groups (**Figure 3.3D**). Consistently, MKO macrophages showed an increase in Xbp1s, ATF4 and CHOP transcription factors (**Figure 3.3E**). Similar to the IRE1 α pathway, total PERK protein increased over 4-6 fold in *MKO* macrophages (**Figure 3.3F**). Slight mobility-shift of PERK protein was noted in MKO cells at both basal and Tg-treated conditions (**Figure 3.3F**). Phosphorylation of e-IF2 α , a downstream of the PERK pathway, was not elevated in *Sel1L* KO macrophages (**Figure 3.3G**). While the underlying mechanism for IRE1 α and PERK accumulation in MKO macrophages remains unclear, our data demonstrated that IRE1 α and PERK signaling pathways were modestly elevated in MKO macrophages compared to

the WT cohorts. To be noted, the accumulation of IRE1 α and PERK protein in MKO were not only due to the ERAD defect, as blocking cytosolic proteasome by MG-132 only induced a mild increase of IRE1 α and PERK (**Figure S3.5**). Moreover, the half-life of IRE1 α , PERK, GRP78 and HRD1 seem to be shorter in Sel1L KO macrophages compared to WT (**Figure S3.6**). Since the mRNA level of IRE1 α and PERK is not induced in MKO (**Figure S3.4**), we assume IRE1 α and PERK protein degradation might be dependent on Sel1L/HRD1. At the transcription level, some chaperones such as GRP78 was elevated, while others were unaffected at the basal conditions (**Figure S3.4**). Overall, WT and MKO cells exhibited similar ER stress-induced transcription profiles (**Figure S3.4**).

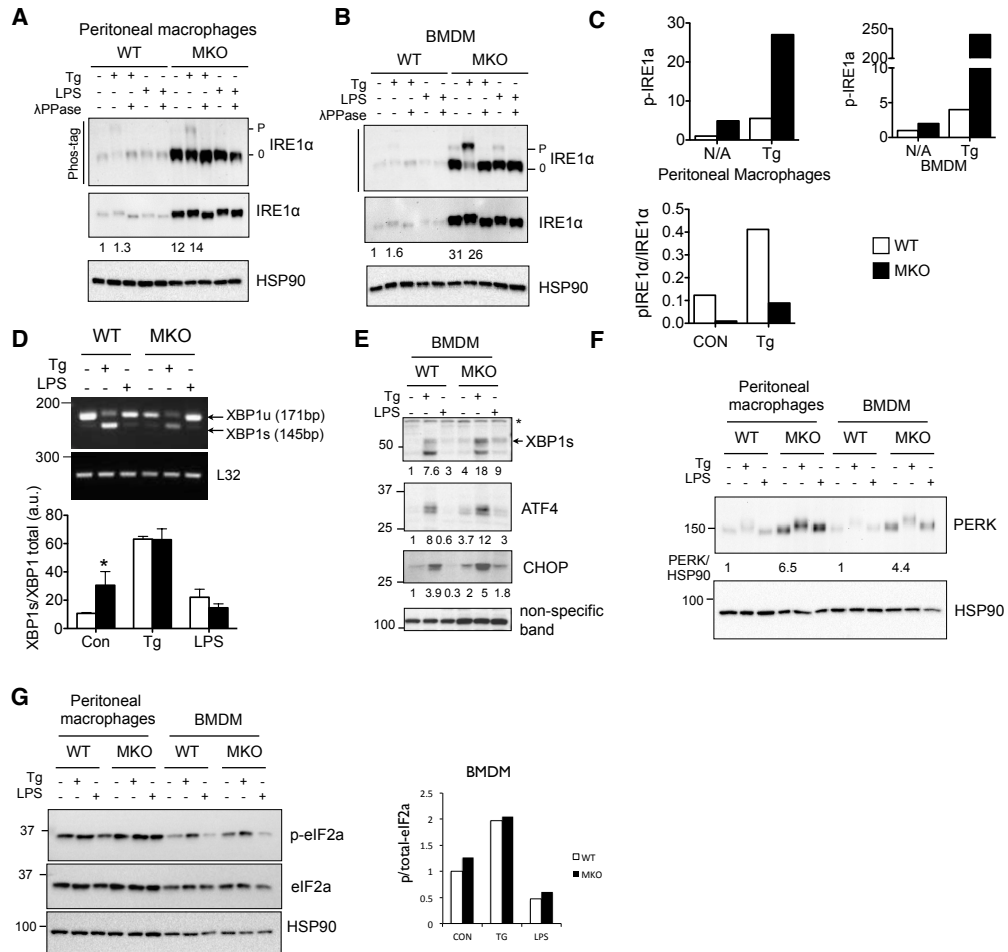


Figure 3.3 Sel1L/HRD1 ERAD deficiency caused a mild UPR activation in MKO macrophages.

Thioglycollate induced peritoneal macrophages and bone marrow derived macrophages (BMDM) were cultured and treated by Thapsigargin (Tg, 300nM) or lipopolysaccharides (LPS, 1000ng/ml) for 4 hours or as indicated time course. Whole cell lysates were extracted and performed SDS-page western blots. Data were representative of 2 independent experiments. Western blot showed peritoneal macrophages (A) and BMDM (B) p-IRE1 α in phos-tag gels, total IRE1 α and loading control hsp90 on regular SDS page gel. Cell lysates were treated with/without λ PPase. The absolute amount of p-IRE1 α and p-IRE1 α /total IRE1 α were shown in (C). N/A, non-treated control. (D) XBP1 splicing by RT PCR under basal condition, Tg and LPS treatment. Quantification of XBP1s/total XBP1 was shown below. (E) Nuclear extraction protein lysates run on western blots showed transcription factors XBP1s, ATF4 and CHOP. (F) PERK protein levels in both peritoneal macrophages and BMDM from WT and MKO mice under the listed treatment conditions. (G) p- or total eIF2 α protein levels in both peritoneal macrophages and BMDM from WT and MKO mice under listed treatment conditions. Quantification of p/total eIF2 α in BMDM was shown on the right side.

As ER stress is linked to cell death (63), we next asked whether MKO cells are predisposed to cell death. Surprisingly, at the basal condition, MKO cells exhibited similar levels of caspase-3 cleavage (**Figure 3.4A,C**) and Annexin V levels (**Figure 3.4F**). However, *MKO* cells exhibited increased caspase-3 cleavage and Annexin V levels under ER stress condition (**Figure 3.4A-B, D, F**) but not with LPS stimulation (**Figure 3.4C, E, F**).

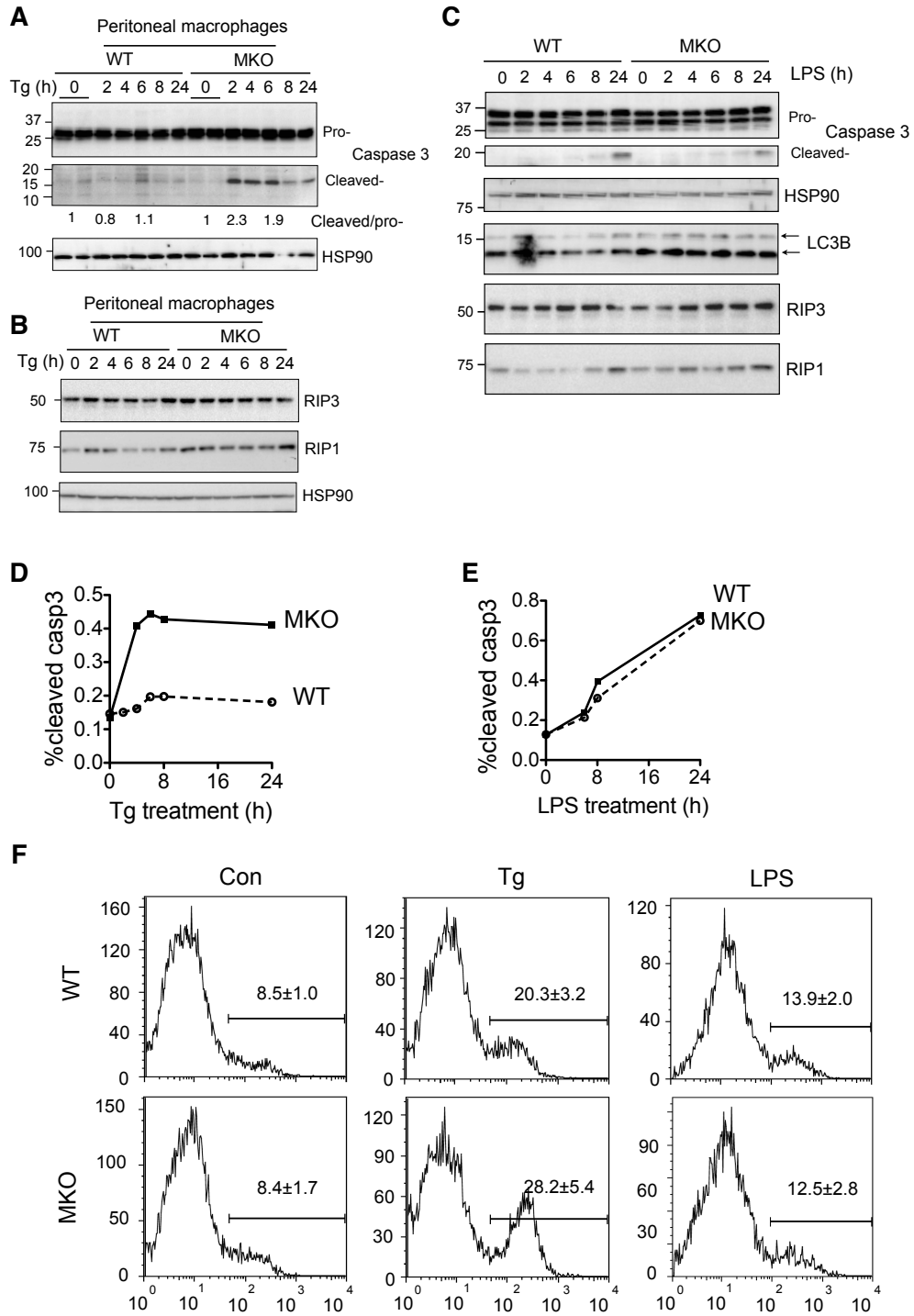


Figure 3.4 Increased sensitivity to ER stress in MKO macrophages.

(A) Peritoneal macrophages were treated by Thapsigargin (Tg, 300nM) for the indicated time course. Western blot for pro- and cleaved form of caspase-3 were shown in (A). Quantification of cleaved caspase-3 was shown in numbers below. (B) For the same conditions as (A), western blot for RIP3 and RIP1. (C) Peritoneal macrophages were treated by LPS (1000ng/ml) for a time course as listed. Western blots showed pro- and cleaved form of caspase-3, RIP3, RIP1, LC3-B and quantification of caspase-3 was shown in (E). (F) FACS data showed the percentage of Annexin-V positive peritoneal macrophages in the conditions listed.

Normal immune functions of MKO macrophages in vitro. As macrophages play a key role in both innate and acquired immunity, we next asked how Sel1L deficiency affects immune functions of macrophages such as antigen presenting and cytokine secretion upon stimulation. Macrophages are professional antigen presenting cells to process peptide and lipid antigens and present them in complex with MHC class I/II and CD1d proteins to activate CD8⁺, CD4⁺ T cells and natural killer T (NKT) cells, respectively. Assembly and maturation of MHC class I/II and CD1d proteins occurs in the ER, as well as the loading of endogenous peptides onto the MHC class I molecules. Thus, we anticipated that Sel1L deficiency might affect antigen presentation function of macrophages via the regulation of the assembly, maturation and presentation of MHC-peptides or CD1d-lipid complexes.

To our surprise, protein levels of MHC class I and II molecules at the cellular surface were comparable between MKO and WT macrophages (**Figure 3.5A**). In a co-culture system with both macrophages and CD8⁺ T cells, supplemented with corresponding ovalbumin 257-264 (SIINFEKL) peptides, there was no difference in the activation of CD8⁺ T cells, because IL-2 released from the CD8⁺ T cells showed no differences (**Figure 3.5B**). Similarly, when pulsed with lipid agonist α -galactoceramides (α GalCer, binds to CD1d), MKO

cells had no defect in activating NKT cell line DN32 (**Figure 3.5C**). Thus, these data showed that despite the dilation of the ER, the assembly and maturation of functional surface MHC-peptide complex and antigen presentation by MHC class I and CD1d molecules were not compromised by Sel1L deficiency.

We next examined the immunological response to LPS. Sel1L protein levels were not changed upon the stimulation of various Toll-Like Receptors (TLR) agonists (**Figure S3.7A**). In vitro, LPS increased inflammation in both *MKO* and WT macrophages at a comparable level and dynamic pattern, as shown by IKappaB (**Figure 3.5D-E**) and p-JNK (**Figure S3.7B**). Commassie blue staining of secreted proteins in the culture medium of WT and *MKO* macrophages revealed comparable levels of overall protein secretion in response to LPS and Tg (**Figure 3.5F**). Furthermore, Tumor Necrosis Factor alpha (TNF α) and Interleukin-6 (IL-6) secreted by *MKO* macrophages in response to LPS were similar to those of WT macrophages (**Figure 3.5G**). At the molecular level, an ER-transmembrane protein iRhome2, a key regulator of TNF α activation (365, 366), was not altered in *MKO* macrophages (**Figure 3.5H**). Thus, these data strongly support that Sel1L deficiency does not affect LPS-induced acute macrophage activation and inflammatory cytokine secretion.

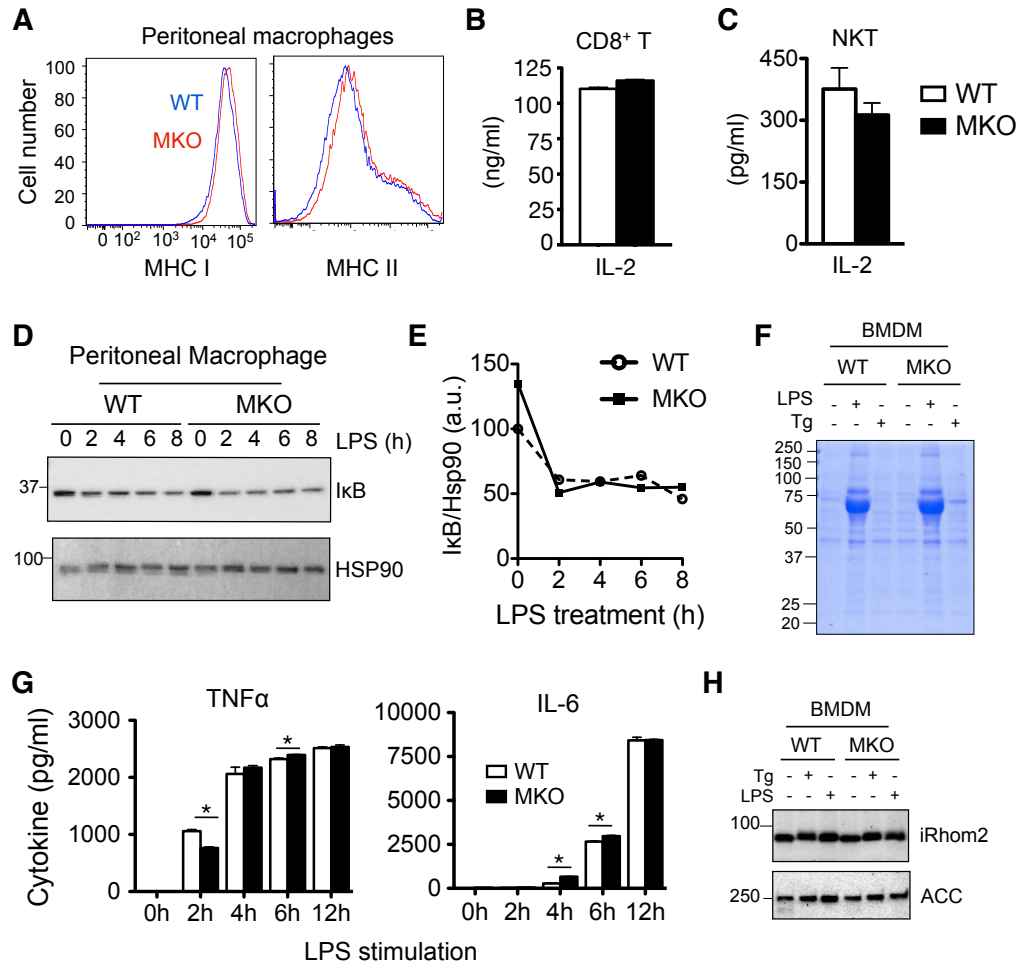


Figure 3.5 Normal innate function of MKO macrophages in vitro.

(A) Peritoneal macrophages were collected fresh from both WT and MKO mice and performed FACS to detect MHC-I and II expression levels. (B) BMDM from both WT and MKO were cultured in 96 well (4×10^5 BMDM/well), together with 4×10^5 CD8⁺ T cells that were isolated from OT1 mouse spleens. To each well, 5 μ M OVA257-264 (SIINFEKL, Biomatik) or control-DMSO (data not shown) were added and incubated in 37°C incubator for 48 hours. The culture medium was collected at the end of incubation and ELISA was performed to measure IL-2. (C) NKT cells (1×10^4 /well) and 1×10^5 peritoneal macrophages were co-cultured in a 96 well for 12 hours and the culture medium was pulsed with lipid agonist α -galactoceramides. Then the medium was collected for analyzing IL-2 by ELISA. (D) Western blot showed I κ B levels of peritoneal macrophages treated with LPS by indicated time points. Hsp90, a loading control. Quantification of I κ B/Hsp90 was shown in (E). (F) BMDM were cultured on 10 cm plates (1.8×10^6 /dish) and treated with Tg or LPS in DMEM without FBS for 4 hours. The culture medium was then collected and concentrated from 6ml to 100 μ l and run a SDS-page gel, followed by Commassie Blue Staining. (G) Stimulated by LPS in a time course, macrophage cytokine TNFa and IL-6 levels in culture medium were analyzed by ELISA. (H) Protein levels of iRhom2 in WT/MKO BMDM in basal level, Tg and LPS treatments. ACC, a loading control.

Sel1L is not required for inflammatory responses against pathogens in vivo. Next we examined the whole body responses to LPS endotoxin shock and the *listeria* pathogen infection, the outcome of which were known to be determined by the function of macrophages (365, 366). First, WT and *MKO* mice were challenged with LPS. *MKO* mice exhibited no difference from WT littermates in survival rate with 100% death within 24 hours (**Figure 3.6A**). Serum cytokine levels (TNF α , IL-6 and IL-1 β) were dramatically induced within hours post injection, which were not different between WT and *MKO* mice (**Figure 3.6B**). Second, we challenged mice with *L. monocytogenes*, an intracellular anaerobe causing listeriosis (367). There were no differences in bacterial load in the liver and spleen (**Figure 3.6C**). Moreover, serum levels of IFN γ and TNF α were also comparable (**Figure 3.6D**). Taken together, our data demonstrated that macrophage innate immunity functions against pathogens in vivo were not perturbed by Sel1L deficiency and alterations in ER homeostasis.

In addition, inflammasomes have been shown to be activated upon both bacterial and viral infections, and inflammasomes activation was known to be dependent on monocytes and macrophages (368-373). Here, we also tested in vivo inflammasome activation by an LPS and Adenosine Triphosphate (ATP) two-step signaling model. Macrophages and dendritic cells need a TLR-ligand

activation to induce pro-IL-1 β transcription and a second signal ATP to induce caspase-1 cleavage that leads to IL-1 β maturation and secretion (357, 374). We were surprised to find no severe activation of inflammasomes in MKO mice in vivo (**Figure 3.6E**). Although there was an increase of TNF α both in the serum and lavage fluid, IL1 β levels, as well as the number of total cells, neutrophils, macrophages, B cells, and T cells were all the same between MKO and WT groups. In addition, the cellular surface and intracellular ATP receptor P2X7 levels remained similar between WT and MKO cells (**Figure S3.8**), consistent with the results that showed similar levels of pro-inflammatory cytokines and MHC class I proteins (374-376). These results thus prove there was no defect or enhancement of inflammasomes activation in Sel1L MKO mice; indicating Sel1L in macrophages is dispensable for the maintenance of normal inflammasomes function in vivo.

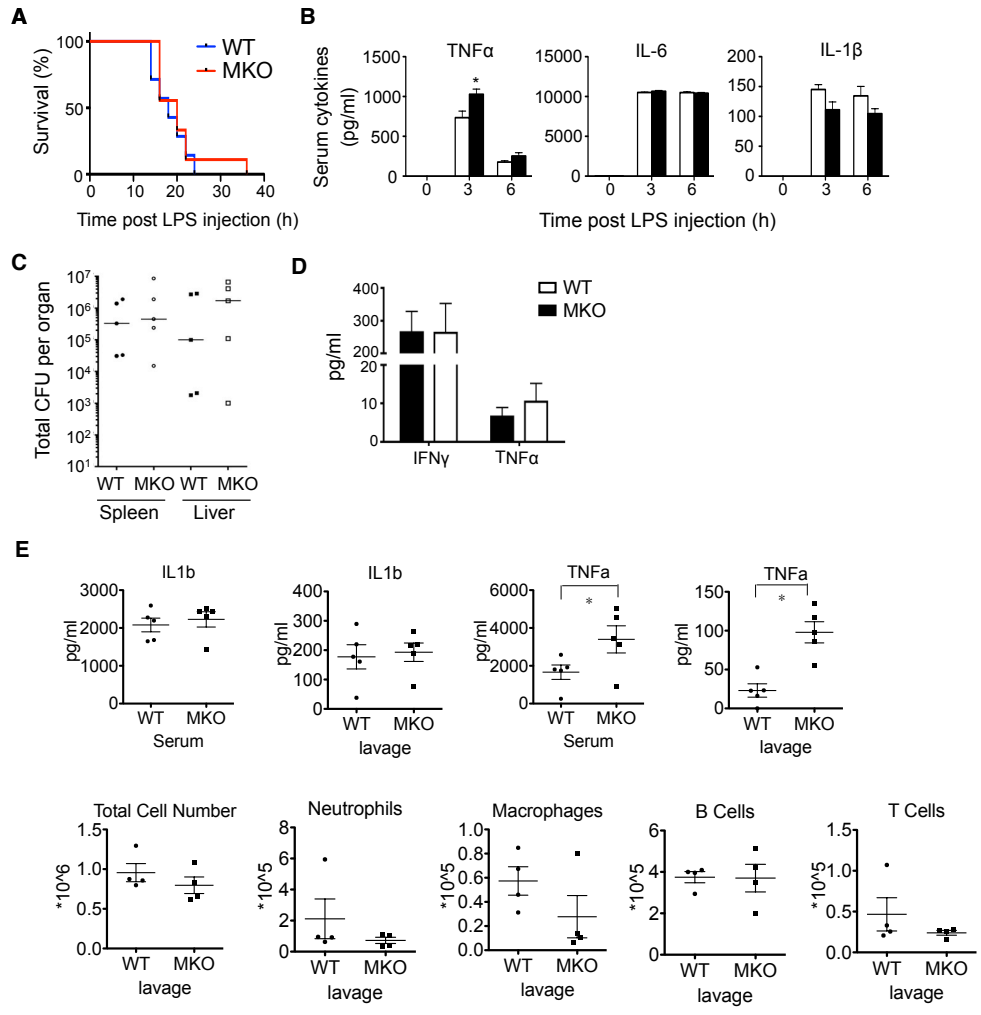


Figure 3.6 Sell1L is not required for inflammatory responses against pathogens in vivo.

(A) Survival curve of MKO and WT mice that were challenged by 40mg/kg LPS in an endotoxin shock model. (B) Serum levels of TNF α , IL-6 and IL-1b at the indicated time points from mice challenged with LPS. (C) Tissue bacterial burdens from both WT and MKO mice at the third day post *Listeria monocytogenes* infection. (D) Cytokine levels of IFN γ and TNF α in serum 3d post-infection as analyzed by ELISA. (E) 8w-old mice were injected (i.p.) with LPS, and 1.5 h later injected with ATP, then after 1 hour, the blood and peritoneal lavage fluid was collected. ELISA was performed to measure cytokines IL-1 β and TNF α . Total cell number, Gr-1 $^{+}$ CD11b $^{+}$ neutrophils, F4/80 $^{+}$ macrophages, B220 $^{+}$ B cells, and CD4 $^{+}$ or CD8 $^{+}$ T cells numbers were all measured by the flow cytometer.

Sel1L in macrophages is not required for chronic inflammatory responses in obesity. ER stress in adipose tissue and the liver has been causally linked to obesity-induced type-2 diabetes (219, 377). Indeed, chemical chaperones that may help protein folding have been shown to be effective in treating type-2 diabetic mouse models (377). In obesity, macrophage infiltration into white adipose tissue (WAT) may play a significant role in the development of inflammatory tone in the adipose tissue and hence insulin resistance (378-380). Based on these studies, we postulated that Sel1L deficiency in macrophages might influence adipose inflammation in obese animals.

To this end, mice were placed on a 60% high fat diet (HFD), in which 60% calories were derived from fat for up to 20 weeks. There was no difference in body and liver/adipose weight between *MKO* and WT mice upon 20-week HFD feeding (**Figure 3.7A-C**). Histological assessment of WAT revealed comparable levels of immune cell infiltration (**Figure 3.7D**), which was further confirmed by Q-PCR and Western blot analyses of macrophage markers and inflammatory genes in WAT (**Figure 3.7E-F**). No dramatic difference in morphology was observed in the liver as assessed by H&E staining (**Figure 3.7D**). Serum cytokine levels of IL-6 and TNF α were comparable (**Figure 3.7G**), indicative of comparable systemic inflammatory responses. Finally, glucose and

insulin tolerance as measured by glucose tolerance test (GTT) and insulin tolerance test (ITT) were similar between the two cohorts (**Figure 3.7H-I**). Taken together, our data supported that macrophage Sel1L is dispensable for adipose inflammation in obesity.

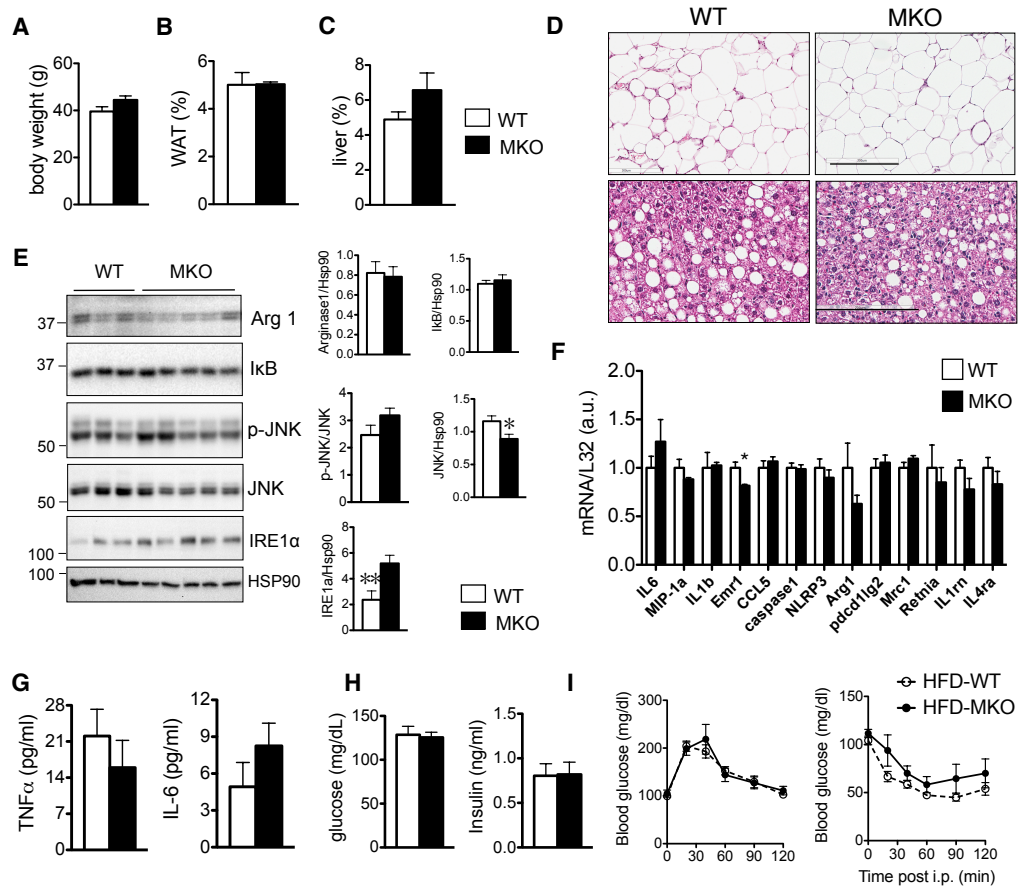


Figure 3.7 Sell1L in macrophages is not required for chronic inflammatory responses in obesity.

WT and MKO mice (n=6 each) were set on HFD from week 6 continuously till week 20. (A) Body weight (B) Percentage of WAT weight and (C) Percentage of liver weight of WT or MKO mice. (D) HE staining of WAT and liver tissue sections of MKO or WT mice fed on HFD. (E) Western blots of Arginase 1 (Arg 1), I-kappa-B (I κ B), phosphorylated JNK (p-JNK), total JNK and IRE1 α in WAT after 20w HFD. Quantification of proteins as normalized to hsp90 was shown at the right side. (F) Q-PCR showed M1 M2 gene markers in WAT tissue in MKO and WT mice fed on HFD. (G) Serum TNF α and IL-6 levels were measured by ELISA. (H) Serum glucose level and insulin level after 18 hours fasting. (I) GTT and ITT in MKO or WT mice fed on HFD. Values represent mean \pm S.E. *, $p < 0.05$, and ***, $p < 0.005$.

SUPPLEMENTAL FIGURES

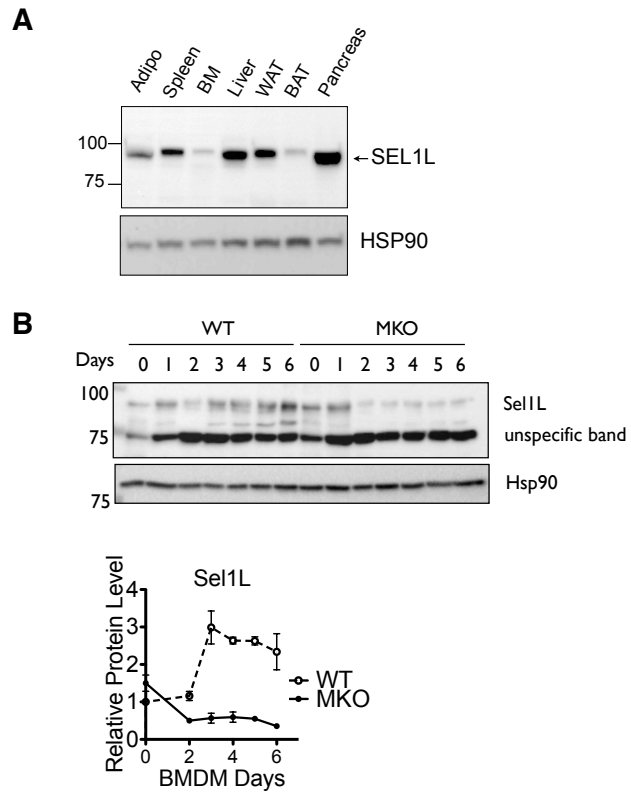


Figure S3.1 Distribution of Sel1L protein level in MKO mouse model.

(A) Sel1L protein levels in different adult mouse tissues. (B) Collected bone marrow cells from WT and MKO mice were cultured and stimulated by macrophage colony-stimulating factor (M-CSF) by a time course. Sel1L protein levels were shown in the western blot and the quantification was shown below. Hsp90, a loading control.

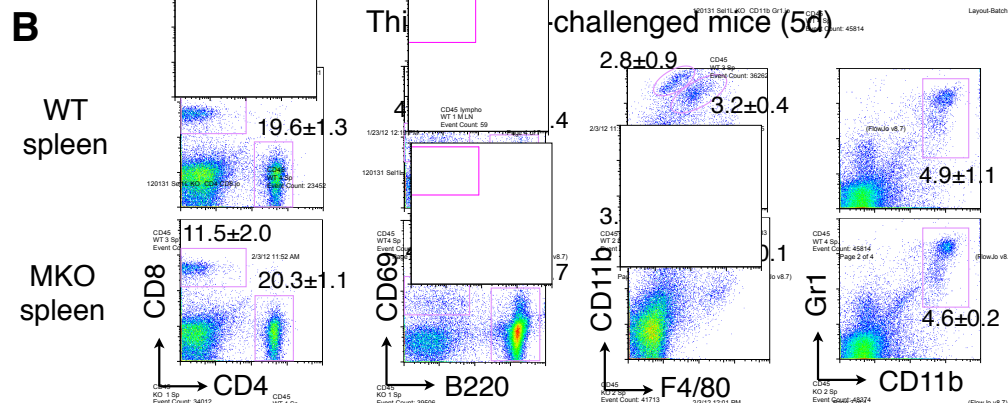
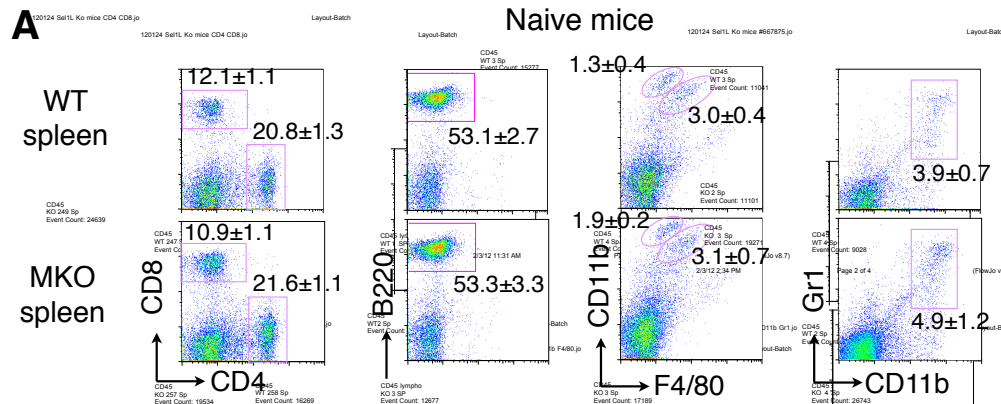


Figure S3.2 Normal spleen T cell and B cell population in naïve WT and MKO mice.

Naïve (A) or Thioglycollate-injected mice (B) spleens were dissected and analyzed by FACS. CD4 and CD8 antibodies were used to gate and quantify the percentage of T cells; B220 and CD69 were used to gate and quantify the percentage of B cells; CD11b and F4/80 antibodies were used to gate and quantify the percentage of macrophages. CD11b and Gr1 were used to gate and quantify the percentage of myeloid cell lines. (N=7 each and 2 repeats for CD4⁺, CD8⁺, B220⁺ FACS; N=4 each for F4/80⁺, Gr1⁺ FACS)

Peritoneal macrophages

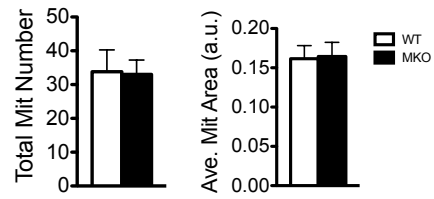
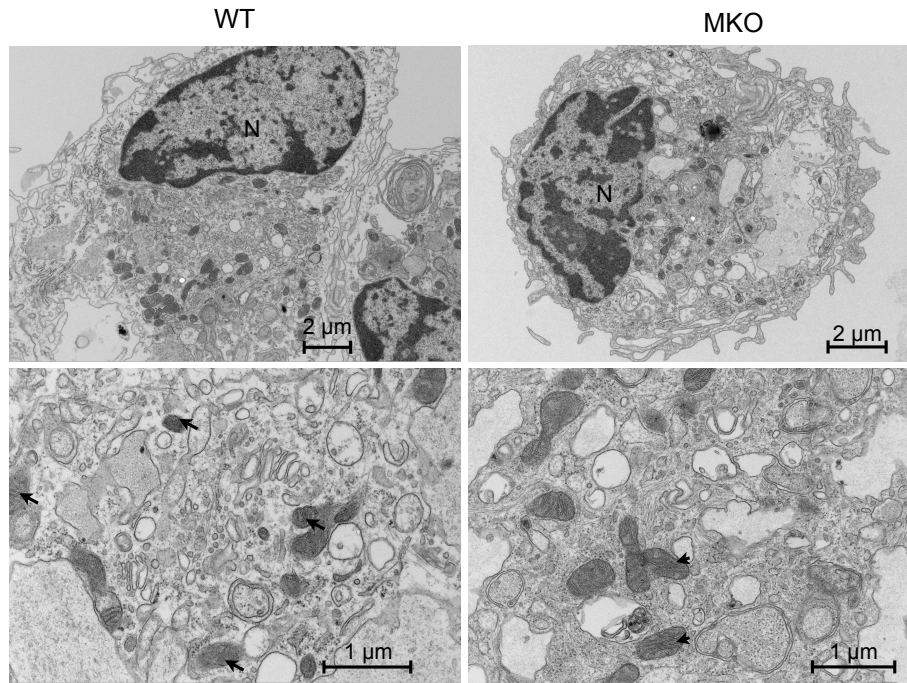


Figure S3.3 Normal Mitochondria number and morphology in MKO peritoneal macrophages.

Representative transmission electron microscopy (TEM) images of peritoneal macrophages are shown here. The scale bars were shown in the picture, with arrows indicating mitochondria and N indicating nucleus. Quantifications were shown on the right side.

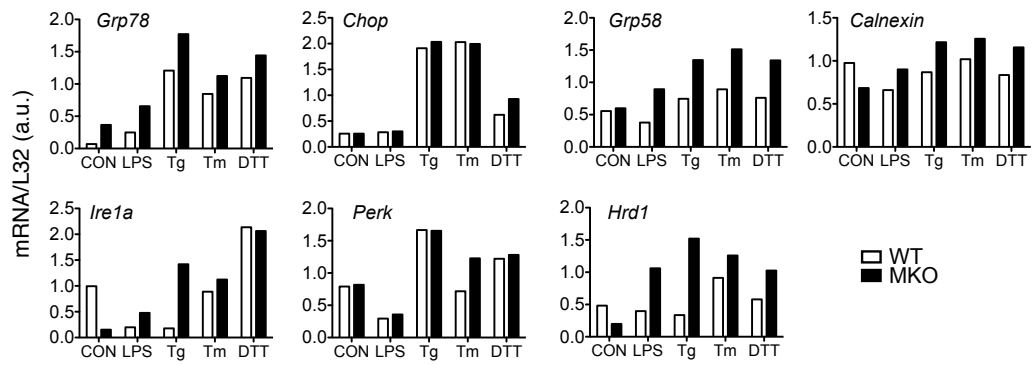


Figure S3.4 UPR genes in MKO peritoneal macrophages.

Peritoneal macrophages were cultured and treated in the conditions as listed above. Q-PCR was performed to show relative UPR gene expression levels in both the WT and MKO peritoneal macrophages.

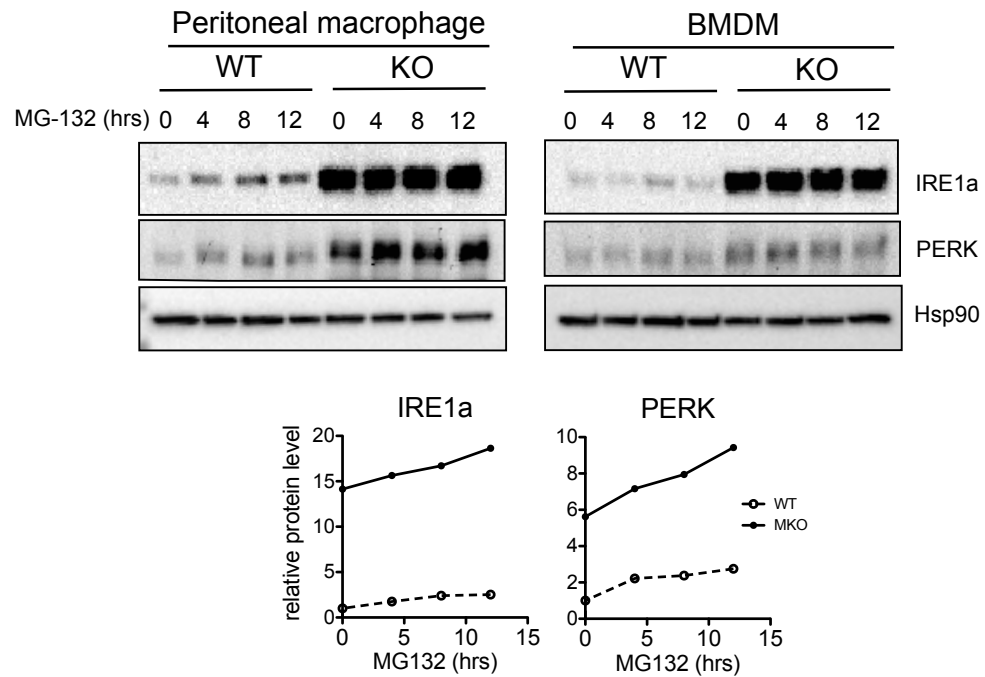


Figure S3.5 Accumulation of IRE1 α and PERK by blocking cytosolic proteasomes.

Peritoneal macrophages were collected and cultured overnight, then treated with MG-132 (1mM) for the indicated time course. Western blots showed the protein levels of IRE1 α and PERK. Hsp90 was a loading control. Quantifications were shown below.

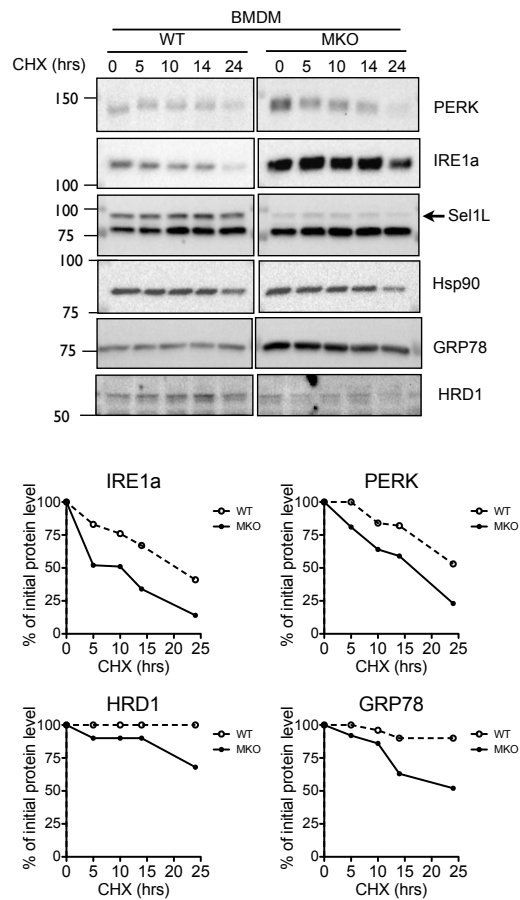


Figure S3.6 The half-life of UPR and ERAD component proteins in MKO macrophages.

Peritoneal macrophages were collected and cultured overnight, then treated with cycloheximide (CHX) (100 μ g/ml) for indicated time points. Western blots showed the protein levels of UPR and ERAD components. Hsp90 was a loading control. Quantifications of half-lives were shown below.

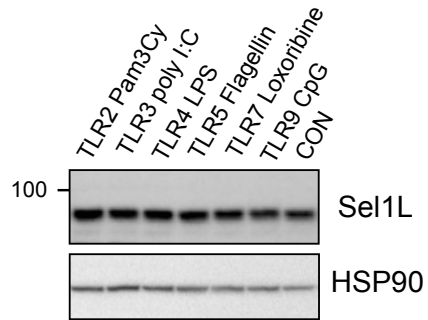
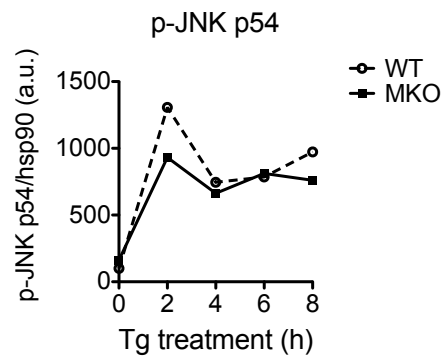
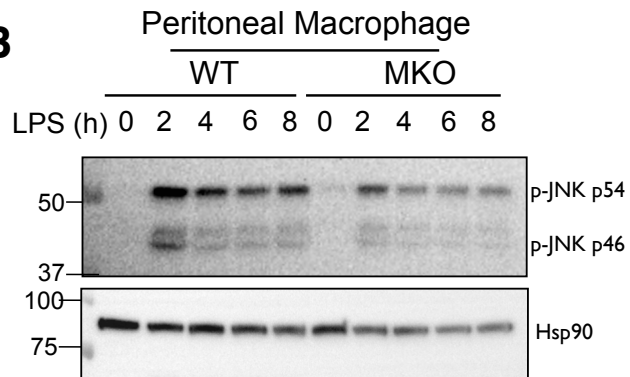
A**B**

Figure S3.7 MKO peritoneal macrophage inflammatory response model in vitro.

(A) Sel1L protein levels under the stimulation of various TLR agonists were indicated in the western blots. (B) Peritoneal macrophages were treated with LPS (1000ng/ml) by the indicated time points. P-JNKs were shown in the western blot. Hsp90 was a loading control. Quantification of p-JNK normalized to hsp90 was shown below.

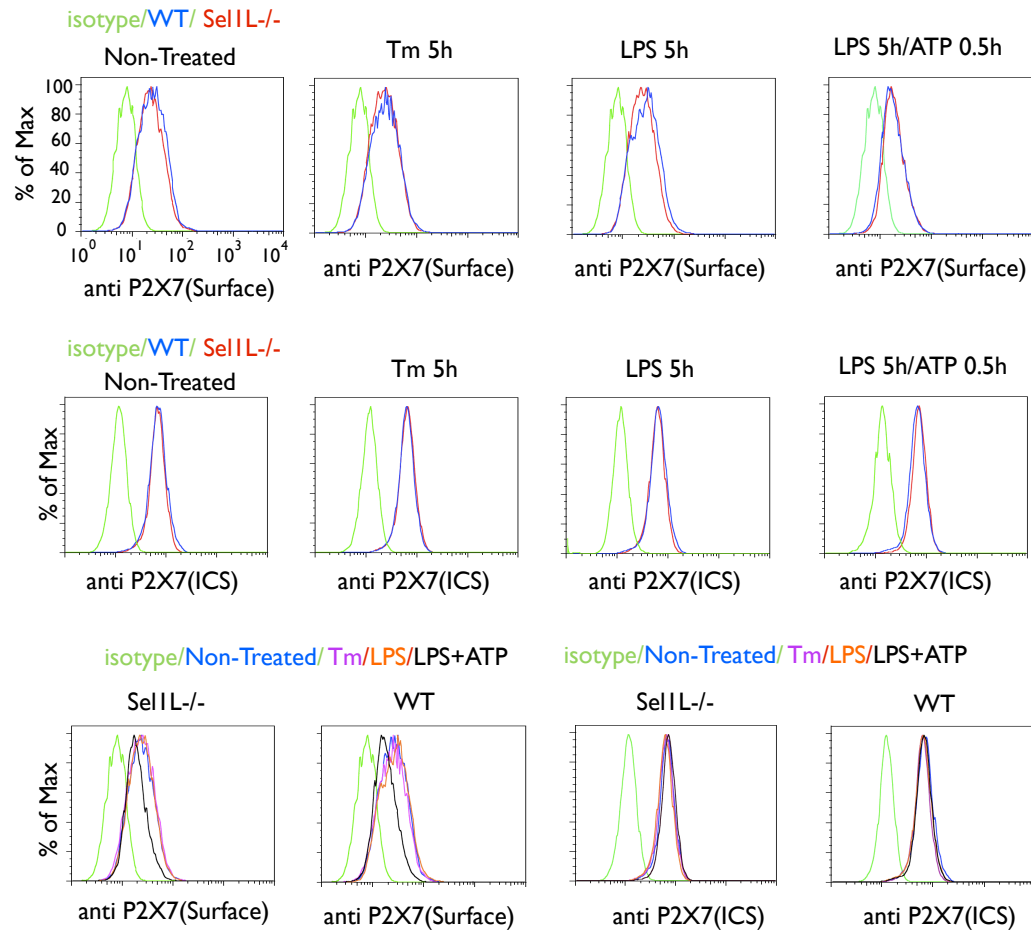


Figure S3.8 P2X7 levels in MKO peritoneal macrophages.

Peritoneal macrophages were treated with 0.1 $\mu\text{g/ml}$ LPS for 5 h followed by addition of 5 mM ATP for 30 min. Intracellular and cellular surface P2X7 levels with or without the treatment were measured by the flow cytometer.

3.5 DISCUSSION

The link between ER homeostasis, UPR and inflammation is an emerging paradigm for the inflammatory responses in many disease settings. The prevailing view that the ERAD functions as a critical regulator of cellular function is based largely on the premise that ERAD deficiency causes an accumulation of misfolded proteins, perturbs ER homeostasis and stimulates ER stress response. However, the physiological significance of ERAD pathways and the necessity of a particular ERAD pathway in the normal cellular function of a specific cell type remain largely unknown.

A recent study using liver-specific gp78 (a membrane-anchored ubiquitin ligase and main component of gp78 ERAD complex) knock-out mice showed that gp78 mediated the degradation of HMGCR via Insig proteins and ER stress is not activated based on chaperone GRP78 protein levels (381). By contrast, our present data in macrophages demonstrate that Sel1L deficiency significantly alters ER homeostasis with elevated protein levels of IRE1 α and a subset of chaperones. Nonetheless, we believe that the Sel1L-deficient macrophages have adapted to the loss of the Sel1-Hrd1 ERAD function through the function of UPR, thus rendering cells with very modest ER stress as judged by direct sensor phosphorylation (IRE1 α and PERK) and Xbp1 mRNA splicing (Figure 3.3). Indeed, compared to WT cells, MKO macrophages have significantly increased ER volume with dilated ER cisternae while cell apoptosis is normal under basal culture conditions. This suggests alterations of ER homeostasis and successful

cellular adaptation. The notion of cellular adaptation is further supported by both in vitro and in vivo studies of macrophage functions: innate responses to LPS shock, pathogen infection (cytokine release and survival), inflammasome activation and inflammation related to obesity were completely normal. Furthermore, using the phos-tag approach, we showed that although total IRE1 α protein is dramatically increased, IRE1 α in MKO macrophages are only slightly hyperphosphorylated. Consistently, *Xbp1* mRNA splicing is only slightly upregulated in MKO macrophages. These observations were supported by recent in vitro studies where no-to-low UPR activation was noted in Sel1L-knockdown HeLa cells (186, 382). Collectively, these and our data suggest cellular adaptation to Sel1L and ERAD deficiency.

Our data provided direct and strong evidence that Sel1L plays a critical role in ERAD function, as indicated by previous elegant biochemical studies (166, 196, 345, 350). However, whether Sel1L function in vivo is exclusively mediated through the Hrd1 ERAD complex remains unknown. Earlier in vitro studies have shown that in the absence of Sel1L, Hrd1-mediated degradation of model substrate antigens such as T-cell receptor (TCR), mutant transthyretin (TTR^{D18G}) and null Hong Kong variant of α 1-antitrypsin (A1AT^{NHK}) is attenuated. Interestingly, a recent study showed that the Hrd1 substrate glutamate receptor subunit (GluR1) may be Sel1L-independent (345), suggesting that Sel1L may not be involved in the degradation of all Hrd1 substrates. On the other hand, Sel1L may have Hrd1-independent functions as it has been reported that not all Sel1L is associated with Hrd1 (135, 383, 384). Nonetheless, proteomic analyses from two

laboratories in HEK293T and HeLa cells have identified a number of Sel1L-interacting proteins, most of which are involved in the ERAD function (166, 345, 350). This list includes Hrd1 and p97, key components of ERAD; and OS-9 and XTP-3B, two lectins that help define substrate specificity for the ERAD complex. More studies are required to determine whether other aspects of macrophage function, such as iron metabolism, are impaired in MKO mice and whether Sel1L has additional ERAD-independent functions. The identification of bona fide Sel1L-Hrd1 substrates in macrophages will help address these questions.

Our data showed that both IRE1 α and PERK protein levels are dramatically elevated in Sel1L-deficient macrophages, although IRE1 α phosphorylation and RNase activity are not. The increase of IRE1 α protein has also been observed, albeit to a much lesser extent, in Derlin 2- and XBP1- deficient cells (222, 364). Whether IRE1 α and PERK are direct substrates of the Sel1L-Hrd1 ERAD complex remains to be demonstrated. Moreover, unlike that in Sel1L-deficient macrophages, IRE1 α in XBP1-deficient hepatocytes is hyperphosphorylated with elevated IRE1 α RNase activity (222). The authors proposed that this might be due to the negative feedback regulatory mechanism of IRE1 α by XBP1s. Thus, the difference in IRE1 α activity between Sel1L- and XBP1-deficient cells may be due to the different levels of XBP1s proteins. In addition, unlike our MKO mice, mice with macrophage-specific deletion in *Xbp1* gene are defective in inflammatory responses against LPS challenges and bacterial infections (298). Mechanistically, Martinon et al. (2010) showed that the TLR signaling synergizes with the IRE1 α -XBP1 pathway, in part through XBP1s-mediated transcriptional

regulation of various inflammatory cytokines. Thus, the Sel1L MKO mouse model is not equivalent to the UPR sensor- or effector- null mouse models, as in MKO mice, the three UPR branches are intact thus allowing them to respond efficiently to the disturbance of ER homeostasis.

Why MKO macrophages and mice showed no defects in immunity functions could also be explained by multiple compensatory mechanisms: First, increases in the levels of chaperones and ER volume via the UPR pathway could explain this phenomenon. Second, the function of Sel1L/HRD1 ERAD complex could also be compensated for by other ERAD complexes (385). And third, increased autophagy functions or other proteasome pathways could compensate for the defect of ERAD function. Another possibility is the existence of macrophage specific Sel1L isoforms. Currently, there are five predicted isoforms of Sel1L based on computational predictions and experimental confirmations: Sel1LA/B/C/D/E (348). These isoforms are the result of alternative splicing. Although none of the predicted sizes of known Sel1L isoforms match the lower bands found on the Sel1L western blot, there is still a possibility that macrophage-specific Sel1L variants may exist. These isoforms may not be completely knocked out by the Flox-Cre system. It could be an isoform with a random start codon after the exon 6, or it could be an isoform that skips the exon 6. Thus, more research needs to be performed to identify the mechanisms for these unexpected results, which show that Sel1L is dispensable for macrophages immunity functions.

Sel1L is ubiquitously expressed in tissues and most abundantly in secretory organs such as the pancreas. Although the *Sel-1* null worm and *Hrd3* deficient yeast are viable, whole body Sel1L knock out mice are embryonic lethal (352). The embryos did not survive embryonic day e14.5, indicating a critical developmental stage that requires the Sel1L function. Whether this is related to its ERAD function or other functions such as the Notch signaling pathway remains unclear. Interestingly, in addition to two isoforms of Sel1L, there are two homologs of Sel1L in mice and humans: Sel1L2 and Sel1L3 (<http://genome.ucsc.edu>). The functions of these two homologs are completely unknown. As Sel1L2 shares more than a 50 percent identity with Sel1L and is predicted to be a transmembrane protein, it may be able to compensate for Sel1L ERAD function in the absence of Sel1L. Further characterization of tissue-specific functions of Sel1L and its isoforms may help identify the importance of Sel1L in various cell types in vivo.

We have concluded that although Sel1L deficiency disrupts a key ERAD function, it does not result in a sustained UPR. This is probably due to the compensatory function of other quality-control systems that allow adaptation to Sel1L knock out. In other words, Sel1L-deficient cells have re-set their ER homeostasis, also known as “proteostasis” (386, 387). Whether this is true in cell types other than macrophages or tissues remains to be seen. It is also interesting to note the similarities between our macrophage-specific Sel1L-deficient mice and mice with Derlin 2 deficiency, specifically in hepatocytes and B cells where the increased protein levels of several chaperones and IRE1 α were noted (364).

3.6 ACKNOWLEDGEMENTS

We thank Drs. Cindy Leifer, H. Ploegh and M. Freeman for reagents and antibodies; John L. Grazul for assistant in TEM analysis; and members of the Qi Lab for technical assistance and discussions. This study is supported by NIH R01DK082582, ADA 07-08-JF-47 and 1-12-CD-04 (L.Q.).

AUTHOR CONTRIBUTIONS

Z.X. designed and performed most experiments, revised the manuscript; Y.J. performed flow cytometric analysis of ER mass, immunotyping in adipose tissue and spleen, and assisted with in vivo study in LPS study; S.S. performed Q-PCR and assisted with some in vivo studies; H.K. performed surface MHC class I/II analysis and T cell activation in vitro; H.M. performed the Listeria infection study; Q.L. provided the floxed mice; L.Q. designed the experiments and wrote the manuscript. Everybody analyzed data and commented on the manuscript.

COMPETING FINANCIAL INTERESTS The authors declare no competing financial interests.

Chapter 4 SUMMARY AND FUTURE DIRECTIONS

It has been concluded that the unfolded protein response plays an important role in maintaining cell ER protein homeostasis. IRE1 α , PERK and ATF6, the three major UPR pathways, respond to ER stress by up-regulating protein folding capacity, global translation attenuation and enhancing ER protein degradation. The activation of the UPR pathways is tightly regulated under various physiological and pathological conditions in a both tissue specific and temporally specific manner, depending on the kind of stimulation received. The UPR plays an essential role, not only in normal developmental process, but also in metabolic diseases such as obesity and diabetes, cardiovascular diseases, cancer, neurodegenerative diseases and immune diseases. Therefore, it is desired, yet challenging, to dissect the UPR pathways under variable conditions. At the same time, the molecular mechanism of UPR regulation is also of importance for further research into new therapies that target UPR pathways.

This thesis focused on both the physiological functions of ERAD and on the molecular mechanisms of UPR activation. In Chapter 2, a highly conserved proline residue at IRE1 α position 830 (P830) was determined to be critical for IRE1 α structural integrity, as well as the activation of both kinase and RNase domains. Structural analysis revealed that P830 may form a highly conserved structural linker with adjacent tryptophan and tyrosine residues at positions 833 and 945 (W833 and Y945), thereby bridging the kinase and RNase domains. Mutation of P830 to leucine (P830L) completely abolished the kinase and RNase

activities, thus significantly decreasing protein stability and preventing oligomerization of IRE1 α upon ER stress.

Besides the individual amino acid residue functions and inner-molecule or inter-molecule interactions, there are several other aspects to be further studied for a better understanding of the molecular mechanism of IRE1 α activation.

1) IRE1 is known to interact with multiple cofactors to facilitate diversified downstream effects. For example IRE1-TRAF2-ASK1 complex activates the JNK pathway (131), and IRE1 α -TXNIP activates the NLRP3 inflammasome and terminal UPR pathway to induce apoptosis (339). Certain cofactors are also required to resolve IRE1 α activation; e.g. nonmuscle myosin heavy chain IIB is required for IRE1 α aggregation and foci formation. It is likely there are more interactive proteins associated with IRE1 α to regulate its activation function, particularly in a tissue-specific manner. Therefore, in future research, I propose to perform IRE1 α Immunoprecipitation in different detergent buffers. Further, I will perform protein mass spectrometry to identify more interacting proteins with IRE1 α and then use specific knock-out or overexpression model to study the relevant biological functions.

2) Based on IRE1 α kinase activation, RNase domain of IRE α will undergo conformational change and cleave the mRNA XBP1u to form XBP1s. However, it is still not clear how XBP1u is recruited to IRE1 α and whether there is cross-talk between IRE1 α sensor and XBP1 trafficking. On the other hand, it's not clear

yet how the cleaved XBPs regulate the negative feedback to suppress IRE1 α . Understanding the cross-talk between IRE1 α -XBP1 is essential for further manipulating of this pathway.

3) Under ER stress conditions, IRE1 α mRNA and total protein levels are not significantly increased (Fig S3.4). This indicates a fast reaction based on phosphorylation and conformational change. Chemical compounds are now being developed to modulate the signaling output from IRE1 α . For yeast IRE1 α , Papa first made a L745G mutant IRE1 α which, while bypassing the kinase activity and phosphorylation, can constitutively activate all downstream functions at the presence of ATP-competitive inhibitor 1NM-PP1 through conformational change in the kinase domain (320). In addition, ADP, APY29, Cdk1/2 inhibitor III, and JAK inhibitor 1 all bound the IRE1 α cytosolic domain and help conformational change in back-to-back dimers, which correlates with stimulation of IRE1 nuclease activity (388). More importantly, these chemical compounds need to be studied in mammalian IRE1 α , as mammalian IRE1 α are able to form high order oligomers (334), indicating a slightly different activation mechanism. I would propose to work on the crystal structure of mammalian IRE1 α structure, test the compatibility of chemical compounds and identify new ones for drug discovery.

4) In Sel1L knock-out macrophages, we observed more than a ten-fold increase in IRE1 α protein levels. It was indicated in the previous research that IRE1 α is degraded through HRD1 (389). Data in Chapter 3 also suggested a possibility that Sel1L regulates the IRE1 α degradation by HRD1. Therefore I

propose in future research to delineate the relative role of Sel1L, HRD1, Derlin1 or Derlin2, and other interaction proteins facilitating IRE1 α degradation. It is interesting that the increase in phosphorylated forms of IRE1 α is much less than the total IRE1 α protein accumulation. This indicates that the constitutive dephosphorylation process was increased. Whether Sel1L regulates the IRE1 α dephosphorylation process is still unknown.

In chapter 3, the physiological role of Sel1L in macrophage innate immunology was studied. Although ERAD plays an important role in maintaining ER protein homeostasis, and previous research has shown a close link between UPR activation and inflammatory response (reviewed in chapter 1.5.2), surprisingly our results showed that Sel1L is dispensable for macrophage immune functions including antigen presentation, cytokine secretion, pathogen defense and mild inflammatory response in metabolic diseases. This indicates compensatory mechanisms exist to cope with Sel1L defects. For future study, I propose to focus on possible compensatory mechanisms. This is important because it helps us understand the cross-talk between ERAD and UPR pathways, as well as the tissue specific function of ERAD, since other tissue Sel1L knock-out models in our lab showed different defective phenotypes.

The first hypothesis is that other mammalian ERAD E3 complex compensates for Sel1L knock-out and a decrease in HRD1 protein level. Secondly, it is possible that the overall process of protein transportation, from the ER to the Golgi and then to lysosome or extracellular, is enhanced. Third, it could be the

activation of autophagosomes. Fourth, other protein degradation pathways such as a proteasome system in the nuclear could compensate for protein degradation. And fifth, it could be that in macrophages there are no important physiological substrates that are strictly dependent on Sel1L-HRD1 degradation. Therefore, future study could utilize different antagonists to block individual compensatory pathways to identify the most important ones. For example 3-Methyladenine (3-MA) could be used to block autophagy (390), MG-132 to block the proteasome, the downstream common pathway of ERAD, and Eeyarestatin to inhibit P97 (391). Identification of compensatory pathways will reveal the overall protein degradation cross-talk in macrophages.

REFERENCES

1. Brodsky JL, Wojcikiewicz RJH. Substrate-specific mediators of ER associated degradation (ERAD). *Curr Opin Cell Biol.* 2009;21(4):516–521.
2. Walter P, Ibrahimi I, Blobel G. Translocation of proteins across the endoplasmic reticulum. I. Signal recognition protein (SRP) binds to in-vitro-assembled polysomes synthesizing secretory protein. *J Cell Biol.* 1981;91(2 Pt 1):545–550.
3. Walter P, Blobel G. Translocation of proteins across the endoplasmic reticulum. II. Signal recognition protein (SRP) mediates the selective binding to microsomal membranes of in-vitro-assembled polysomes synthesizing secretory protein. *J Cell Biol.* 1981;91(2 Pt 1):551–556.
4. Walter P, Blobel G. Translocation of proteins across the endoplasmic reticulum III. Signal recognition protein (SRP) causes signal sequence-dependent and site-specific arrest of chain elongation that is released by microsomal membranes. *J Cell Biol.* 1981;91(2 Pt 1):557–561.
5. Lingappa VR, Blobel G. Early events in the biosynthesis of secretory and membrane proteins: the signal hypothesis. *Recent Prog Horm Res.* 1980;36:451–475.
6. Hyde M, Block-Alper L, Felix J, Webster P, Meyer DI. Induction of secretory pathway components in yeast is associated with increased stability of their mRNA. *J Cell Biol.* 2002;156(6):993–1001.
7. Unsworth H, Raguz S, Edwards HJ, Higgins CF, Yagüe E. mRNA escape from stress granule sequestration is dictated by localization to the endoplasmic reticulum. *FASEB J.* 2010;24(9):3370–3380.
8. Reid DW, Nicchitta CV. Primary role for endoplasmic reticulum-bound ribosomes in cellular translation identified by ribosome profiling. *J Biol Chem.* 2012;287(8):5518–5527.
9. Chen Q, Jagannathan S, Reid DW, Zheng T, Nicchitta CV. Hierarchical regulation of mRNA partitioning between the cytoplasm and the endoplasmic reticulum of mammalian cells. *Mol Biol Cell.* 2011;22(14):2646–2658.
10. Besse F, Ephrussi A. Translational control of localized mRNAs: restricting protein synthesis in space and time. *Nat Rev Mol Cell Biol.* 2008;9(12):971–980.

11. Kondrashov N et al. Ribosome-mediated specificity in Hox mRNA translation and vertebrate tissue patterning. *Cell*. 2011;145(3):383–397.
12. Palmiter RD. Quantitation of parameters that determine the rate of ovalbumin synthesis. *Cell*. 1975;4(3):189.
13. Bouadloun F, Donner D, Kurland CG. Codon-specific missense errors in vivo. *EMBO J*. 1983;2(8):1351–1356.
14. Edelmann P, Gallant J. Mistranslation in *E. coli*. *Cell*. 1977;10(1):131–137.
15. Kramer EB, Farabaugh PJ. The frequency of translational misreading errors in *E. coli* is largely determined by tRNA competition. *RNA*. 2007;13(1):87–96.
16. Ogle JM, Ramakrishnan V. Structural insights into translational fidelity. *Annu Rev Biochem*. 2005;74:129–177.
17. Stephens SB, Nicchitta CV. Divergent regulation of protein synthesis in the cytosol and endoplasmic reticulum compartments of mammalian cells. *Mol Biol Cell*. 2008;19(2):623–632.
18. Hebert DN, Molinari M. In and out of the ER: protein folding, quality control, degradation, and related human diseases 2007;
19. Lee AS. The glucose-regulated proteins: stress induction and clinical applications. *Trends Biochem Sci*. 2001;26(8):504–510.
20. Shiu RP, Pouyssegur J, Pastan I. Glucose depletion accounts for the induction of two transformation-sensitive membrane proteins in Rous sarcoma virus-transformed chick embryo fibroblasts. *Proc Natl Acad Sci USA*. 1977;74(9):3840–3844.
21. Cabral CM, Liu Y, Moremen KW, Sifers RN. Organizational diversity among distinct glycoprotein endoplasmic reticulum-associated degradation programs. *Mol Biol Cell*. 2002;13(8):2639–2650.
22. Kabani M et al. Dependence of endoplasmic reticulum-associated degradation on the peptide binding domain and concentration of BiP. *Mol Biol Cell*. 2003;14(8):3437–3448.
23. Molinari M, Galli C, Piccaluga V, Pieren M, Paganetti P. Sequential assistance of molecular chaperones and transient formation of covalent complexes during protein degradation from the ER. *J Cell Biol*. 2002;158(2):247–257.

24. Sörgjerd K et al. Retention of misfolded mutant transthyretin by the chaperone BiP/GRP78 mitigates amyloidogenesis. *J Mol Biol.* 2006;356(2):469–482.
25. Schröder M, Kaufman RJ. The mammalian unfolded protein response. *Annu Rev Biochem.* 2005;
26. Parodi AJ. Protein glucosylation and its role in protein folding. *Annu Rev Biochem.* 2000;69:69–93.
27. Parodi AJ, Behrens NH, Leloir LF, Carminatti H. The role of polyprenol-bound saccharides as intermediates in glycoprotein synthesis in liver. *Proc Natl Acad Sci USA.* 1972;69(11):3268–3272.
28. Deprez P, Gautschi M, Helenius A. More than one glycan is needed for ER glucosidase II to allow entry of glycoproteins into the calnexin/calreticulin cycle. *Mol Cell.* 2005;
29. Coe H, Michalak M. ERp57, a multifunctional endoplasmic reticulum resident oxidoreductase. *Int J Biochem Cell Biol.* 2010;42(6):796–799.
30. Pearse BR et al. The role of UDP-Glc:glycoprotein glucosyltransferase 1 in the maturation of an obligate substrate prosaposin. *J Cell Biol.* 2010;189(5):829–841.
31. Molinari M, Galli C, Vanoni O, Arnold SM, Kaufman RJ. Persistent Glycoprotein Misfolding Activates the Glucosidase II/UGT1-Driven Calnexin Cycle to Delay Aggregation and Loss of Folding Competence. *Mol Cell.* 2005;20(4):503–512.
32. Pearse BR, Gabriel L, Wang N, Hebert DN. A cell-based reglucosylation assay demonstrates the role of GT1 in the quality control of a maturing glycoprotein. *J Cell Biol.* 2008;181(2):309–320.
33. Brodsky JL. Cleaning up: ER-associated degradation to the rescue. *Cell.* 2012;151(6):1163–1167.
34. Molinari M. N-glycan structure dictates extension of protein folding or onset of disposal. *Nature chemical biology.* 2007;
35. Malhotra JD, Kaufman RJ. The endoplasmic reticulum and the unfolded protein response. *Seminars in Cell & Developmental Biology.* 2007;18(6):716–731.

36. Molinari M, Eriksson KK, Calanca V, Galli C. Contrasting functions of calreticulin and calnexin in glycoprotein folding and ER quality control. *Mol Cell*. 2004;
37. Soldà T, Garbi N, Hämmerling GJ, Molinari M. Consequences of ERp57 deletion on oxidative folding of obligate and facultative clients of the calnexin cycle. *Journal of Biological ...*. 2006;
38. Garbi N, Tanaka S, Momburg F, Hämmerling GJ. Impaired assembly of the major histocompatibility complex class I peptide-loading complex in mice deficient in the oxidoreductase ERp57. *Nat Immunol*. 2005;7(1):93–102.
39. Mesaeli N, Nakamura K, Zvaritch E, Dickie P. Calreticulin is essential for cardiac development. *The Journal of cell ...*. 1999;
40. Groenendyk J, Lynch J, Michalak M. Calreticulin, Ca²⁺, and calcineurin-signaling from the endoplasmic reticulum. *Mol Cells*. 2004;
41. Denzel A et al. Early Postnatal Death and Motor Disorders in Mice Congenitally Deficient in Calnexin Expression. *Mol Cell Biol*. 2002;22(21):7398–7404.
42. De Praeter CM et al. A Novel Disorder Caused by Defective Biosynthesis of N-Linked Oligosaccharides Due to Glucosidase I Deficiency. *The American Journal of Human Genetics*. 2000;66(6):1744–1756.
43. Gao B, Adhikari R, Howarth M, Nakamura K, Gold MC. Assembly and antigen-presenting function of MHC class I molecules in cells lacking the ER chaperone calreticulin. *Immunity*. 2002;
44. Sevier CS, Kaiser CA. Formation and transfer of disulphide bonds in living cells. *Nat Rev Mol Cell Biol*. 2002;3(11):836–847.
45. Tsai B, Rodighiero C, Lencer WI, Rapoport TA. Protein disulfide isomerase acts as a redox-dependent chaperone to unfold cholera toxin. *Cell*. 2001;
46. Ferrari D, Soling H. The protein disulphide-isomerase family: unravelling a string of folds. *Biochem J*. 1999;
47. Freedman RB, Klappa P, Ruddock LW. Protein disulfide isomerases exploit synergy between catalytic and specific binding domains. *EMBO Rep*. 2002;
48. Oliver JD, van der Wal FJ, Bulleid NJ, High S. Interaction of the thiol-

- dependent reductase ERp57 with nascent glycoproteins. *Science*. 1997;
49. Molinari M, Helenius A. Glycoproteins form mixed disulphides with oxidoreductases during folding in living cells. *Nature*. 1999;
50. Bu G. The roles of receptor-associated protein (RAP) as a molecular chaperone for members of the LDL receptor family. *International review of cytology*. 2001;
51. Li Y, Lu W, Schwartz AL, Bu G. Receptor-associated protein facilitates proper folding and maturation of the low-density lipoprotein receptor and its class 2 mutants. *Biochemistry*. 2002;
52. Tasab M, Batten MR, Bulleid NJ. Hsp47: a molecular chaperone that interacts with and stabilizes correctly-folded procollagen. *EMBO J*. 2000;
53. Nagai N et al. Embryonic lethality of molecular chaperone hsp47 knockout mice is associated with defects in collagen biosynthesis. *J Cell Biol*. 2000;150(6):1499–1506.
54. Claessen JHL, Kundrat L, Ploegh HL. Protein quality control in the ER: balancing the ubiquitin checkbook. *Trends in Cell Biology*. 2012;22(1):22–32.
55. Kaufman RJ et al. The unfolded protein response in nutrient sensing and differentiation. *Nat Rev Mol Cell Biol*. 2002;3(6):411–421.
56. Benali-Furet NL, Chami M, Houel L, De Giorgi F. Hepatitis C virus core triggers apoptosis in liver cells by inducing ER stress and ER calcium depletion. *Oncogene*. 2005;
57. Peters LR, Raghavan M. Endoplasmic reticulum calcium depletion impacts chaperone secretion, innate immunity, and phagocytic uptake of cells. *J Immunol*. 2011;187(2):919–931.
58. Wang H et al. The ubiquitin ligase Hrd1 promotes degradation of the Z variant alpha 1-antitrypsin and increases its solubility. *Mol Cell Biochem*. 2011;346(1-2):137–145.
59. Imai Y et al. An Unfolded Putative Transmembrane Polypeptide, which Can Lead to Endoplasmic Reticulum Stress, Is a Substrate of Parkin. *Cell*. 2001;105(7):891–902.
60. Sagara Y, Inesi G. Inhibition of the sarcoplasmic reticulum Ca²⁺ transport

- ATPase by thapsigargin at subnanomolar concentrations. *Journal of Biological Chemistry*. 1991;
61. Kuo SC, Lampen JO. Tunicamycin—an inhibitor of yeast glycoprotein synthesis. *Biochemical and biophysical research* 1974;
 62. Shen X, Zhang K, Kaufman RJ. The unfolded protein response—a stress signaling pathway of the endoplasmic reticulum. *Journal of Chemical Neuroanatomy*. 2004;28(1-2):79–92.
 63. Walter P, Ron D. The unfolded protein response: from stress pathway to homeostatic regulation. *Science*. 2011;334(6059):1081–1086.
 64. Hetz C, Glimcher LH. Fine-tuning of the unfolded protein response: Assembling the IRE1alpha interactome. *Mol Cell*. 2009;35(5):551–561.
 65. Kohno K. Stress-sensing mechanisms in the unfolded protein response: similarities and differences between yeast and mammals. *Journal of Biochemistry*. 2010;147(1):27–33.
 66. Iwawaki T, Akai R, Yamanaka S, Kohno K. Function of IRE1 alpha in the placenta is essential for placental development and embryonic viability. *Proc Natl Acad Sci USA*. 2009;106(39):16657–16662.
 67. Tsuru A et al. Negative feedback by IRE1β optimizes mucin production in goblet cells. *Proc Natl Acad Sci USA*. 2013;110(8):2864–2869.
 68. Yoshida H, Matsui T, Yamamoto A, Okada T, Mori K. XBP1 mRNA Is Induced by ATF6 and Spliced by IRE1 in Response to ER Stress to Produce a Highly Active Transcription Factor. *Cell*. 2001;107(7):881–891.
 69. Yoshida H, Oku M, Suzuki M, Mori K. pXBP1(U) encoded in XBP1 pre-mRNA negatively regulates unfolded protein response activator pXBP1(S) in mammalian ER stress response. *J Cell Biol*. 2006;172(4):565–575.
 70. Masaki T, Yoshida M, Noguchi S. Targeted disruption of CRE-binding factor TREB5 gene leads to cellular necrosis in cardiac myocytes at the embryonic stage. *Biochem Biophys Res Commun*. 1999;261(2):350–356.
 71. Reimold AM et al. An essential role in liver development for transcription factor XBP-1. *Genes Dev*. 2000;14(2):152–157.
 72. Reimold AM et al. Plasma cell differentiation requires the transcription factor

- XBP-1. *Nature*. 2001;412(6844):300–307.
73. Lee A-H, Chu GC, Iwakoshi NN, Glimcher LH. XBP-1 is required for biogenesis of cellular secretory machinery of exocrine glands. *EMBO J*. 2005;24(24):4368–4380.
74. Acosta-Alvear D et al. XBP1 Controls Diverse Cell Type- and Condition-Specific Transcriptional Regulatory Networks. *Mol Cell*. 2007;27(1):53–66.
75. Hollien J, Weissman JS. Decay of endoplasmic reticulum-localized mRNAs during the unfolded protein response. *Science*. 2006;313(5783):104–107.
76. Dong B, Niwa M, Walter P, Silverman RH. Basis for regulated RNA cleavage by functional analysis of RNase L and Ire1p. *RNA*. 2001;7(3):361–373.
77. Doma MK, Parker R. Endonucleolytic cleavage of eukaryotic mRNAs with stalls in translation elongation. *Nature*. 2006;440(7083):561–564.
78. Kimmig P et al. The unfolded protein response in fission yeast modulates stability of select mRNAs to maintain protein homeostasis. *Elife*. 2012;1:e00048.
79. Hur KY et al. IRE1 α activation protects mice against acetaminophen-induced hepatotoxicity. *J Exp Med*. 2012;209(2):307–318.
80. Shore GC, Papa FR, Oakes SA. Signaling cell death from the endoplasmic reticulum stress response. *Curr Opin Cell Biol*. 2011;23(2):143–149.
81. Lin JH et al. IRE1 signaling affects cell fate during the unfolded protein response. *Science*. 2007;318(5852):944–949.
82. Lin JH, Li H, Zhang Y, Ron D, Walter P. Divergent effects of PERK and IRE1 signaling on cell viability. *PLoS ONE*. 2009;4(1):e4170.
83. Hetz C. The unfolded protein response: controlling cell fate decisions under ER stress and beyond. *Nat Rev Mol Cell Biol*. 2012;13(2):89–102.
84. Upton J-P et al. IRE1 α cleaves select microRNAs during ER stress to derepress translation of proapoptotic Caspase-2. *Science*. 2012;338(6108):818–822.
85. Nishitoh H et al. ASK1 is essential for endoplasmic reticulum stress-induced neuronal cell death triggered by expanded polyglutamine repeats. *Genes Dev*. 2002;16(11):1345–1355.

86. Takeda K, Matsuzawa A, Nishitoh H, Ichijo H. Roles of MAPKKK ASK1 in Stress-Induced Cell Death. *Cell Struct Funct.* 2003;28(1):23–29.
87. Kato H et al. mTORC1 serves ER stress-triggered apoptosis via selective activation of the IRE1–JNK pathway. *Cell Death Differ.* 2011;19(2):310–320.
88. Lei K, Davis RJ. JNK phosphorylation of Bim-related members of the Bcl2 family induces Bax-dependent apoptosis. *Proc Natl Acad Sci USA.* 2003;100(5):2432–2437.
89. Hetz C et al. Proapoptotic BAX and BAK modulate the unfolded protein response by a direct interaction with IRE1alpha. *Science.* 2006;312(5773):572–576.
90. Yamaguchi H, Wang H-G. CHOP is involved in endoplasmic reticulum stress-induced apoptosis by enhancing DR5 expression in human carcinoma cells. *J Biol Chem.* 2004;279(44):45495–45502.
91. Puthalakath H et al. ER stress triggers apoptosis by activating BH3-only protein Bim. *Cell.* 2007;129(7):1337–1349.
92. McCullough KD, Martindale JL, Klotz LO, Aw TY, Holbrook NJ. Gadd153 sensitizes cells to endoplasmic reticulum stress by down-regulating Bcl2 and perturbing the cellular redox state. *Mol Cell Biol.* 2001;21(4):1249–1259.
93. Sano R, Reed JC. ER stress-induced cell death mechanisms. *Biochim Biophys Acta.* [published online ahead of print: July 10, 2013]; doi:10.1016/j.bbamcr.2013.06.028
94. Kimata Y, Oikawa D, Shimizu Y, Ishiwata-Kimata Y, Kohno K. A role for BiP as an adjustor for the endoplasmic reticulum stress-sensing protein Ire1. *J Cell Biol.* 2004;167(3):445–456.
95. Gardner BM, Walter P. Unfolded Proteins Are Ire1-Activating Ligands That Directly Induce the Unfolded Protein Response. *Science.* 2011;333(6051):1891–1894.
96. Oikawa D, Kimata Y, Takeuchi M, Kohno K. An essential dimer-forming subregion of the endoplasmic reticulum stress sensor Ire1. *Biochem J.* 2005;391(Pt 1):135–142.
97. Oikawa D, Kimata Y, Kohno K. Self-association and BiP dissociation are not sufficient for activation of the ER stress sensor Ire1. *Journal of Cell Science.*

2007;120(9):1681–1688.

98. Credle JJ, Finer-Moore JS, Papa FR, Stroud RM, Walter P. On the mechanism of sensing unfolded protein in the endoplasmic reticulum. *Proc Natl Acad Sci USA*. 2005;102(52):18773–18784.

99. Oikawa D, Kimata Y, Kohno K, Iwawaki T. Activation of mammalian IRE1 α upon ER stress depends on dissociation of BiP rather than on direct interaction with unfolded proteins. *Experimental Cell Research*. 2009;315(15):2496–2504.

100. Pincus D et al. BiP binding to the ER-stress sensor Ire1 tunes the homeostatic behavior of the unfolded protein response. *PLoS Biol*. 2010;8(7):e1000415.

101. Oikawa D, Kitamura A, Kinjo M, Iwawaki T. Direct association of unfolded proteins with mammalian ER stress sensor, IRE1 β . *PLoS ONE*. 2012;7(12):e51290.

102. Liu CY, Wong HN, Schauerte JA, Kaufman RJ. The protein kinase/endoribonuclease IRE1 α that signals the unfolded protein response has a luminal N-terminal ligand-independent dimerization domain. *J Biol Chem*. 2002;277(21):18346–18356.

103. Ali MMU et al. Structure of the Ire1 autophosphorylation complex and implications for the unfolded protein response. *EMBO J*. 2011;30(5):894–905.

104. Korennykh AV et al. The unfolded protein response signals through high-order assembly of Ire1. *Nature*. 2009;457(7230):687–693.

105. Li H, Korennykh AV, Behrman SL, Walter P. Mammalian endoplasmic reticulum stress sensor IRE1 signals by dynamic clustering. *Proc Natl Acad Sci USA*. 2010;107(37):16113–16118.

106. He Y et al. Nonmuscle myosin IIB links cytoskeleton to IRE1 α signaling during ER stress. *Dev Cell*. 2012;23(6):1141–1152.

107. Ariyama H, Kono N, Matsuda S, Inoue T, Arai H. Decrease in membrane phospholipid unsaturation induces unfolded protein response. *J Biol Chem*. 2010;285(29):22027–22035.

108. Pineau L et al. Lipid-Induced ER Stress: Synergistic Effects of Sterols and Saturated Fatty Acids. *Traffic*. 2009;10(6):673–690.

109. Fu S et al. Aberrant lipid metabolism disrupts calcium homeostasis causing liver endoplasmic reticulum stress in obesity. *Nature*. 2011;473(7348):528–531.
110. Feng B et al. The endoplasmic reticulum is the site of cholesterol-induced cytotoxicity in macrophages. *Nat Cell Biol*. 2003;5(9):781–792.
111. Volmer R, van der Ploeg K, Ron D. Membrane lipid saturation activates endoplasmic reticulum unfolded protein response transducers through their transmembrane domains. *Proc Natl Acad Sci USA*. 2013;110(12):4628–4633.
112. Kebache S, Cardin E, Nguyễn DT, Chevet E, Larose L. Nck-1 antagonizes the endoplasmic reticulum stress-induced inhibition of translation. *J Biol Chem*. 2004;279(10):9662–9671.
113. Gebauer F, Hentze MW. Molecular mechanisms of translational control. *Nat Rev Mol Cell Biol*. 2004;5(10):827–835.
114. Hamanaka RB, Bobrovnikova-Marjon E, Ji X, Liebhaber SA, Diehl JA. PERK-dependent regulation of IAP translation during ER stress. *Oncogene*. 2009;28(6):910–920.
115. Harding HP, Zhang Y, Zeng H, Novoa I, Lu PD. An integrated stress response regulates amino acid metabolism and resistance to oxidative stress. *Mol Cell*. 2003;
116. Gotoh T, Terada K, Oyadomari S, Mori M. hsp70-DnaJ chaperone pair prevents nitric oxide- and CHOP-induced apoptosis by inhibiting translocation of Bax to mitochondria. *Cell Death Differ*. 2004;11(4):390–402.
117. van Huizen R, Martindale JL, Gorospe M, Holbrook NJ. P58IPK, a novel endoplasmic reticulum stress-inducible protein and potential negative regulator of eIF2alpha signaling. *J Biol Chem*. 2003;278(18):15558–15564.
118. Yan W et al. Control of PERK eIF2alpha kinase activity by the endoplasmic reticulum stress-induced molecular chaperone P58IPK. *Proc Natl Acad Sci USA*. 2002;99(25):15920–15925.
119. Novoa I, Zeng H, Harding HP, Ron D. Feedback inhibition of the unfolded protein response by GADD34-mediated dephosphorylation of eIF2alpha. *J Cell Biol*. 2001;153(5):1011–1022.
120. Jousse C et al. Inhibition of a constitutive translation initiation factor 2alpha phosphatase, CReP, promotes survival of stressed cells. *J Cell Biol*.

2003;163(4):767–775.

121. Chakrabarti A, Chen AW, Varner JD. A review of the mammalian unfolded protein response. *Biotechnol Bioeng*. 2011;108(12):2777–2793.

122. Haze K, Yoshida H, Yanagi H, Yura T. Mammalian transcription factor ATF6 is synthesized as a transmembrane protein and activated by proteolysis in response to endoplasmic reticulum stress. *Molecular biology of the ...*. 1999;

123. Ye J et al. ER stress induces cleavage of membrane-bound ATF6 by the same proteases that process SREBPs. *Mol Cell*. 2000;6(6):1355–1364.

124. Shen J, Chen X, Hendershot L, Prywes R. ER stress regulation of ATF6 localization by dissociation of BiP/GRP78 binding and unmasking of Golgi localization signals. *Dev Cell*. 2002;3(1):99–111.

125. Hong M et al. Underglycosylation of ATF6 as a novel sensing mechanism for activation of the unfolded protein response. *J Biol Chem*. 2004;279(12):11354–11363.

126. Nakanaka S, Okada T, Yoshida H, Mori K. Role of disulfide bridges formed in the luminal domain of ATF6 in sensing endoplasmic reticulum stress. *Mol Cell Biol*. 2007;27(3):1027–1043.

127. Yoshida H et al. ATF6 activated by proteolysis binds in the presence of NF- κ B directly to the cis-acting element responsible for the mammalian unfolded protein response. *Mol Cell Biol*. 2000;20(18):6755–6767.

128. Kokame K. Identification of ERSE-II, a New cis-Acting Element Responsible for the ATF6-dependent Mammalian Unfolded Protein Response. *Journal of Biological Chemistry*. 2000;276(12):9199–9205.

129. Belmont PJ et al. Coordination of growth and endoplasmic reticulum stress signaling by regulator of calcineurin 1 (RCAN1), a novel ATF6-inducible gene. *J Biol Chem*. 2008;283(20):14012–14021.

130. Wang HG, Pathan N, Ethell IM, Krajewski S. Ca²⁺-induced apoptosis through calcineurin dephosphorylation of BAD. *Science*. 1999;

131. Ron D, Walter P. Signal integration in the endoplasmic reticulum unfolded protein response. *Nat Rev Mol Cell Biol*. 2007;8(7):519–529.

132. Zeng L et al. ATF6 modulates SREBP2-mediated lipogenesis. *EMBO J*.

2004;23(4):950–958.

133. Yoshida H, Uemura A, Mori K. pXBP1(U), a Negative Regulator of the Unfolded Protein Response Activator pXBP1(S), Targets ATF6 but not ATF4 in Proteasome-mediated Degradation. *Cell Struct Funct.* 2009;34(1):1–10.

134. Smith MH, Ploegh HL, Weissman JS. Road to ruin: targeting proteins for degradation in the endoplasmic reticulum. *Science.* 2011;334(6059):1086–1090.

135. Gardner RG et al. Endoplasmic reticulum degradation requires lumen to cytosol signaling. Transmembrane control of Hrd1p by Hrd3p. *J Cell Biol.* 2000;151(1):69–82.

136. Gauss R, Sommer T, Jarosch E. The Hrd1p ligase complex forms a linchpin between ER-luminal substrate selection and Cdc48p recruitment. *EMBO J.* 2006;25(9):1827–1835.

137. Ravid T, Kreft SG, Hochstrasser M. Membrane and soluble substrates of the Doa10 ubiquitin ligase are degraded by distinct pathways. *EMBO J.* 2006;25(3):533–543.

138. Ismail N, Ng DTW. Have you HRD? Understanding ERAD is DOAble! *Cell.* 2006;126(2):237–239.

139. Kostova Z, Tsai YC, Weissman AM. Ubiquitin ligases, critical mediators of endoplasmic reticulum-associated degradation. *Seminars in Cell & Developmental Biology.* 2007;18(6):770–779.

140. Lenk U et al. A role for mammalian Ubc6 homologues in ER-associated protein degradation. *Journal of Cell Science.* 2002;115(Pt 14):3007–3014.

141. Arteaga MF, Wang L, Ravid T, Hochstrasser M, Canessa CM. An amphipathic helix targets serum and glucocorticoid-induced kinase 1 to the endoplasmic reticulum-associated ubiquitin-conjugation machinery. *Proc Natl Acad Sci USA.* 2006;103(30):11178–11183.

142. Younger JM et al. Sequential quality-control checkpoints triage misfolded cystic fibrosis transmembrane conductance regulator. *Cell.* 2006;126(3):571–582.

143. Chen B et al. The activity of a human endoplasmic reticulum-associated degradation E3, gp78, requires its Cue domain, RING finger, and an E2-binding site. *Proc Natl Acad Sci USA.* 2006;103(2):341–346.

144. Kikkert M et al. Human HRD1 is an E3 ubiquitin ligase involved in degradation of proteins from the endoplasmic reticulum. *J Biol Chem.* 2004;279(5):3525–3534.
145. Varga K et al. Efficient intracellular processing of the endogenous cystic fibrosis transmembrane conductance regulator in epithelial cell lines. *J Biol Chem.* 2004;279(21):22578–22584.
146. Alberti S, Böhse K, Arndt V, Schmitz A, Höhfeld J. The cochaperone HspBP1 inhibits the CHIP ubiquitin ligase and stimulates the maturation of the cystic fibrosis transmembrane conductance regulator. *Mol Biol Cell.* 2004;15(9):4003–4010.
147. Arndt V, Daniel C, Nastainczyk W, Alberti S, Höhfeld J. BAG-2 acts as an inhibitor of the chaperone-associated ubiquitin ligase CHIP. *Mol Biol Cell.* 2005;16(12):5891–5900.
148. Mimura N et al. Altered quality control in the endoplasmic reticulum causes cortical dysplasia in knock-in mice expressing a mutant BiP. *Mol Cell Biol.* 2008;28(1):293–301.
149. Caramelo JJ, Castro OA, Alonso LG. UDP-Glc: glycoprotein glucosyltransferase recognizes structured and solvent accessible hydrophobic patches in molten globule-like folding intermediates. In: 2003:
150. D'Alessio C, Caramelo JJ, Parodi AJ. UDP-Glc: glycoprotein glucosyltransferase-glucosidase II, the ying-yang of the ER quality control. *Seminars in cell & developmental* 2010;
151. Caramelo JJ, Parodi AJ. Getting in and out from calnexin/calreticulin cycles. *J Biol Chem.* 2008;283(16):10221–10225.
152. Groisman B, Shenkman M, Ron E, Lederkremer GZ. Mannose trimming is required for delivery of a glycoprotein from EDEM1 to XTP3-B and to late endoplasmic reticulum-associated degradation steps. *J Biol Chem.* 2011;286(2):1292–1300.
153. Fagioli C, Sitia R. Glycoprotein quality control in the endoplasmic reticulum. Mannose trimming by endoplasmic reticulum mannosidase I times the proteasomal degradation of unassembled immunoglobulin subunits. *J Biol Chem.* 2001;276(16):12885–12892.
154. Schelhaas M et al. Simian Virus 40 depends on ER protein folding and

- quality control factors for entry into host cells. *Cell*. 2007;131(3):516–529.
155. Ushioda R et al. ERdj5 is required as a disulfide reductase for degradation of misfolded proteins in the ER. *Science*. 2008;321(5888):569–572.
156. Vashist S, Ng DTW. Misfolded proteins are sorted by a sequential checkpoint mechanism of ER quality control. *J Cell Biol*. 2004;165(1):41–52.
157. Denic V, Quan EM, Weissman JS. A luminal surveillance complex that selects misfolded glycoproteins for ER-associated degradation. *Cell*. 2006;126(2):349–359.
158. Carvalho P, Goder V, Rapoport TA. Distinct ubiquitin-ligase complexes define convergent pathways for the degradation of ER proteins. *Cell*. 2006;126(2):361–373.
159. Hosokawa N et al. A novel ER alpha-mannosidase-like protein accelerates ER-associated degradation. *EMBO Rep*. 2001;2(5):415–422.
160. Oda Y, Hosokawa N, Wada I, Nagata K. EDEM as an acceptor of terminally misfolded glycoproteins released from calnexin. *Science*. 2003;299(5611):1394–1397.
161. Molinari M, Calanca V, Galli C, Lucca P, Paganetti P. Role of EDEM in the release of misfolded glycoproteins from the calnexin cycle. *Science*. 2003;299(5611):1397–1400.
162. Mast SW et al. Human EDEM2, a novel homolog of family 47 glycosidases, is involved in ER-associated degradation of glycoproteins. *Glycobiology*. 2005;15(4):421–436.
163. Olivari S, Galli C, Alanen H, Ruddock L, Molinari M. A novel stress-induced EDEM variant regulating endoplasmic reticulum-associated glycoprotein degradation. *J Biol Chem*. 2005;280(4):2424–2428.
164. Hirao K, Natsuka Y, Tamura T, Wada I, Morito D. EDEM3, a soluble EDEM homolog, enhances glycoprotein endoplasmic reticulum-associated degradation and mannose trimming. *Journal of Biological ...*. 2006;
165. Gauss R, Jarosch E, Sommer T, Hirsch C. A complex of Yos9p and the HRD ligase integrates endoplasmic reticulum quality control into the degradation machinery. *Nat Cell Biol*. 2006;8(8):849–854.

166. Christianson JC, Shaler TA, Tyler RE, Kopito RR. OS-9 and GRP94 deliver mutant alpha1-antitrypsin to the Hrd1-SEL1L ubiquitin ligase complex for ERAD. *Nat Cell Biol.* 2008;10(3):272–282.
167. Hosokawa N et al. Human XTP3-B forms an endoplasmic reticulum quality control scaffold with the HRD1-SEL1L ubiquitin ligase complex and BiP. *J Biol Chem.* 2008;283(30):20914–20924.
168. Richly H, Rape M, Braun S, Rumpf S, Hoegge C. A series of ubiquitin binding factors connects CDC48/p97 to substrate multiubiquitylation and proteasomal targeting. *Cell.* 2005;
169. Kleiger G, Saha A, Lewis S, Kuhlman B, Deshaies RJ. Rapid E2-E3 assembly and disassembly enable processive ubiquitylation of cullin-RING ubiquitin ligase substrates. *Cell.* 2009;
170. Jarosch E et al. Protein dislocation from the ER requires polyubiquitination and the AAA-ATPase Cdc48. *Nat Cell Biol.* 2002;4(2):134–139.
171. Bays NW, Gardner RG, Seelig LP, Joazeiro CA. Hrd1p/Der3p is a membrane-anchored ubiquitin ligase required for ER-associated degradation. *Nature cell* 2000;
172. Yoshida Y et al. E3 ubiquitin ligase that recognizes sugar chains. *Nature.* 2002;418(6896):438–442.
173. Morito D et al. Gp78 cooperates with RMA1 in endoplasmic reticulum-associated degradation of CFTRDeltaF508. *Mol Biol Cell.* 2008;19(4):1328–1336.
174. Nakatsukasa K, Huyer G, Michaelis S, Brodsky JL. Dissecting the ER-associated degradation of a misfolded polytopic membrane protein. *Cell.* 2008;132(1):101–112.
175. Iida Y et al. SEL1L protein critically determines the stability of the HRD1-SEL1L endoplasmic reticulum-associated degradation (ERAD) complex to optimize the degradation kinetics of ERAD substrates. *J Biol Chem.* 2011;286(19):16929–16939.
176. Horn SC et al. Usa1 functions as a scaffold of the HRD-ubiquitin ligase. *Mol Cell.* 2009;36(5):782–793.
177. Wahlman J et al. Real-time fluorescence detection of ERAD substrate retrotranslocation in a mammalian in vitro system. *Cell.* 2007;129(5):943–955.

178. Ye Y, Shibata Y, Yun C, Ron D, Rapoport TA. A membrane protein complex mediates retro-translocation from the ER lumen into the cytosol. *Nature*. 2004;429(6994):841–847.
179. Lilley BN, Ploegh HL. A membrane protein required for dislocation of misfolded proteins from the ER. *Nature*. 2004;429(6994):834–840.
180. Greenblatt EJ, Olzmann JA, Kopito RR. Derlin-1 is a rhomboid pseudoprotease required for the dislocation of mutant α -1 antitrypsin from the endoplasmic reticulum. *Nat Struct Mol Biol*. 2011;18(10):1147–1152.
181. Lee RJ et al. Uncoupling retro-translocation and degradation in the ER-associated degradation of a soluble protein. *EMBO J*. 2004;23(11):2206–2215.
182. Zhou X et al. Structural and biochemical studies of the C-terminal domain of mouse peptide-N-glycanase identify it as a mannose-binding module. *Proc Natl Acad Sci USA*. 2006;103(46):17214–17219.
183. Zhao G et al. Structural and mutational studies on the importance of oligosaccharide binding for the activity of yeast PNGase. 2009;
184. Hirsch C, Blom D, Ploegh HL. A role for N-glycanase in the cytosolic turnover of glycoproteins. *EMBO J*. 2003;22(5):1036–1046.
185. Ernst R, Mueller B, Ploegh HL, Schlieker C. The otubain YOD1 is a deubiquitinating enzyme that associates with p97 to facilitate protein dislocation from the ER. *Mol Cell*. 2009;36(1):28–38.
186. Bernasconi R et al. Role of the SEL1L:LC3-I complex as an ERAD tuning receptor in the mammalian ER. *Mol Cell*. 2012;46(6):809–819.
187. Merulla J, Fasana E, Soldà T, Molinari M. Specificity and regulation of the endoplasmic reticulum-associated degradation machinery. *Traffic*. 2013;14(7):767–777.
188. Wu Y, Termine DJ, Swulius MT, Moremen KW, Sifers RN. Human endoplasmic reticulum mannosidase I is subject to regulated proteolysis. *J Biol Chem*. 2007;282(7):4841–4849.
189. Termine DJ, Moremen KW, Sifers RN. The mammalian UPR boosts glycoprotein ERAD by suppressing the proteolytic downregulation of ER mannosidase I. *Journal of Cell Science*. 2009;122(Pt 7):976–984.

190. Cali T, Galli C, Olivari S, Molinari M. Segregation and rapid turnover of EDEM1 by an autophagy-like mechanism modulates standard ERAD and folding activities. *Biochem Biophys Res Commun*. 2008;371(3):405–410.
191. Le Fourn V et al. Basal autophagy is involved in the degradation of the ERAD component EDEM1. *Cell Mol Life Sci*. 2009;66(8):1434–1445.
192. Reggiori F, Monastyrska I, Verheije MH, Cali T. Coronaviruses Hijack the LC3-I-positive EDEMosomes, ER-derived vesicles exporting short-lived ERAD regulators, for replication. *Cell host &* 2010;
193. Gauss R, Kanehara K, Carvalho P, Ng DTW, Aebi M. A complex of Pdi1p and the mannosidase Htm1p initiates clearance of unfolded glycoproteins from the endoplasmic reticulum. *Mol Cell*. 2011;42(6):782–793.
194. Hori O et al. Role of Herp in the endoplasmic reticulum stress response. *Genes Cells*. 2004;9(5):457–469.
195. Miura H et al. Deletion of Herp facilitates degradation of cytosolic proteins. *Genes Cells*. 2010;15(8):843–853.
196. Mueller B, Lilley BN, Ploegh HL. SEL1L, the homologue of yeast Hrd3p, is involved in protein dislocation from the mammalian ER. *J Cell Biol*. 2006;175(2):261–270.
197. Cattaneo M et al. Secretion of novel SEL1L endogenous variants is promoted by ER stress/UPR via endosomes and shed vesicles in human cancer cells. *PLoS ONE*. 2011;6(2):e17206.
198. Xie Y, Avello M, Schirle M, McWhinnie E, Feng Y. Deubiquitinase FAM/USP9X interacts with the E3 ubiquitin ligase SMURF1 protein and protects it from ligase activity-dependent self-degradation. *Journal of Biological* 2013;
199. Guo X et al. The E3 ligase Smurf1 regulates Wolfram syndrome protein stability at the endoplasmic reticulum. *J Biol Chem*. 2011;286(20):18037–18047.
200. Shmueli A, Tsai YC, Yang M, Braun MA, Weissman AM. Targeting of gp78 for ubiquitin-mediated proteasomal degradation by Hrd1: Cross-talk between E3s in the endoplasmic reticulum. *Biochem Biophys Res Commun*. 2009;390(3):758–762.
201. Ballar P, Ors AU, Yang H, Fang S. Differential regulation of CFTRDeltaF508 degradation by ubiquitin ligases gp78 and Hrd1. *Int J Biochem*

Cell Biol. 2010;42(1):167–173.

202. Tcherpakov M et al. JAMP optimizes ERAD to protect cells from unfolded proteins. *Mol Biol Cell.* 2008;19(11):5019–5028.

203. Ying Z, Wang H, Fan H, Zhu X, Zhou J. Gp78, an ER associated E3, promotes SOD1 and ataxin-3 degradation. *Human molecular* 2009;

204. Durcan TM, Kontogiannea M, Bedard N, Wing SS, Fon EA. Ataxin-3 deubiquitination is coupled to Parkin ubiquitination via E2 ubiquitin-conjugating enzyme. *J Biol Chem.* 2012;287(1):531–541.

205. Leitman J, Ron E, Ogen-Shtern N, Lederkremer GZ. Compartmentalization of endoplasmic reticulum quality control and ER-associated degradation factors. *DNA Cell Biol.* 2013;32(1):2–7.

206. Olzmann JA, Kopito RR. The mammalian endoplasmic reticulum-associated degradation system. *Cold Spring Harbor* 2012;

207. Kny M, Standera S, Hartmann-Petersen R, Kloetzel P-M, Seeger M. Herp regulates Hrd1-mediated ubiquitylation in a ubiquitin-like domain-dependent manner. *J Biol Chem.* 2011;286(7):5151–5156.

208. Kopito RR, Ron D. Conformational disease. *Nat Cell Biol.* 2000;

209. Carrell RW, Lomas DA. Conformational disease. *The Lancet.* 1997;

210. Selkoe DJ. Folding proteins in fatal ways. *Nature.* 2003;426(6968):900–904.

211. Sitia R, Braakman I. Quality control in the endoplasmic reticulum protein factory. *Nature.* 2003;426(6968):891–894.

212. Stutts MJ, Canessa CM, Olsen JC, Hamrick M, Cohn JA. CFTR as a cAMP-dependent regulator of sodium channels. *Science.* 1995;

213. Cheng SH, Gregory RJ, Marshall J, Paul S, Souza DW. Defective intracellular transport and processing of CFTR is the molecular basis of most cystic fibrosis. *Cell.* 1990;

214. Welch WJ, Brown CR. Influence of molecular and chemical chaperones on protein folding. *Cell Stress Chaperones.* 1996;1(2):109–115.

215. Morello JP, Petäjä-Repo UE, Bichet DG, Bouvier M. Pharmacological

- chaperones: a new twist on receptor folding. *Trends Pharmacol Sci.* 2000;21(12):466–469.
216. Cohen FE, Kelly JW. Therapeutic approaches to protein-misfolding diseases. *Nature.* 2003;
217. Conn PM, Leañós-Miranda A, Janovick JA. Protein origami: therapeutic rescue of misfolded gene products. *Mol Interv.* 2002;2(5):308–316.
218. Bernier V, Lagacé M, Bichet DG, Bouvier M. Pharmacological chaperones: potential treatment for conformational diseases. *Trends in Endocrinology & Metabolism.* 2004;15(5):222–228.
219. Ozcan U et al. Endoplasmic reticulum stress links obesity, insulin action, and type 2 diabetes. *Science.* 2004;306(5695):457–461.
220. Ozcan L et al. Endoplasmic reticulum stress plays a central role in development of leptin resistance. *Cell Metab.* 2009;9(1):35–51.
221. Lee A-H, Heidtman K, Hotamisligil GS, Glimcher LH. Dual and opposing roles of the unfolded protein response regulated by IRE1alpha and XBP1 in proinsulin processing and insulin secretion. *Proc Natl Acad Sci USA.* 2011;108(21):8885–8890.
222. Lee A-H, Scapa EF, Cohen DE, Glimcher LH. Regulation of hepatic lipogenesis by the transcription factor XBP1. *Science.* 2008;320(5882):1492–1496.
223. Zhang K et al. The unfolded protein response transducer IRE1 α prevents ER stress-induced hepatic steatosis. *EMBO J.* 2011;30(7):1357–1375.
224. Scheuner D et al. Translational control is required for the unfolded protein response and in vivo glucose homeostasis. *Mol Cell.* 2001;7(6):1165–1176.
225. Harding HP et al. Diabetes mellitus and exocrine pancreatic dysfunction in perk^{-/-} mice reveals a role for translational control in secretory cell survival. *Mol Cell.* 2001;7(6):1153–1163.
226. Zhang P et al. The PERK eukaryotic initiation factor 2 alpha kinase is required for the development of the skeletal system, postnatal growth, and the function and viability of the pancreas. *Mol Cell Biol.* 2002;22(11):3864–3874.
227. Zhang W et al. PERK EIF2AK3 control of pancreatic beta cell

- differentiation and proliferation is required for postnatal glucose homeostasis. *Cell Metab.* 2006;4(6):491–497.
228. Gupta S, McGrath B, Cavener DR. PERK (EIF2AK3) regulates proinsulin trafficking and quality control in the secretory pathway. *Diabetes.* 2010;59(8):1937–1947.
229. Oyadomari S, Harding HP, Zhang Y, Oyadomari M, Ron D. Dephosphorylation of Translation Initiation Factor 2 α Enhances Glucose Tolerance and Attenuates Hepatosteatosis in Mice. *Cell Metab.* 2008;7(6):520–532.
230. Song B, Scheuner D, Ron D, Pennathur S, Kaufman RJ. Chop deletion reduces oxidative stress, improves beta cell function, and promotes cell survival in multiple mouse models of diabetes. *J Clin Invest.* 2008;118(10):3378–3389.
231. Maron BJ, Ferrans VJ, Roberts WC. Ultrastructural features of degenerated cardiac muscle cells in patients with cardiac hypertrophy. *Am J Pathol.* 1975;79(3):387–434.
232. Okada K-I et al. Prolonged endoplasmic reticulum stress in hypertrophic and failing heart after aortic constriction: possible contribution of endoplasmic reticulum stress to cardiac myocyte apoptosis. *Circulation.* 2004;110(6):705–712.
233. Yamaguchi O et al. Targeted deletion of apoptosis signal-regulating kinase 1 attenuates left ventricular remodeling. *Proc Natl Acad Sci USA.* 2003;100(26):15883–15888.
234. Dally S, Monceau V, Corvazier E, Bredoux R, Raies A. Compartmentalized expression of three novel sarco/endoplasmic reticulum Ca²⁺ ATPase 3 isoforms including the switch to ER stress, SERCA3f, in non *Cell calcium.* 2009;
235. Scull CM, Tabas I. Mechanisms of ER stress-induced apoptosis in atherosclerosis. *Arterioscler Thromb Vasc Biol.* 2011;31(12):2792–2797.
236. Brown MS, Goldstein JL. Lipoprotein metabolism in the macrophage: implications for cholesterol deposition in atherosclerosis. *Annu Rev Biochem.* 1983;52:223–261.
237. Maxfield FR, Tabas I. Role of cholesterol and lipid organization in disease. *Nature.* 2005;
238. Sun Y et al. Free cholesterol accumulation in macrophage membranes

activates Toll-like receptors and p38 mitogen-activated protein kinase and induces cathepsin K. *Circ Res*. 2009;104(4):455–465.

239. Ozcan L, Tabas I. Pivotal role of calcium/calmodulin-dependent protein kinase II in ER stress-induced apoptosis. *Cell Cycle*. 2010;9(2):223–224.

240. Timmins JM et al. Calcium/calmodulin-dependent protein kinase II links ER stress with Fas and mitochondrial apoptosis pathways. *J Clin Invest*. 2009;119(10):2925–2941.

241. Li G et al. Role of ERO1- α -mediated stimulation of inositol 1,4,5-triphosphate receptor activity in endoplasmic reticulum stress-induced apoptosis. *J Cell Biol*. 2009;186(6):783–792.

242. Devries-Seimon T et al. Cholesterol-induced macrophage apoptosis requires ER stress pathways and engagement of the type A scavenger receptor. *J Cell Biol*. 2005;171(1):61–73.

243. Seimon TA, Nadolski MJ, Liao X, Magallon J. Atherogenic lipids and lipoproteins trigger CD36-TLR2-dependent apoptosis in macrophages undergoing endoplasmic reticulum stress. *Cell Metab*. 2010;

244. Li G, Scull C, Ozcan L, Tabas I. NADPH oxidase links endoplasmic reticulum stress, oxidative stress, and PKR activation to induce apoptosis. *J Cell Biol*. 2010;191(6):1113–1125.

245. Pedruzzi E et al. NAD(P)H oxidase Nox-4 mediates 7-ketocholesterol-induced endoplasmic reticulum stress and apoptosis in human aortic smooth muscle cells. *Mol Cell Biol*. 2004;24(24):10703–10717.

246. Kedi X, Ming Y, Yongping W, Yi Y, Xiaoxiang Z. Free cholesterol overloading induced smooth muscle cells death and activated both ER- and mitochondrial-dependent death pathway. *Atherosclerosis*. 2009;207(1):123–130.

247. Zhou J et al. Association of multiple cellular stress pathways with accelerated atherosclerosis in hyperhomocysteinemic apolipoprotein E-deficient mice. *Circulation*. 2004;110(2):207–213.

248. Werstuck GH et al. Glucosamine-induced endoplasmic reticulum dysfunction is associated with accelerated atherosclerosis in a hyperglycemic mouse model. *Diabetes*. 2006;55(1):93–101.

249. Zeng L et al. Sustained activation of XBP1 splicing leads to endothelial

- apoptosis and atherosclerosis development in response to disturbed flow. *Proc Natl Acad Sci USA*. 2009;106(20):8326–8331.
250. Civelek M, Manduchi E, Riley RJ, Stoeckert CJ, Davies PF. Chronic endoplasmic reticulum stress activates unfolded protein response in arterial endothelium in regions of susceptibility to atherosclerosis. *Circ Res*. 2009;105(5):453–461.
251. Zhang C et al. Homocysteine induces programmed cell death in human vascular endothelial cells through activation of the unfolded protein response. *J Biol Chem*. 2001;276(38):35867–35874.
252. Outinen PA et al. Homocysteine-induced endoplasmic reticulum stress and growth arrest leads to specific changes in gene expression in human vascular endothelial cells. *Blood*. 1999;94(3):959–967.
253. Gargalovic PS et al. The unfolded protein response is an important regulator of inflammatory genes in endothelial cells. *Arterioscler Thromb Vasc Biol*. 2006;26(11):2490–2496.
254. Gora S et al. Phospholipolyzed LDL induces an inflammatory response in endothelial cells through endoplasmic reticulum stress signaling. *FASEB J*. 2010;24(9):3284–3297.
255. Thuerauf DJ et al. Activation of the unfolded protein response in infarcted mouse heart and hypoxic cultured cardiac myocytes. *Circ Res*. 2006;99(3):275–282.
256. Severino A et al. Identification of protein disulfide isomerase as a cardiomyocyte survival factor in ischemic cardiomyopathy. *J Am Coll Cardiol*. 2007;50(11):1029–1037.
257. Tadimalla A et al. Mesencephalic astrocyte-derived neurotrophic factor is an ischemia-inducible secreted endoplasmic reticulum stress response protein in the heart. *Circ Res*. 2008;103(11):1249–1258.
258. Nickson P, Toth A, Erhardt P. PUMA is critical for neonatal cardiomyocyte apoptosis induced by endoplasmic reticulum stress. *Cardiovasc Res*. 2007;73(1):48–56.
259. Vandewynckel Y-P et al. The paradox of the unfolded protein response in cancer. *Anticancer Res*. 2013;33(11):4683–4694.

260. Dong D et al. A critical role for GRP78/BiP in the tumor microenvironment for neovascularization during tumor growth and metastasis. *Cancer Res.* 2011;71(8):2848–2857.
261. Mahadevan NR, Zanetti M. Tumor stress inside out: cell-extrinsic effects of the unfolded protein response in tumor cells modulate the immunological landscape of the tumor microenvironment. *The Journal of Immunology.* 2011;
262. Shuda M et al. Activation of the ATF6, XBP1 and grp78 genes in human hepatocellular carcinoma: a possible involvement of the ER stress pathway in hepatocarcinogenesis. *J Hepatol.* 2003;38(5):605–614.
263. Chang K-C, Chen PC-H, Chen Y-P, Chang Y, Su I-J. Dominant expression of survival signals of endoplasmic reticulum stress response in Hodgkin lymphoma. *Cancer Sci.* 2011;102(1):275–281.
264. Shoulders MD, Ryno LM, Genereux JC, Moresco JJ. Stress-Independent Activation of XBP1s and/or ATF6 Reveals Three Functionally Diverse ER Proteostasis Environments. *Cell reports.* 2013;
265. Adachi Y et al. ATF6 is a transcription factor specializing in the regulation of quality control proteins in the endoplasmic reticulum. *Cell Struct Funct.* 2008;33(1):75–89.
266. Schewe DM, Aguirre-Ghiso JA. ATF6alpha-Rheb-mTOR signaling promotes survival of dormant tumor cells in vivo. *Proc Natl Acad Sci USA.* 2008;105(30):10519–10524.
267. Thorpe JA, Schwarze SR. IRE1 α controls cyclin A1 expression and promotes cell proliferation through XBP-1. *Cell Stress Chaperones.* 2010;
268. Zhong Y et al. X-box binding protein 1 is essential for the anti-oxidant defense and cell survival in the retinal pigment epithelium. *PLoS ONE.* 2012;7(6):e38616.
269. Carrasco DR et al. The differentiation and stress response factor XBP-1 drives multiple myeloma pathogenesis. *Cancer Cell.* 2007;11(4):349–360.
270. Auf G et al. Inositol-requiring enzyme 1 α is a key regulator of angiogenesis and invasion in malignant glioma. *Proc Natl Acad Sci USA.* 2010;107(35):15553–15558.
271. Drogat B, Auguste P, Nguyễn DT, Bouche-careilh M. IRE1 signaling is

- essential for ischemia-induced vascular endothelial growth factor-A expression and contributes to angiogenesis and tumor growth in vivo. *Cancer Res.* 2007;
272. Zeng L et al. Vascular endothelial cell growth-activated XBP1 splicing in endothelial cells is crucial for angiogenesis. *Circulation.* 2013;127(16):1712–1722.
273. Gomez BP et al. Human X-box binding protein-1 confers both estrogen independence and antiestrogen resistance in breast cancer cell lines. *FASEB J.* 2007;21(14):4013–4027.
274. Yoneda T et al. Activation of caspase-12, an endoplasmic reticulum (ER) resident caspase, through tumor necrosis factor receptor-associated factor 2-dependent mechanism in response to the ER stress. *J Biol Chem.* 2001;276(17):13935–13940.
275. Jing G, Wang JJ, Zhang SX. ER stress and apoptosis: a new mechanism for retinal cell death. *Exp Diabetes Res.* 2012;2012:589589.
276. Bi M et al. ER stress-regulated translation increases tolerance to extreme hypoxia and promotes tumor growth. *EMBO J.* 2005;24(19):3470–3481.
277. Fels DR, Koumenis C. The PERK/eIF2 α /ATF4 module of the UPR in hypoxia resistance and tumor growth. *Cancer Biology & Therapy.* 2006;5(7):723–728.
278. Bobrovnikova-Marjon E et al. PERK promotes cancer cell proliferation and tumor growth by limiting oxidative DNA damage. *Oncogene.* 2010;29(27):3881–3895.
279. Luo B, Lee AS. The critical roles of endoplasmic reticulum chaperones and unfolded protein response in tumorigenesis and anticancer therapies. *Oncogene.* 2013;32(7):805–818.
280. Ranganathan AC, Ojha S, Kourtidis A, Conklin DS, Aguirre-Ghiso JA. Dual function of pancreatic endoplasmic reticulum kinase in tumor cell growth arrest and survival. *Cancer Res.* 2008;68(9):3260–3268.
281. Gorman AM, Healy SJM, Jäger R, Samali A. Stress management at the ER: regulators of ER stress-induced apoptosis. *Pharmacol Ther.* 2012;134(3):306–316.
282. Zhang K, Kaufman RJ. From endoplasmic-reticulum stress to the inflammatory response. *Nature.* 2008;454(7203):455–462.

283. Tu BP, Weissman JS. The FAD-and O₂-Dependent Reaction Cycle of Ero1-Mediated Oxidative Protein Folding in the Endoplasmic Reticulum. *Mol Cell*. 2002;
284. Cuozzo JW, Kaiser CA. Competition between glutathione and protein thiols for disulphide-bond formation. *Nat Cell Biol*. 1999;1(3):130–135.
285. Urano F et al. Coupling of stress in the ER to activation of JNK protein kinases by transmembrane protein kinase IRE1. *Science*. 2000;287(5453):664–666.
286. Hu P, Han Z, Couvillon AD, Kaufman RJ, Exton JH. Autocrine tumor necrosis factor alpha links endoplasmic reticulum stress to the membrane death receptor pathway through IRE1alpha-mediated NF-kappaB activation and down-regulation of TRAF2 expression. *Mol Cell Biol*. 2006;26(8):3071–3084.
287. Davis RJ. Signal transduction by the JNK group of MAP kinases. *Inflammatory Processes*.. 2000;
288. Deng J et al. Translational repression mediates activation of nuclear factor kappa B by phosphorylated translation initiation factor 2. *Mol Cell Biol*. 2004;24(23):10161–10168.
289. Todd DJ, Lee A-H, Glimcher LH. The endoplasmic reticulum stress response in immunity and autoimmunity. *Nature Reviews Immunology*. 2008;8(9):663–674.
290. Iwakoshi NN et al. Plasma cell differentiation and the unfolded protein response intersect at the transcription factor XBP-1. *Nat Immunol*. 2003;4(4):321–329.
291. Shaffer AL et al. XBP1, downstream of Blimp-1, expands the secretory apparatus and other organelles, and increases protein synthesis in plasma cell differentiation. *Immunity*. 2004;21(1):81–93.
292. Zhang K et al. The unfolded protein response sensor IRE1alpha is required at 2 distinct steps in B cell lymphopoiesis. *J Clin Invest*. 2005;115(2):268–281.
293. Gass JN, Gifford NM, Brewer JW. Activation of an unfolded protein response during differentiation of antibody-secreting B cells. *J Biol Chem*. 2002;277(50):49047–49054.
294. Gass JN, Jiang H-Y, Wek RC, Brewer JW. The unfolded protein response of

- B-lymphocytes: PERK-independent development of antibody-secreting cells. *Mol Immunol*. 2008;45(4):1035–1043.
295. Reimold AM et al. Transcription factor B cell lineage-specific activator protein regulates the gene for human X-box binding protein 1. *J Exp Med*. 1996;183(2):393–401.
296. Obeng EA et al. Proteasome inhibitors induce a terminal unfolded protein response in multiple myeloma cells. *Blood*. 2006;107(12):4907–4916.
297. Davenport EL et al. Heat shock protein inhibition is associated with activation of the unfolded protein response pathway in myeloma plasma cells. *Blood*. 2007;110(7):2641–2649.
298. Martinon F, Chen X, Lee A-H, Glimcher LH. TLR activation of the transcription factor XBP1 regulates innate immune responses in macrophages. *Nat Immunol*. 2010;11(5):411–418.
299. Smith JA et al. Endoplasmic reticulum stress and the unfolded protein response are linked to synergistic IFN- β induction via X-box binding protein 1. *Eur J Immunol*. 2008;38(5):1194–1203.
300. Zeng L et al. XBP-1 couples endoplasmic reticulum stress to augmented IFN- β induction via a cis-acting enhancer in macrophages. *J Immunol*. 2010;185(4):2324–2330.
301. Iwakoshi NN, Pypaert M, Glimcher LH. The transcription factor XBP-1 is essential for the development and survival of dendritic cells. *Journal of Experimental Medicine*. 2007;204(10):2267–2275.
302. Woo CW et al. Adaptive suppression of the ATF4–CHOP branch of the unfolded protein response by toll-like receptor signalling. *Nat Cell Biol*. 2009;11(12):1473–1480.
303. Kaser A et al. XBP1 Links ER Stress to Intestinal Inflammation and Confers Genetic Risk for Human Inflammatory Bowel Disease. *Cell*. 2008;134(5):743–756.
304. Adolph TE et al. Paneth cells as a site of origin for intestinal inflammation. *Nature*. 2013;503(7475):272–276.
305. Xue X et al. Tumor necrosis factor alpha (TNF α) induces the unfolded protein response (UPR) in a reactive oxygen species (ROS)-dependent fashion,

- and the UPR counteracts ROS accumulation by TNFalpha. *J Biol Chem.* 2005;280(40):33917–33925.
306. Zhang K et al. Endoplasmic reticulum stress activates cleavage of CREBH to induce a systemic inflammatory response. *Cell.* 2006;124(3):587–599.
307. Cox JS, Shamu CE, Walter P. Transcriptional induction of genes encoding endoplasmic reticulum resident proteins requires a transmembrane protein kinase. *Cell.* 1993;73(6):1197–1206.
308. Mori K, Ma W, Gething MJ, Sambrook J. A transmembrane protein with a cdc2+/CDC28-related kinase activity is required for signaling from the ER to the nucleus. *Cell.* 1993;74(4):743–756.
309. He Y et al. Emerging roles for XBP1, a sUPeR transcription factor. *Gene Expr.* 2010;15(1):13–25.
310. Cox JS, Walter P. A novel mechanism for regulating activity of a transcription factor that controls the unfolded protein response. *Cell.* 1996;87(3):391–404.
311. Sidrauski C, Walter P. The transmembrane kinase Ire1p is a site-specific endonuclease that initiates mRNA splicing in the unfolded protein response. *Cell.* 1997;
312. Travers KJ et al. Functional and genomic analyses reveal an essential coordination between the unfolded protein response and ER-associated degradation. *Cell.* 2000;101(3):249–258.
313. Calton M et al. IRE1 couples endoplasmic reticulum load to secretory capacity by processing the XBP-1 mRNA. *Nature.* 2002;415(6867):92–96.
314. Lee K et al. IRE1-mediated unconventional mRNA splicing and S2P-mediated ATF6 cleavage merge to regulate XBP1 in signaling the unfolded protein response. *Genes Dev.* 2002;16(4):452–466.
315. Liu CY, Schröder M, Kaufman RJ. Ligand-independent dimerization activates the stress response kinases IRE1 and PERK in the lumen of the endoplasmic reticulum. *J Biol Chem.* 2000;275(32):24881–24885.
316. Liu CY, Xu Z, Kaufman RJ. Structure and intermolecular interactions of the luminal dimerization domain of human IRE1alpha. *J Biol Chem.* 2003;278(20):17680–17687.

317. Zhou J et al. The crystal structure of human IRE1 luminal domain reveals a conserved dimerization interface required for activation of the unfolded protein response. *Proc Natl Acad Sci USA*. 2006;103(39):14343–14348.
318. Lee KPK et al. Structure of the dual enzyme Ire1 reveals the basis for catalysis and regulation in nonconventional RNA splicing. *Cell*. 2008;132(1):89–100.
319. Han D et al. IRE1 α Kinase Activation Modes Control Alternate Endoribonuclease Outputs to Determine Divergent Cell Fates. *Cell*. 2009;138(3):562–575.
320. Papa FR, Zhang C, Shokat K, Walter P. Bypassing a kinase activity with an ATP-competitive drug. *Science*. 2003;302(5650):1533–1537.
321. Greenman C et al. Patterns of somatic mutation in human cancer genomes. *Nature*. 2007;446(7132):153–158.
322. Sha H et al. The IRE1 α -XBP1 pathway of the unfolded protein response is required for adipogenesis. *Cell Metab*. 2009;9(6):556–564.
323. Chen H, Qi L. SUMO modification regulates the transcriptional activity of XBP1. *Biochem J*. 2010;429(1):95–102.
324. Yang L et al. A Phos-tag-based approach reveals the extent of physiological endoplasmic reticulum stress. *PLoS ONE*. 2010;5(7):e11621.
325. Qi L, Yang L, Chen H. Detecting and quantitating physiological endoplasmic reticulum stress. *Meth Enzymol*. 2011;490:137–146.
326. Tirasophon W, Welihinda AA. A stress response pathway from the endoplasmic reticulum to the nucleus requires a novel bifunctional protein kinase/endoribonuclease (Ire1p) in mammalian cells. ... *& development*. 1998;
327. Tirasophon W, Lee K, Callaghan B, Welihinda A, Kaufman RJ. The endoribonuclease activity of mammalian IRE1 autoregulates its mRNA and is required for the unfolded protein response. *Genes Dev*. 2000;14(21):2725–2736.
328. Davies FE et al. Insights into the multistep transformation of MGUS to myeloma using microarray expression analysis. *Blood*. 2003;102(13):4504–4511.
329. Juric D, Lacayo NJ, Ramsey MC. Differential gene expression patterns and interaction networks in BCR-ABL–positive and–negative adult acute

- lymphoblastic leukemias. *Journal of Clinical ...* 2007;
330. Leleu X et al. Expression of regulatory genes for lymphoplasmacytic cell differentiation in Waldenstrom Macroglobulinemia. *Br J Haematol.* 2009;145(1):59–63.
331. Munshi NC et al. Identification of genes modulated in multiple myeloma using genetically identical twin samples. *Blood.* 2004;103(5):1799–1806.
332. Doane AS, Danso M, Lal P, Donaton M, Zhang L. An estrogen receptor-negative breast cancer subset characterized by a hormonally regulated transcriptional program and response to androgen. *Oncogene.* 2006;
333. Romero-Ramirez L et al. X box-binding protein 1 regulates angiogenesis in human pancreatic adenocarcinomas. *Transl Oncol.* 2009;2(1):31–38.
334. Taouji S, Wolf S, Chevet E. Oligomerization in endoplasmic reticulum stress signaling. *Progress in molecular biology and ...* 2013;
335. Jenkins SJ et al. Local macrophage proliferation, rather than recruitment from the blood, is a signature of TH2 inflammation. *Science.* 2011;332(6035):1284–1288.
336. Meusser B, Hirsch C, Jarosch E, Sommer T. ERAD: the long road to destruction. *Nat Cell Biol.* 2005;7(8):766–772.
337. Tabas I. The role of endoplasmic reticulum stress in the progression of atherosclerosis. *Circ Res.* 2010;107(7):839–850.
338. Sha H, He Y, Yang L, Qi L. Stressed out about obesity: IRE1 α -XBP1 in metabolic disorders. *Trends Endocrinol Metab.* 2011;22(9):374–381.
339. Lerner AG et al. IRE1 α induces thioredoxin-interacting protein to activate the NLRP3 inflammasome and promote programmed cell death under irremediable ER stress. *Cell Metab.* 2012;16(2):250–264.
340. Osowski CM et al. Thioredoxin-interacting protein mediates ER stress-induced β cell death through initiation of the inflammasome. *Cell Metab.* 2012;16(2):265–273.
341. Schroder K, Tschopp J. The inflammasomes. *Cell.* 2010;
342. Bergsbaken T, Fink SL, Cookson BT. Pyroptosis: host cell death and

inflammation. *Nature Reviews Microbiology*. 2009;

343. Mehnert M, Sommer T, Jarosch E. ERAD ubiquitin ligases: multifunctional tools for protein quality control and waste disposal in the endoplasmic reticulum. *Bioessays*. 2010;32(10):905–913.

344. Hetz C, Martinon F, Rodriguez D, Glimcher LH. The unfolded protein response: integrating stress signals through the stress sensor IRE1 α . *Physiol Rev*. 2011;91(4):1219–1243.

345. Christianson JC et al. Defining human ERAD networks through an integrative mapping strategy. *Nat Cell Biol*. 2012;14(1):93–105.

346. Plemper RK et al. Genetic interactions of Hrd3p and Der3p/Hrd1p with Sec61p suggest a retro-translocation complex mediating protein transport for ER degradation 1999;

347. Biunno I et al. Cross-species conservation of SEL1L, a human pancreas-specific expressing gene. *OMICS*. 2002;6(2):187–198.

348. Biunno I et al. SEL1L a multifaceted protein playing a role in tumor progression. *J Cell Physiol*. 2006;208(1):23–38.

349. Donoviel DB, Donoviel MS, Fan E, Hadjantonakis A, Bernstein A. Cloning and characterization of Sel-11, a murine homolog of the *C. elegans* sel-1 gene. *Mech Dev*. 1998;78(1-2):203–207.

350. Mueller B, Klemm EJ, Spooner E, Claessen JH, Ploegh HL. SEL1L nucleates a protein complex required for dislocation of misfolded glycoproteins. *Proc Natl Acad Sci USA*. 2008;105(34):12325–12330.

351. Grant B, Greenwald I. The *Caenorhabditis elegans* sel-1 gene, a negative regulator of lin-12 and glp-1, encodes a predicted extracellular protein. *Genetics*. 1996;143(1):237–247.

352. Francisco AB et al. Deficiency of suppressor enhancer Lin12 1 like (SEL1L) in mice leads to systemic endoplasmic reticulum stress and embryonic lethality. *J Biol Chem*. 2010;285(18):13694–13703.

353. Ban Y et al. SEL1L microsatellite polymorphism in Japanese patients with autoimmune thyroid diseases. *Thyroid*. 2001;11(4):335–338.

354. Kyöstilä K et al. A SEL1L mutation links a canine progressive early-onset

- cerebellar ataxia to the endoplasmic reticulum-associated protein degradation (ERAD) machinery. *PLoS Genet.* 2012;8(6):e1002759.
355. Saltini G et al. A novel polymorphism in SEL1L confers susceptibility to Alzheimer's disease. *Neurosci Lett.* 2006;398(1-2):53–58.
356. Rodríguez CI et al. High-efficiency deleter mice show that FLPe is an alternative to Cre-loxP. *Nat Genet.* 2000;25(2):139–140.
357. Sun S, Xia S, Ji Y, Kersten S, Qi L. The ATP-P2X7 signaling axis is dispensable for obesity-associated inflammasome activation in adipose tissue. *Diabetes.* 2012;61(6):1471–1478.
358. Ferrero S et al. SEL1L expression in non-small cell lung cancer. *Hum Pathol.* 2006;37(5):505–512.
359. Granelli P et al. SEL1L and squamous cell carcinoma of the esophagus. *Clin Cancer Res.* 2004;10(17):5857–5861.
360. Barberis MCP, Roz E, Biunno I. SEL1L expression in prostatic intraepithelial neoplasia and adenocarcinoma: an immunohistochemical study. *Histopathology.* 2006;48(5):614–616.
361. LIDA Y et al. SEL1 L Protein Critically Determines the Stability of the HRD1-SEL1L Endoplasmic Reticulum-associated Degradation (ERAD) Complex to Optimize the Degradation Kinetics of ERAD Substrates. *J Biol Chem.* 2011;286(19):16929–16939.
362. Bulua AC, Simon A, Maddipati R. Mitochondrial reactive oxygen species promote production of proinflammatory cytokines and are elevated in TNFR1-associated periodic syndrome (TRAPS). *The Journal of* 2011;
363. Naik E, Dixit VM. Mitochondrial reactive oxygen species drive proinflammatory cytokine production 2011;
364. Dougan SK et al. Derlin-2-deficient mice reveal an essential role for protein dislocation in chondrocytes. *Mol Cell Biol.* 2011;31(6):1145–1159.
365. Adrain C, Zettl M, Christova Y, Taylor N, Freeman M. Tumor necrosis factor signaling requires iRhom2 to promote trafficking and activation of TACE. *Science.* 2012;335(6065):225–228.
366. McIlwain DR et al. iRhom2 regulation of TACE controls TNF-mediated

- protection against *Listeria* and responses to LPS. *Science*. 2012;335(6065):229–232.
367. Yeung PSM, Na Y, Kreuder AJ, Marquis H. Compartmentalization of the broad-range phospholipase C activity to the spreading vacuole is critical for *Listeria monocytogenes* virulence. *Infect Immun*. 2007;75(1):44–51.
368. van de Veerdonk FL, Netea MG, Dinarello CA, Joosten LAB. Emerging roles for XBP1, a sUPeR transcription factor. *Trends Immunol*. 2011;32(3):110–116.
369. Yang Y et al. The AIM2 Inflammasome Is Involved in Macrophage Activation During Infection With Virulent *Mycobacterium bovis* Strain. *J Infect Dis*. [published online ahead of print: September 11, 2013]; doi:10.1093/infdis/jit347
370. Hernandez JC, Latz E, Urcuqui-Inchima S. HIV-1 Induces the First Signal to Activate the NLRP3 Inflammasome in Monocyte-Derived Macrophages. *Intervirology*. [published online ahead of print: September 5, 2013]; doi:10.1159/000353902
371. Lima-Junior DS et al. Inflammasome-derived IL-1 β production induces nitric oxide-mediated resistance to *Leishmania*. *Nat Med*. 2013;19(7):909–915.
372. Wu M-F, Chen S-T, Hsieh S-L. Distinct regulation of dengue virus-induced inflammasome activation in human macrophage subsets. *J Biomed Sci*. 2013;20:36.
373. Negash AA et al. IL-1 β production through the NLRP3 inflammasome by hepatic macrophages links hepatitis C virus infection with liver inflammation and disease. *PLoS Pathog*. 2013;9(4):e1003330.
374. Pelegrin P, Barroso-Gutierrez C, Surprenant A. P2X₇ receptor differentially couples to distinct release pathways for IL-1 β in mouse macrophage. *J Immunol*. 2008;180(11):7147–7157.
375. Miller CM et al. The role of the P2X₇ receptor in infectious diseases. *PLoS Pathog*. 2011;7(11):e1002212.
376. Baroja-Mazo A, Barberà-Cremades M, Pelegrin P. P2X₇ receptor activation impairs exogenous MHC class I oligopeptides presentation in antigen presenting cells. *PLoS ONE*. 2013;8(8):e70577.

377. Ozcan U et al. Chemical chaperones reduce ER stress and restore glucose homeostasis in a mouse model of type 2 diabetes. *Science*. 2006;313(5790):1137–1140.
378. Sun S, Ji Y, Kersten S, Qi L. Mechanisms of inflammatory responses in obese adipose tissue. *Annu Rev Nutr*. 2012;32:261–286.
379. Weisberg SP, McCann D, Desai M. Obesity is associated with macrophage accumulation in adipose tissue. *Journal of Clinical ...*. 2003;
380. Xu H et al. Chronic inflammation in fat plays a crucial role in the development of obesity-related insulin resistance. *J Clin Invest*. 2003;112(12):1821–1830.
381. Liu T-F et al. Ablation of gp78 in liver improves hyperlipidemia and insulin resistance by inhibiting SREBP to decrease lipid biosynthesis. *Cell Metab*. 2012;16(2):213–225.
382. Cattaneo M et al. SEL1L and HRD1 are involved in the degradation of unassembled secretory Ig-mu chains. *J Cell Physiol*. 2008;215(3):794–802.
383. Kislinger T et al. Global survey of organ and organelle protein expression in mouse: combined proteomic and transcriptomic profiling. *Cell*. 2006;125(1):173–186.
384. Lilley BN, Ploegh HL. Multiprotein complexes that link dislocation, ubiquitination, and extraction of misfolded proteins from the endoplasmic reticulum membrane. *Proc Natl Acad Sci USA*. 2005;102(40):14296–14301.
385. Bernasconi R, Galli C, Calanca V, Nakajima T, Molinari M. Stringent requirement for HRD1, SEL1L, and OS-9/XTP3-B for disposal of ERAD-LS substrates. *J Cell Biol*. 2010;188(2):223–235.
386. Balch WE, Morimoto RI, Dillin A, Kelly JW. Adapting proteostasis for disease intervention. *Science*. 2008;319(5865):916–919.
387. Powers ET, Morimoto RI, Dillin A, Kelly JW, Balch WE. Biological and chemical approaches to diseases of proteostasis deficiency. *Annu Rev Biochem*. 2009;78:959–991.
388. Conn PM. The Unfolded Protein Response and Cellular Stress 2011;
389. Gao B et al. Synoviolin promotes IRE1 ubiquitination and degradation in

synovial fibroblasts from mice with collagen-induced arthritis. *EMBO Rep.* 2008;9(5):480–485.

390. Wu Y-T et al. Dual role of 3-methyladenine in modulation of autophagy via different temporal patterns of inhibition on class I and III phosphoinositide 3-kinase. *J Biol Chem.* 2010;285(14):10850–10861.

391. Wang Q, Li L, Ye Y. Inhibition of p97-dependent protein degradation by Eeyarestatin I. *J Biol Chem.* 2008;283(12):7445–7454.